The Thesis Committee for Homar Molina Jr.
Certifies that this is the approved version of the following thesis:

Using the FRDPARRC Design Methodology to Drive Innovation in the HETDEX PFIP Support Adjustable Strut Assembly

APPROVED BY
SUPERVISING COMMITTEE:

Supervisor:

Steven P. Nichols

Joseph H. Beno

Using the FRDPARRC Design Methodology to Drive Innovation in the HETDEX PFIP Support Adjustable Strut Assembly

by

Homar Molina Jr., B.S.M.E.

Thesis

Presented to the Faculty of the Graduate School of

The University of Texas at Austin

in Partial Fulfillment

of the Requirements

for the Degree of

Master of Science in Engineering

The University of Texas at Austin

December 2010

Dedication

To Eva L. and Eva N. the two most beautiful ladies inside and out.

Acknowledgements

I would like acknowledge those instrumental in my academic and personal achievements of which this thesis is no small part.

First of all, I would like to thank Professor Steve Nichols for his expertise, advice, and direction with regards to this thesis and my Master's program. I would like to express thanks to the University of Texas for the generous opportunity afforded me to pursue my Master's degree in their mechanical engineering department.

To those I worked with at the Center for Electromechanics, I appreciate all of you. I especially want to thank the following people: Joey Zierer and Rex Jackson whose expertise and advice on CAD, engineering, and machining made this thesis possible; Mike Worthington and Ian Soukup for their help both on the job and in the classroom; Richard Hayes and Dr. Joe Beno for allowing me to study and work on their team; and Tim Beets and Robert Pearsall for providing much-needed laughs.

I would like to acknowledge Professor Mary Boyce, Professor Martin Culpepper, Professor Alex Slocum, Professor Doug Hart, Patrick McAtamney, Donna Friedman, and Wayne Johnson of MIT.

I would like to thank my father, sister, Aaron Buchok, Seth Forster, and Rusty Trapps for their friendship and support during my time at UT. Finally thanks to God whose gracious blessings and gifts have given me all I have.

December 2010

Abstract

Using the FRDPARRC Design Methodology to Drive Innovation in the HETDEX PFIP Support Adjustable Strut Assembly

Homar Molina Jr., MSE

The University of Texas at Austin, 2010

Supervisor: Steven P. Nichols

This thesis provides background information on the Hobby-Eberly Telescope (HET), HET Dark Energy Experiment (HETDEX), Gough-Stewart platforms (GSP), the Prime Focus Instrument Package (PFIP) support structure, and the design methodology used to design said support structure. Each component is analyzed from the point of view of Professor Alex Slocum's FRDPARRC design methodology. Each aspect of the design is shown to have been derived by following the steps of Slocum's design method. Material selection, manufacturing techniques, and integration of off-the-shelf components into the support system are also discussed in reference to FRDPARRC. The assembly procedure for the PFIP structure is outlined. Finally, using specific examples from the detailed design, the FRDPARRC method itself is analyzed and its ability to drive innovation in design is evaluated.

Table of Contents

List of Tables

List of Figures

Chapter 1: Background

THE HOBBY-EBERLY TELESCOPE, DARK ENERGY, AND HETDEX

The Hobby-Eberly Telescope (HET)

The Hobby-Eberly Telescope, or HET, is the third largest optical telescope in the world and resides on Mount Fowlkes at the McDonald Observatory in Fort Davis, Texas [**1**]. The HET design allows it to gather data comparable to telescopes that cost 5-8 times more. Instead of moving the entirety of the telescope to observe and follow object in apparent motion across the sky, the HET relies on the reflection of a fixed-elevation 11 meter primary mirror consisting of 91 hexagonal contoured segments arranged in a spherical shape and a moving tracker that follows the object being observed as its reflection moves along the mirror [**2**]. Additionally, the HET is slanted at 55 degrees to the horizon [**3**]. The HET can rotate in azimuth a full 360 degrees on air bearings to point the mirror in the desired direction for observation to regain some of the sky coverage lost by its fixed-elevation, fixed-tilt design [**2**]. The moving mass of this telescope is kept low by restricting the motion of the full mass of the telescope to rotation only having the tracker move predominantly in 2 dimensions with respect to a plane tangent to the spherical contour of the primary mirror arrangement [**2**]. Since the height of the telescope is kept constant, there is little change in gravitational forces over time; this provides the advantage of using simplified 9-point Hindle mounts to make minor corrections in the position of the mirror segments and employing optical correctors to compensate for resultant image distortion [**2**]. HET currently has a field of view of approximately 4 arcminutes of sky and can use an area of the mirror that forms a circle up to 9.2 meters in diameter [**3**].

Dark Energy

In 1997-1998 two research groups independently happened upon "Dark Energy" whilst observing distant supernovae [**4**]. Up until their discovery, it was assumed that the universe was expanding at a decelerating or at most a constant rate. Operating under this

assumption, one team found that some supernovae were much further than expected. Furthermore, their data "suggest an externally expanding universe that is accelerated by energy in the vacuum" [**5**]. The other team independently concluded that "the data are strongly inconsistent with… the simplest inflationary universe model" [**6**]. The "energy in the vacuum" that increases the universe's rate of expansion with increasing age was dubbed "Dark Energy" [**7**]. It is named as such in much the same way as the 'Dark Ages'—that is to convey a sense of ignorance or lack of understanding; it is not meant to convey any foreboding or malicious form of energy as connotations of the word 'dark' would suggest [**8**]. The source or cause of the acceleration is not known, but it is suggested that its discovery and study will affect current scientific understanding of the universe and its basic properties [**8**]. Astronomers, cosmologists, and physicists have all put forth that the study of Dark Energy can mean the discovery of new sub-atomic particles, revamping of the understanding of gravity, formulation of alternate origin-of-the-universe theories that update/supersede the Big Bang theory, or have other unforeseen profound effects on the scientific community and the study of the universe [**7**]. However, these are conjectures as only the existence of Dark Energy is known, and there is no data as to its properties or their implications [**9**].

The Hobby-Eberly Telescope Dark Energy Experment (HETDEX)

The McDonald Observatory (MDO) at The University of Texas at Austin along with numerous partners, donors, and academic institutions are embarking on a $34M study into the nature of Dark Energy which will employ the HET to survey around one million galaxies in 140 nights [**10**]. However, the HET in its current condition is insufficient for the task at hand [**3**]. The telescope's optical complement is to undergo an upgrade with an array of spectrographs called the Visible Integral-Field-Unit (IFU) Replicable Ultra-cheap Spectrograph or VIRUS that will use 132 simple IFU spectrographs that reduce total engineering costs while increasing field of view to approximately 22 square arcminutes of sky up from its current 4 arcminute capability [**9**]. A new Wide Field Corrector (WFC) that is capable of feeding VIRUS at the increased

field of view must also be constructed to enable HET to complete the HETDEX survey at around 2 degrees of sky per night over an estimated 3 spring trimesters with the appropriate accuracy [**9**].

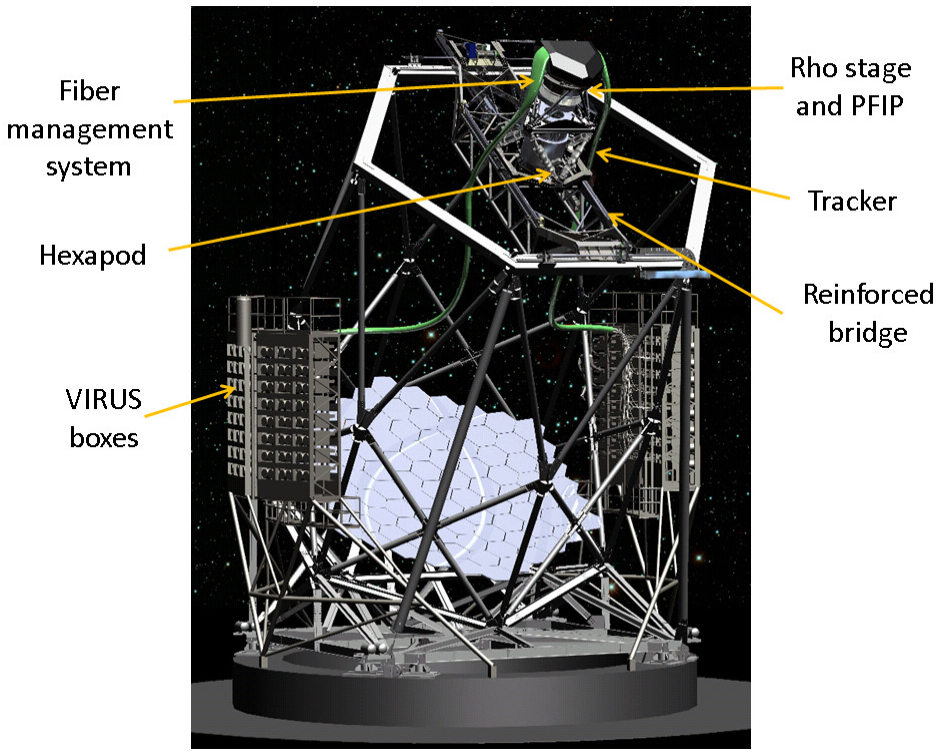

Figure 1-1: Solid-model rendering of HETDEX Upgrade with key components identified. [**11**]

The instrumentation to support the increased field of view and resolution increases the mass payload beyond HET's current capability. Also, HET was plagued with design shortcomings [**10**] that scientists at MDO decided to rectify during this substantial retrofit/upgrade [**12**]. In totality the HET upgrade will consist of the new WFC, the new Prime Focus Instrument Package (PFIP) that interfaces with the VIRUS array, a new tracker—reinforced and redesigned with performance enhancing features, manually adjustable struts to align and position the PFIP with the WFC, a rotary stage that manipulates only the equipment at the top of the tracker, an upgraded computer-controlled Hexapod, and fiber-optic cable management to route the cabling that transmits

data to the VIRUS [**12**]. These components are visible in the solid model rendering shown in Figure 1-1.

PFIP SUPPORT STRUCTURE AND GOUGH-STEWART PLATFORMS

The PFIP support structure is comprised of six manually adjustable Rho struts and 2 sets of 3 identical blocks that house the spherical bearing strut-ends. One set of blocks is arranged on the strongback and the other on the Rho stage. This configuration forms what is known as a parallel manipulator since the pose of the Rho stage (platform) is determined by the distance between two sets of six points: one on the strongback (base) and the other on the Rho stage [**13**]. The lower planar rigid-body, or base, is considered fixed while the upper planar rigid-body, or platform, is mobile. This particular class of parallel manipulator is known as a Gough-Stewart platform or GSP, and there exist a total of 3,850 possible configurations of GSPs [**14**]. The Gough-Stewart platform is named after V. E. Gough who developed a platform for testing automobile tires in 1956 and D. Stewart who developed a platform similar in concept for the manipulation of flight simulators in 1965 [**15**]. GSPs are used when precision positioning, high stiffness, and 6 degrees-of-freedom (DOF) are required [**15**] [**16**]. GSPs have been used in telescopes, microscopes, circuit fabrication via lithography, vibration isolation [**17**], machining [**16**], and numerous other applications. Advantages of GSPs include the ability to manipulate the platform to at least some extent in 6-DOFs, (namely translation in X, Y, and Z, and roll, pitch, and yaw), the low strut-weight-to-payload ratio [**15**] allows for heavy payloads to be supported with struts of low cross-sectional area [**16**]. However, due to the nature of the kinematics, even basic translation requires adjusting all 6 supports [**16**].

The type of GSP that the PFIP support structure, Rho stage, and strongback form is a 6-6 GSP since the struts attach to the platform and base using 6 separate but geometrically identical spherical joints [**13**], i.e. no joints are shared by struts. This configuration also meets additional criterion put forth by [**18**] since the points on the base

and platform form hexagons, and the hexagons formed by these points are geometrically similar. See Figure 1-2 for a graphical representation of this criterion.

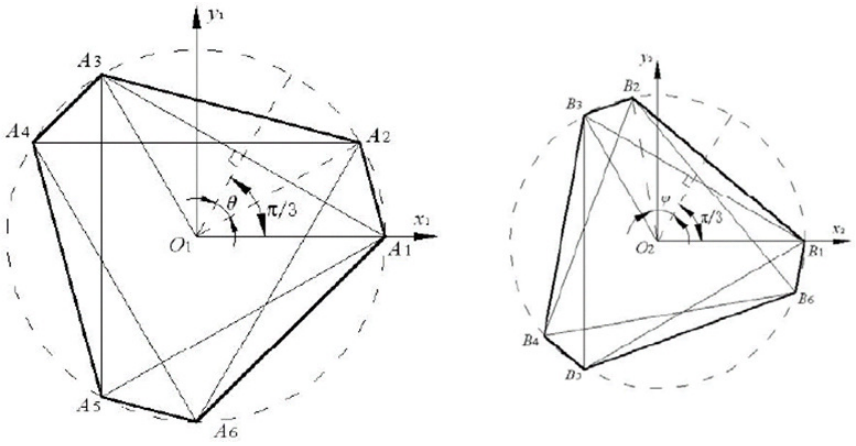

Figure 1-2: Similar hexagons on the base (left) and platform (right) are formed by connecting the centers of the spherical joints in a symmetrical 6-6 GSP [**19**]. Disregard the relative orientations of the hexagons since they are each defined in their own local coordinate system in this figure.

This configuration is known as the 6-6^p GSP [**18**] or a symmetrical 6-6 GSP [**19**] and is shown in Figure 1-3.

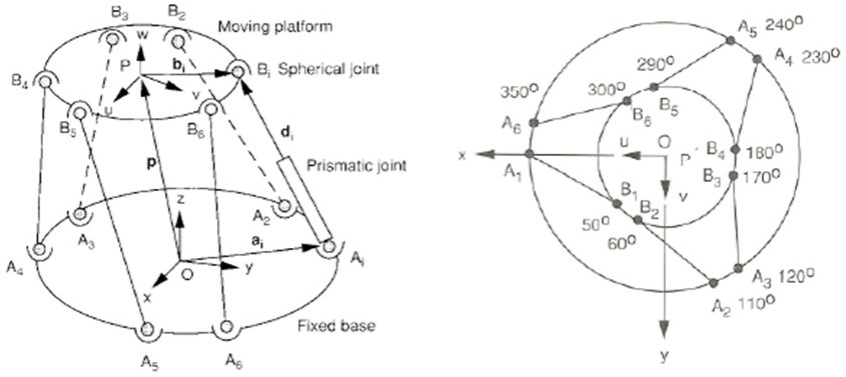

Figure 1-3: A simplified graphical representation of an assembled 6-6^p GSP is shown from a side view (left) and from above (right) [**16**]. The top-view shows how the similar hexagons are situated in relation to one-another. This configuration most closely matches that which is implemented in the PFIP support structure.

There are two general methods of studying the kinematic of GSPs: *directly* which determines pose of the platform with respect to the base by knowing the lengths of each support [**14**] and *indirectly* where the support lengths are determined by the known pose of the platform with respect to the base [**16**]. The direct kinematic method may yield as many as 40 mathematical solutions [**13**], most of which are non-real and therefore physically invalid, and some of which result in negative leg-lengths and are also physically invalid [**19**]. It is important to note that multiple valid solutions often remain. The indirect kinematic method produces two solutions per leg, one of which is negative and therefore invalid [**16**]. Only after evaluating which quantities are known can a solution type be chosen. Typically in a control system, the leg-lengths are known and therefore the direct kinematic approach is usually more popular [**20**]. Solving the kinematic problem can be done numerically using a Newton-Raphson method [**20**] or algebraically, with many choosing the latter to eliminate the need for an initial guess value and for reduction of computing time; many papers have been written about algebraic eliminations methods of direct kinematic GSP systems and the streamlining thereof [**19**] [**15**] [**18**] [**20**]. All methods assume the base is fixed, but this is not the case on HETDEX. The strongback is manipulated along with the WFC by its own Hexapod, i.e. a computer-controlled GSP. However since the PFIP support structure provides alignment between the WFC and the PFIP—two components whose relative position is unaffected by Hexapod position—this poses no problem. Additionally, these methods assume that the center-points of the spherical end-mounts are planar with the base and platform. Again, this is not the case as the spherical bearings rest in blocks fixed distances from the strongback and Rho stage. However, a simple mathematical translation operation along the normal-vectors of each planar surface of magnitude determined by those fixed distances corrects this.

The adjustable Rho struts are shown in the context of the GSP formed with the strongback and Rho stage in Figure 1-4 which is a close-up rendering of just the tracker and payload.

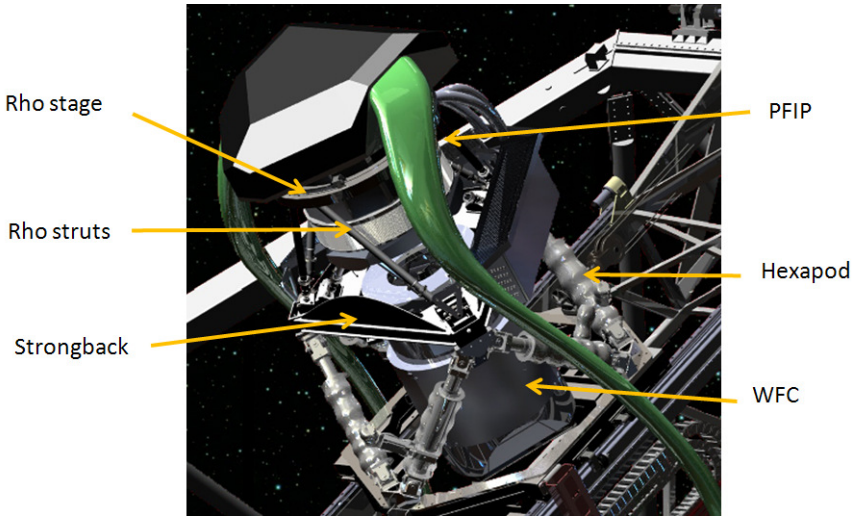

Figure 1-4: A cropped rendering of the tracker with relevant components identified is shown. Note the "stacked" 6-6^p GSPs formed by the Hexapod and the PFIP support structure [**11**].

THE "FRDPARRC" DESIGN METHODOLOGY

FRDPARRC Origin

FRDPARRC (pronounced Fred Park) design methodology was created by Professor Alexander Slocum of MIT for use in the school's 2.007 Design & Manufacturing I course as a way to organize thoughts and introduce students to design engineering [**21**]. FRDPARRC is an acronym that stands for sections of the design process in sequential order. They are Functional Requirements, Design Parameters, Analysis, References (Research), Risks, and Countermeasures. The process is meant to help engineers clearly state the task to be performed and organize their thoughts on how to meet the task as well as identify any potential problems associated with their proposed solutions. It serves a number of purposes: brain storming, idea generation/innovation, risk identification/mitigation, proper research into proposed solutions, feasibility checks, iteration, and elimination of inferior design solutions.

This process is meant to be a top-level view of the design. Therefore details normally considered in product design are left out of this process. Slocum intentionally encourages some degree of generality in this process such as to not limit the engineer's

options in formulating a solution. Additionally, he believes that unless an idea or goal can be expressed in words in the abstract sense, there is no way to describe it in specific terms either through modeling, equations, or specifications [**21**]. However, in practice this process can apply even at the detail level and can help to drive innovation not only in abstract or general terms but in detail design as well. This is true even if design goals are very specifically defined.

Functional Requirements

The first step is to identify Functional Requirements (FRs) or simply the purpose or function the design has to meet or perform [**21**]. Slocum emphasizes that the functional requirements identified be as independently as possible in order to promote modularity and robustness in design. Modularity has been deemed "the most important characteristic of a product's architecture" [**22**]. A modular design uses a single sub-component (or design parameter) to perform a single functional parameter, and sub-component interactions are fundamental to the design functionality [**22**]. Robustness in a design ensures that the product maintains functionality despite non-ideal working conditions [**22**]. Slocum discourages the use of specifications or numbers in defining FRs, but this thesis will include them.

In addition to functional requirements, this first step will be widened to include "Operational Desirements". These are essentially features the design must include at the expressed desire of the customer. These can be either general, overarching features (e.g. components must be light weight) or specific, application dependent features (e.g. component X must not exceed Y pounds in weight).

Design Parameters

The second step is to identify Design Parameters (DPs) that indicate how the design will meet the FRs and ODs [**21**]. The ultimate goal is to apply a single DP to each FR and keep DPs as independent as possible to reduce any unintended consequences of implementing a DP on the performance of the others. In the early stages of conceptual design there may be numerous possible DPs per FR that are systematically eliminated

through evaluation in subsequent steps. For the purposes of this thesis, DPs will mean the specific physical features of a design that serve to accomplish a FR/OD.

Analysis

The third step is to analyze the physics of the design. Again Slocum encourages an abstract view here prior to attempting a mathematical model [**21**]. The analysis can include stress calculations to determine material choices or geometry, feasibility studies to see if the DP can feasibly meet the FR, bench-level experiments to investigate the physical phenomena at work or to provide proof of concept, determine assembly specifications, and identify ideal and functionality in non-ideal working conditions. Because of the heavy mathematical nature of the analysis section, the analysis will be described in this thesis in words with only the results or extremely important mathematical relations shown in the body of the text. Full detailed analysis will be available in the appendices with the proper sections noted in the text.

References

The fourth step is to collect references, or more appropriately to research the design problem and possible DPs. Researching can help identify if current solutions exist to the problem at hand thus allowing the engineer to employ off-the-shelf components in their design. Additionally researching DPs can help inspire ideas or to identify possible patents barring the use of a DP or requiring licensing or other legal steps to be taken prior to implementation. This can help the engineer avoid patent infringement issues. Finally, researching can aid in the analysis of the design. General equations or explanations of the physical phenomena are likely to exist in some printed no matter the nature of the mechanical design. Use the research and provide references to give proper credit and aid in explanation or validation of analysis.

Risks

The analysis and research portions of the design will likely bring to light risks associated with the DPs. A risk is simply what could feasibly go wrong in the

implementation of a design [**21**]. The fifth step is to identify these risks for two reasons: 1) to evaluate which DP best suits the FR and 2) to be able to react to these risks to improve the design and add robustness. This thesis focuses on the latter use as the iterative process is left out for the sake of brevity knowing that this process was carried out. Slocum emphasizes that risk in a design is not necessarily always bad thing since a properly rectified risky design may perform better than a safer alternative.

Countermeasures

The final step is to identify feasible countermeasures that reduce the risk associated with a DP. If a countermeasure is acceptable then the design can progress, but if no acceptable countermeasures are taken the idea must be removed from consideration [**21**]. Slocum also points out that the implementation of countermeasures often reduces the performance of the design. Not only must risk be managed but the performance must also be monitored so that the design still meets its FR/OD effectively.

THESIS CONTENT

What follows is a description of the PFIP support struts and blocks with respect to the FRDPARRC design methodology. Each component/sub-assembly will be dissected and how FRDPARRC led to the design choices will be discussed. The iterative nature and process of elimination that come along with FRDPARRC will be left out for the sake of brevity unless where extremely important. Additionally, assembly and recommended alignment procedures will be discussed. While components are not part of high-volume production runs, certain Design for Manufacture and Design for Assembly [**22**] principles are incorporated and will be discussed as necessary.

Chapter 2: The PFIP Support Structure

Overall Design

The PFIP support structure consists of 5 main components: the struts (adjustment features and spherical ends inclusive), the upper Rho blocks, the Rho stage, the strongback, and the lower Rho blocks. Modular design was expressly requested by MDO on all components of the tracker to aid in assembly [**23**]. When assembled, these components form a symmetric 6-6^p Gough-Stewart platform. A solid model representation of the assembled structure can be seen in Figure 2-1.

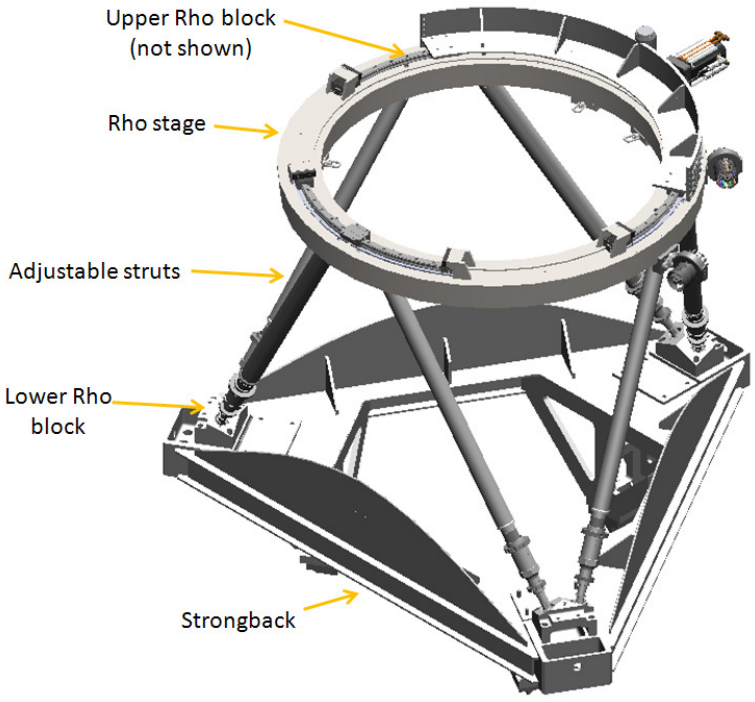

Figure 2-1: A solid model representation of the PFIP support structure is shown with 5 components identified. The strut adjustment features and ends are included in the "strut" assembly. This is not the case for purposes of analysis and assembly, as this convention applies solely to the simplified identification in this figure [**24**].

MDO requested the struts be manually adjustable [**12**] and capable of +/- 25 mm axial adjustment [**25**] that would allow for alignment of PFIP with respect to the WFC

axis [**12**] as well as accommodate any tolerances involved in assembly and manufacturing [**26**]. This requirement was relaxed to +/- 19 mm at Critical Design Review I, which were the adjustment capabilities of the proposed design at the time. Because of the kinematics of a 6-6 GSP the exact optical axis (meaning motion along the axial direction of the WFC as defined in [**27**]) translation achieved depends on the position of the Focal Plane Assembly Mounting Surface [**27**] and the position/geometry of the Upper and Lower Rho blocks. The Rho stage also has to be capable of tipping and/or tilting (rotation about the X and Y axes respectively) at least 10 arcminutes with respect to the WFC reference point [**28**] [**27**]. These two requirements alone dictated the use of a parallel manipulator of some kind with the 6-6^p GSP being the most popular choice.

Additionally, each strut has to support a minimum of 7,557 N axial load in either tension or compression [**29**] to perform its function. This load was increased to 12 kN for analysis purposes to give room for added mass from later design development in the Rho assembly or PFIP as well as act as a safety margin.

To explain how the design works the support structure will be broken up into 3 sub-sections: the Rho blocks (as a pair), the strut ends (with the Rho block bores inclusive), and the adjustment mechanism. Note: for the FRDPARRC analysis and assembly sections these groupings will vary somewhat. After part introduction, all parts will be referred to by their CEM part number.

RHO BLOCKS

There are two sets of three Rho blocks; the lower Rho blocks, 10223-DT-015, and the upper Rho blocks, 10223-DT-083. Three 10223-DT-015 attach to the strong back, and three 10223-DT-083 attach to the Rho platform. These blocks perform a number of functions. They house the spherical bearings at the strut ends and provide adequate stiffness for expected loads. All of the loads in the struts are transmitted through the blocks. Additionally, they set the geometric location of the spherical ends of the struts, thereby dictating the effective lengths of components that comprise the strut and the kinematic motion of the entire support structure.

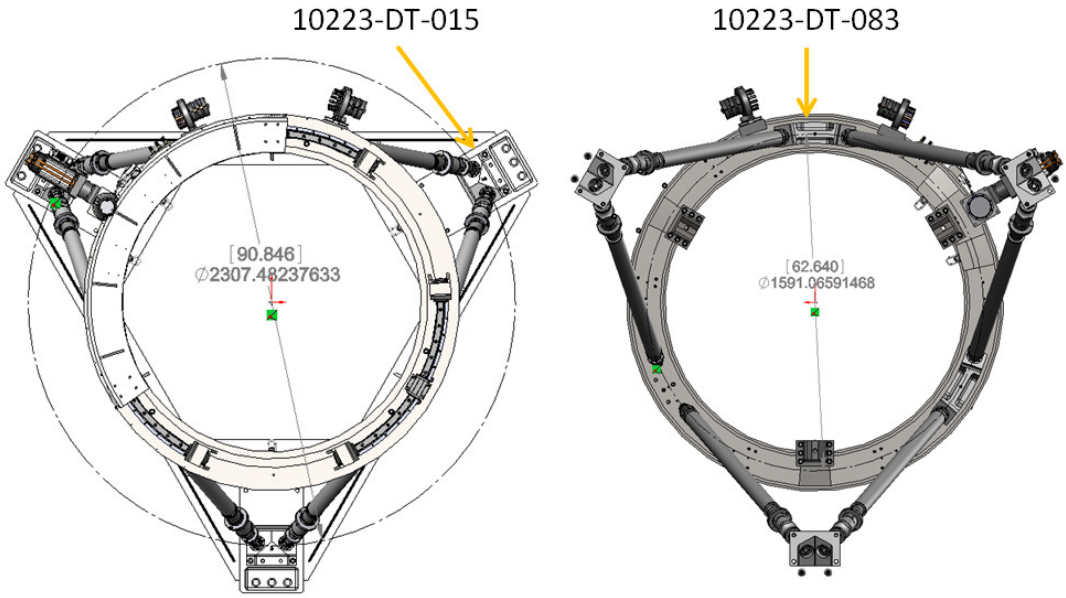

Figure 2-2: A top-view of the PFIP support structure assembly, 10223-AY-400, is shown (left) with some components missing to point out the location of the lower Rho blocks. A bottom-view of the same assembly is shown (right) to identify locations of the lower blocks [**24**]. The diameters of the circles formed by connecting the centers of the spherical bearings in the strut ends are also shown. This data can be used to determine kinematic behavior.

10223-DT-015

Three 10223-DT-015 attach to the strongback via four M16 X 2.0 socket-head cap screws. This places the centers of the spherical bearings about which the struts pivot on a circle that measures approximately 2,307.5 mm in diameter at a height of approximately 91.6 mm from the top of the strongback. The block location and outline/diameter of the circle (to much higher resolution to reduce the effects of round-off error in subsequent calculations) can be found in Figure 2-2. The holes are counter-bored close-fit clearance holes that, despite the surface geometry, terminate at the same depth so that the M16 X 2.0 screws can all be of the same length, 80 mm, to simplify assembly.

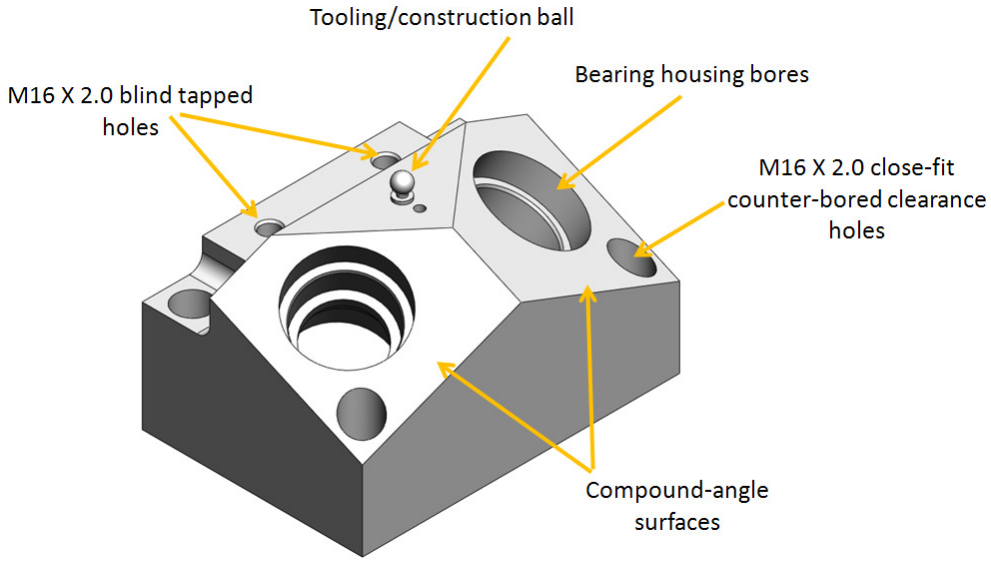

Figure 2-3: The 10223-DT-015 is shown. The design features compound angle-surfaces into which the bores that accommodate the strut-ends are machined (and similar geometries on the underside, not-shown), 4 duplicate clearance holes for mounting fasteners, blind tapped holes for mounting work platforms and electronics boxes, a tooling ball to aid in manual construction should the vendor decide to machine this part manually, and a tapped hole for lifting provisions [**30**].

As seen in Figure 2-3, the block contains compound-angled surfaces. This surface gives the machinist a flat surface to work on when boring the features that accommodate the strut ends. Since this involves threading and a smooth finished surface, as will be discussed in a later section, the parallel surface will help to increase accuracy of these features to the prescribed dimensions. There are similar features on the underside (not shown). When initially designed, these compound angled surfaces were meant to be perpendicular to those on the mating blocks, 10223-DT-083, at nominal height, i.e. 2,320 mm +/- 0 mm. This would ensure that the spherical bearings were parallel to the compound surface so that the full range of motion of the sphere was available when adjusting the structure. However, changes in the strongback geometry late in the design phase disturbed this equilibrium. It does not adversely affect

performance as the structure still meets or exceeds all requirements in terms of adjustment as requested by MDO.

10223-DT-015 also features two blind tapped M16 X 2.0 holes on the far side that are meant to serve as attachment points for work platforms added to the tracker by MDO very late in the design stage. Though 10223-DT-015 was meant to serve only functions related to the adjustable PFIP support structure, the blocks are capable of supporting this additional static load with negligible impact on performance. However, the effects of spring-back on the height of the Rho stage induced by the unloading of weight when technicians leave the platforms after adjusting the struts have yet to be investigated as mass estimates and mounting designs are still in flux.

The two final features are a tooling/construction ball that is placed in a precisely located, reamed locational-clearance hole and a tapped hole for lifting provisions. The tooling ball serves as a reference in component drawings for quality assurance via post-process measurement and machining purposes. This will aid in machining should the vendor decide to machine this component manually. Since the PFIP will be assembled at height upon final assembly of the HET upgrade, MDO has requested all components be equipped with lifting features or attachment points for such procedures [**23**].

10223-DT-083

The 10223-DT-083 attaches to the Rho stage with four M16 X 2.0 socket-head cap screws. However, unlike the 10223-DT-015, these attach from the top-side meaning there are 4 blind tapped holes in the blocks and the Rho stage has the counter-bores. This places the centers of the spherical bearings on a circle approximately 1591.1 mm in diameter and approximately 59.4 mm below the lower surface of the Rho stage, as shown in Figure 2-2. No special machining needs to be done on these blocks for them to accommodate fasteners of the same size. The circular nature of the Rho stage dictates the 10223-DT-083 conform to that shape while leaving plenty of room for possible design changes of the Rho stage.

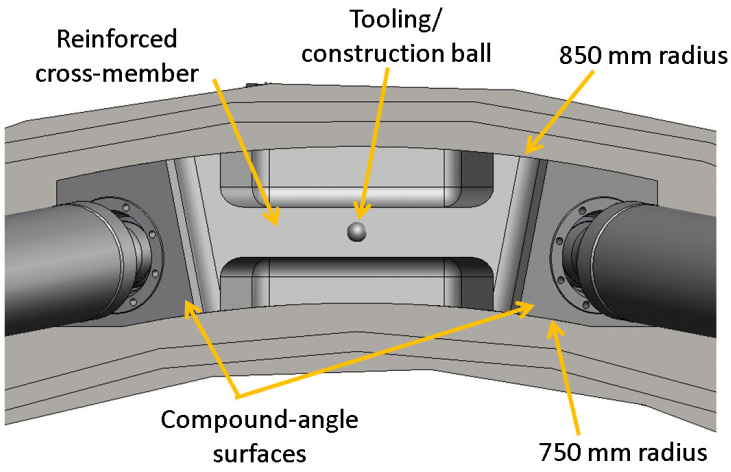

Figure 2-4: A close-up of the 10223-DT-083 in-situ is shown. The radii of curvature of the inner and outer features are labeled. Design features including the compound-angled surfaces, tooling ball, and reinforced cross-member used to stiffen the block against compressive forces between the strut ends are also identified [**31**].

The center of the Rho stage is a 1600 mm diameter circle, so the centers of the 10223-DT-083 were also placed on this circle. This ensures central placement within the stiffening side-walls of the Rho stage. The final design left 39 mm of clearance on either side of the block in case of later upgrades, thickening of the side-wall, or some other unforeseen design change. See Figure 2-4 for an in-situ close up of the 10223-DT-083 attached to the Rho stage. The bore geometries are nearly identical to those on the 10223-DT-015, and the compound-angle surfaces were meant to be parallel to the 10223-DT-015 surfaces as previously mentioned. A tooling ball is once again used to provide a reference point for machining and QA.

A few notable design differences between the blocks exist. The most obvious is the cross-member shown in Figure 2-4. It serves to stiffen the block against compressive or tensile stresses that may exist between the bearing bores. Strategic placement of the cross-member also allows for the use of machined pockets, which can also be seen in the figure above, for weight reduction while keeping adequate stiffness. Differences are also apparent when viewed from the underside.

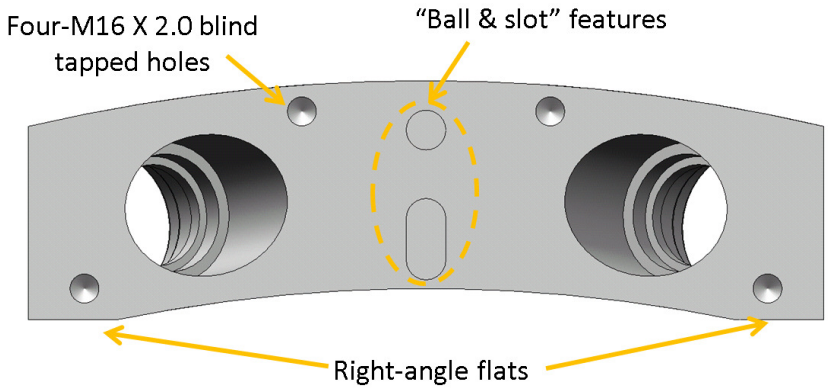

Figure 2-5: The underside of 10223-DT-083 is shown. Ball and slot features to accommodate a repeatable mount, machined indicator flats, and the four tapped M16 x 2.0 holes are shown [**32**].

A view of the 10223-DT-083 surface that interfaces with the Rho stage is shown in Figure 2-5. The ball and slot features are there to meet a requirement that MDO put forth: all mounts that attach the PFIP should be repeatable to reduce readjustment time upon reassembly of the PFIP in case it should ever be removed [**23**]. So long as all other locks on the struts and strut-ends are engaged, the Rho stage can be removed from and accurately replaced onto the plane created by the flat undersides of the three 10223-DT-083. This style of mount has been shown to reduce down-time significantly on the current HET design since tedious and time-consuming readjustments are eliminated [**23**].

Another feature that can be seen in Figure 2-5 is the presence of machined flats in the outline of the part. Since the part is predominantly curved, these flats act as a set of right-angles from which the machinist can indicate and make measurements. This will aid not only in manufacturing but in QA along with the tooling ball that is present on the opposite side of the part.

STRUT ENDS

The strut ends on the PFIP support structure are much more than just the coupling of the Rho blocks to the struts. They function as a locking mechanism that allows for 8.5 degrees of adjustment about the center of the spherical bearing [**33**]. This design uses the bearing in a very non-conventional way to allow the clamping/locking action to take

place. See Figure 2-6 for a section-view through the center of the strut end (along with the lower Rho block).

The strut end consists of the following components:

A: Insert, p/n:10223-DT-458 (also valid for 10223-DT-454)

B: Retaining Ring, p/n: 10223-DT-422

C: H-COM 19 Ball

D: Modified H-COM 19 Bearing Race, p/n: 10223-DT-427

E: Strut Spacer, p/n: 10223-DT-466

F: Bear-lok BLM-05 Lock Nut

G: Upper/Lower Rho Block (10223-DT-015 or 10223-DT-083)

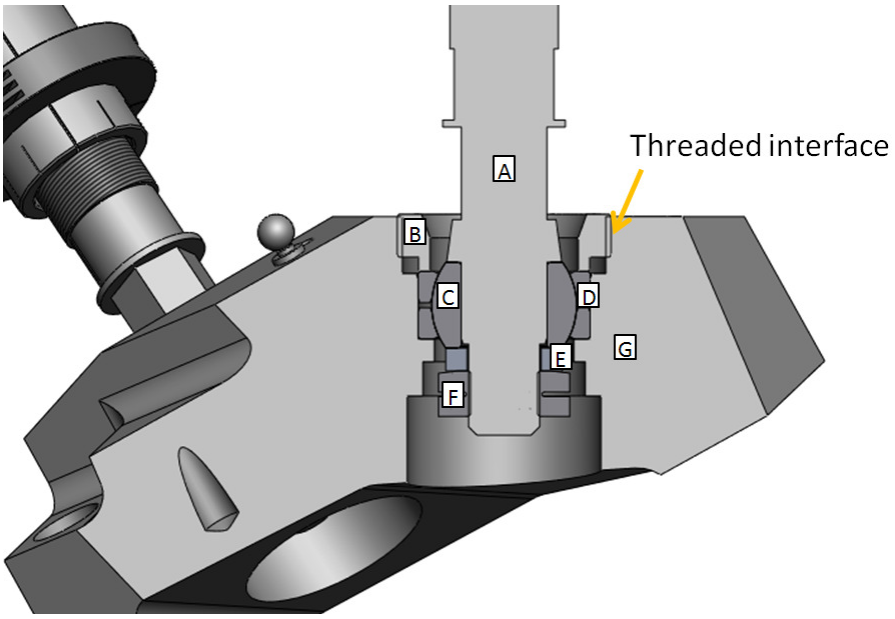

Figure 2-6: A section-view through the center of the strut end and through 10223-DT-015 is shown. Relevant components have been labeled and can be referenced using the key above the figure. The retaining ring threads into the block to place a downward axial force on the modified bearing race to accomplish preload and locking action [**24**].

This section of the design features two off-the-shelf components, one of which is modified. The Bear-lok BLM-05 lock nut is a proprietary nut made by the Whittet-Higgins company; its features will be discussed more in detail when this sub-assembly is

analyzed from the FRDPARRC point of view. Additionally, the H-COM 19 spherical bearing is a product of the Aurora Bearing Company.

The BLM-05 functions to hold the H-COM 19 ball onto the strut end component (represented in Figure 2-6 by the letter A). In addition to being a nut, it has locking features that prevent the nut from loosening once properly installed. The H-COM 19 bearing was initially chosen due to its size and axial strength, but it was later modified thus rendering manufacturer's load capacity data unreliable. It was modified by splitting the race with significant material removal, this way an axial force will cause it to compress and elastically deform causing controlled binding with the spherical ball. This is accomplished by using a spanner wrench to tighten 10223-DT-422 to a specified torque value (See Appendix 1, Section 2, Part 3) thus putting a set axial force in the downward direction (or upward in the case of the 10223-DT-083).

The bearing bore in the Rho block is cut as a locational clearance hole with up to 0.001" of diametric clearance to allow for the upper half to move axially to allow the locking action to occur. It also has a finer finish of 0.8 micron Ra or equivalently 32 CLA. Along with a light coat of lithium grease, this finish helps the locking action remain smooth and decreases the amount of torque required by the user to achieve proper locking action.

All remaining bores are functional with both their depth and diameters carefully selected for operation. The combination of bore geometry and 10223-DT-466 allow for the entire 8.5 degree range of the H-COM 19 ball to be used without having any geometric interference on either the nut-side or strut-side of the block. The final bore on the nut-side of the block is oversized intentionally to allow for the use of a specialized installation socket on the nut to achieve proper installation torque (see Appendix 1, Section 2, Part 1).

ADJUSTMENT MECHANISM

The adjustment mechanism is the crux of the PFIP support adjustable strut design. MDO had requested the strut length be manually adjustable to 50 micron precision. To

accomplish this, a number of goals had to be met not the least of which is making sure that the design is capable of effectively raising or lowering the load while keeping the required user-input torque low enough for the average user/technician to produce safely at elevation.

A number of components come together to form the adjustment mechanism. Outside and section views of the components are shown in Figure 2-7.

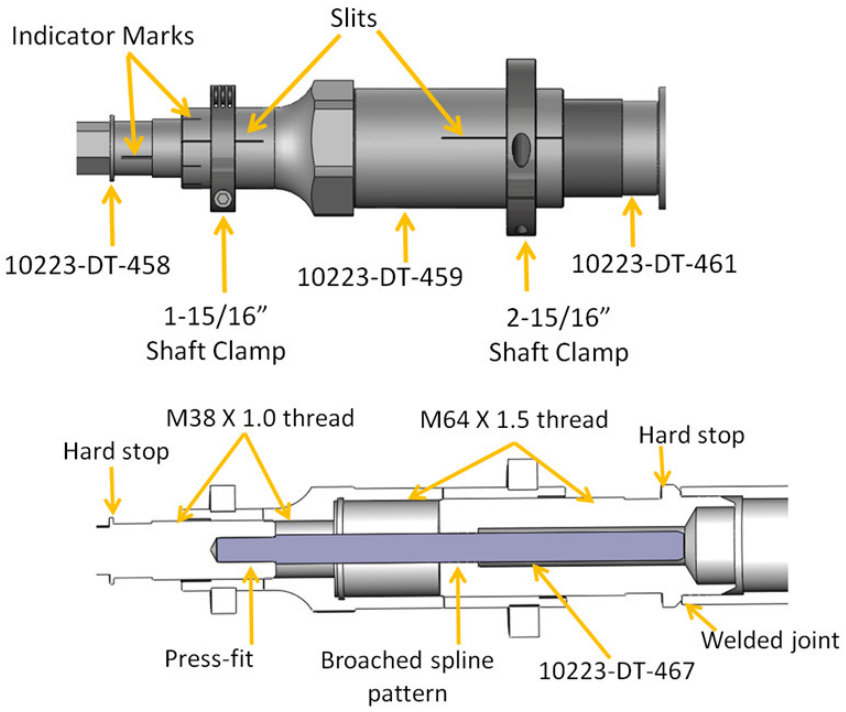

Figure 2-7: A side-view (Top) and section-view (Bottom) of the adjustment mechanism are shown. Key design features are identified in the photos [**24**].

The design functions as a differential thread pitch adjuster. One full revolution of the collar expands or contracts the strut length by 0.5 mm, the difference between the two thread pitches. There are wrench flats on 10223-DT-458 and 10223-DT-459 that allow the user to hold the strut-ends (and by extension via the splined shaft, 10223-DT-467, the strut itself) stationary while using a large wrench to turn the collar. This prevents the strut from rotating about the strut axis via the spherical bearings in the strut ends, thus reducing the effects of friction only to those existing within the threads. The indicator

marks shown in the side-view in Figure 2-7 are 10 in number and are precisely placed at 36° apart. This gives the user a reference point that can adjust the length with 50 micron resolution. However, this design does not incorporate an absolute positioning system, nor does it include a way of having real-time full strut-length feedback. These features were not expressly desired by the MDO.

10223-DT-458

This component is the one onto which the H-COM 19 bearing is attached via interference fit. It is threaded with a high-precision M38 X 1.0 thread with enough threads to allow adequate thread engagement even at the extremes of travel. It also features a set of wrench flats for holding the strut stationary, and an indicator mark that works in conjunction with those on 10223-DT-459.

10223-DT-459 and Shaft Clamps

The 10223-DT-459 features two internal threaded bores, one at M38 X 1.0 and the other at M64 X 1.5. These threads, along with the bores and concentric features, are toleranced tightly to allow for close precision without binding in the case of long thread engagement. Additionally, the threaded areas are slit so to allow for locking once the desired strut length has been attained. The outer surface of 10223-DT-459 is channeled to accommodate the shaft clamps that surround it. The collars are off-the-shelf components that work in conjunction with the slits to make the collar fully adjustable with the ability to lock. They also reinforce the collar to restore hoop strength that is lost after the slitting operation. These clamps function by use of a single socket-head cap screw, effectively reducing the locking operation to simply turning two screws some small amount. The channels in 10223-DT-459 are deep enough to accommodate the clamps in their loosened state so they need not be completely removed during adjustment.

10223-DT-467

Starting out as an approximately 1 foot length of Grob Inc. #0687-16-2 spline stock, 10223-DT-467 is modified to allow for a press-fit into 10223-DT-458. The

function of the spline is to interact with the broached spline pattern in 10223-DT-461 to angularly couple the two externally threaded components. While it does not transfer torque directly, it acts to resist torque introduced by friction in the threads while turning 10223-DT-459 during the adjustment process. The spline resists rotational motion while allowing axial motion along its length. This allows the 10223-DT-458 and 10223-DT-461 to move relative to each other axially (lengthening or shortening the strut) while keeping them from rotating with respect to each other.

10223-DT-461

10223-DT-461 acts as the end of the upper strut assembly. This component features an M64 X 1.5 external thread for its use in the differential thread apparatus. Additionally, the center of the component is broached with the Grob Inc. #0687-16-2 spline profile to interact with 10223-DT-467 in preventing relative rotational motion between the upper and lower strut . The remainder of the center is bored large enough to accommodate aberrations, bends, or out-of-roundness in 10223-DT-467 as the strut is lengthened or shortened. Using a broached feature simplifies the design and reduces part count by eliminating the need for inserts and any risk such a component would introduce.

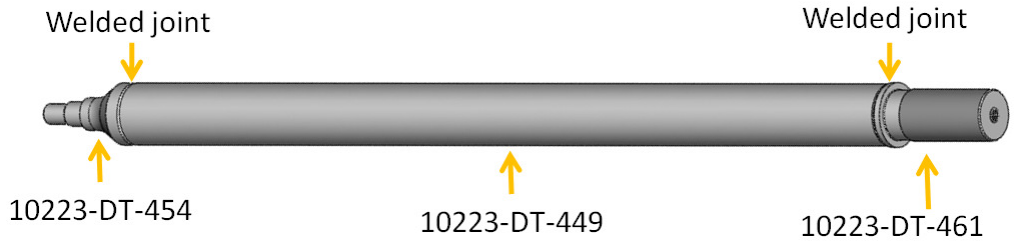

Figure 2-8: The upper strut assembly, 10223-AY-450, with components identified is shown [**24**].

UPPER STRUT COMPONENTS

The simplest subassembly in the PFIP support structure is the upper strut. It consists of three components welded into a full structure (see Figure 2-8). However, its simplicity in design should not devalue its importance in the system. Along with interfacing with the upper strut end and adjustment mechanism, it sets the nominal height

of the Rho platform. Since axial adjustment is only +/- 19 mm, setting the nominal strut length is crucial as any aberration reduces the total amount of available adjustment.

10223-DT-454, 10223-DT-449, and 10223-DT-461 are welded together to form the upper strut. Since this subassembly is critical to the performance of the structure, there are strict manufacturing procedures and tolerances that have been applied to this assembly which are detailed in the FRDPARRC breakdown of these components.

GOING FORWARD

These past sections have served as a primer on the PFIP support strut components and function. Knowledge presented in sections is required for full understanding of how the FRDPARRC process helped shape and influence the final design. As these parts will be discussed in detail in subsequent chapters, familiarity with them to the level established by this chapter on the part of the reader will be assumed.

Chapter 3: PFIP Support Strut Assembly

This chapter discusses the entire assembly without detailed reference to sub-assemblies or components of the system. It is meant as an overview of the design goals of the assembly as a unit as well as a lead-in for familiarity with the FRDPARRC breakdown of components. Subsequent chapters focusing on individual sub-assemblies will be more detailed in nature.

FUNCTIONAL REQUIREMENTS AND OPERATIONAL DESIREMENTS

The main functional requirements of PFIP support structure are to:

1. bear the weight of the PFIP assembly
2. maintain the ability to adjust the relative placement of the Focal Plane Assembly with respect to the WFC reference plane to +/- 21.7 mm [**28**] in 0.050 mm increments [**26**] and achieve tip/tilt of 10 arcminutes [**25**].

MDO has requested the adjustment mechanism:

3. be manually adjustable [**28**]
4. feature a differential thread pitch mechanism of some sort to accomplish the adjustment [**26**]

Additional over-arching requirements are that:

5. all components used be non-reflective such as not to affect data collected by telescope (recall that it functions on the principle of reflection) [**34**]
6. lift provisions be made for all PFIP components or sub-assemblies to be lifted via crane during the final assembly [**23**]
7. designs be modular so that crane lifting capacity is not exceeded [**23**]
8. all removable PFIP components use repeatable mounts to aid in reassembly [**23**]
9. use lightweight components where practical to aid in assembly and reduce energy cost of operation

10. eliminate the use of small removable components (namely loose fasteners) where practical to prevent possible mirror damage should these components fall while being serviced

FR/OD Effects on Design Parameters

Implications of FRs/ODs

Regarding the main purpose of the structure, all that is really implied is that the structure must have at least 3 degrees of freedom: axial translation, roll, and pitch. Yaw is not required as Rho stage serves as a rotational platform. MDO has had success with hexapod structures in the past and decided on a 6-6^p GSP solution. Additionally, precision components requiring precision design and manufacture are going to be required to be able to achieve the required range at the designated resolution.

Since the adjustment mechanism must be manually adjustable and feature a differential-thread pitch solution, this limits the amount of input torque such a mechanism could require from the user. These adjustments must be made at altitude during the assembly process, so minimal operator effort is paramount. These requirements also imply that only one set of hands per strut be required for adjustment.

Additional operational desirements imply rather trivial design choices from the engineer. For example: reducing reflection from components requires painting components flat black or treating components with a process which will yield a flat black finish. These will be discussed in detail as they apply at the sub-assembly or component level of this breakdown.

Design parameters and their implementation

Prior experience with GSPs led MDO to encourage this type of design for use in the PFIP support structure despite it having more degrees of freedom than required. The origins and behavior of GSPs are discussed in detail in the background section. Additionally, with regards to the limits on input torque and interaction, design choices were made to reduce the number of components that require user interaction (namely

fasteners or threaded components for locking/unlocking) and the adjustment procedure itself only requires two wrenches—and therefore only one technician—and a managable input torque to lengthen or shorten the strut.

Repeatable ball-and-slot mounts were used to meet the requirement that the PFIP be easily positioned upon reassembly. To reduce weight, tubing instead of solid bar were used in the strut assemblies, and part geometries were chosen that balance readily available stock sizes, easy to measure/machine feature lengths, and smallest geometry necessary to perform a given function.

Loads/ stresses and their effect on design parameters

Expected design loads heavily influenced most design parameters with regards to material as some components see high stresses or require a certain stiffness to perform properly. While this is not the final word in what material is chosen, the loads determined roughly the class of material to be used: polymer, steel, aluminum, etc. while other factors such as availability, cost, and ease of work to the choices.

Load paths within components determined part geometry. Components with so-called "stress raisers" such as sharp corners or holes, slits, changing diameters, etc. were examined using hand calculations and FEA simulations. These aided in finding and identifying stress "hot-spots" in the components and allowed for modification of geometry wherever warranted to reduce these effects.

Most components in this system were designed with a minimum safety factor of 1.5. This was done for two reasons: 1.) to ensure robust components and 2.) to leave room for growth of other components still in the design phase or additional components to be installed by MDO at a later date. Recall that although this retrofit to the HET is done with Dark Energy experimentation in mind, this telescope is likely to see other use after the HETDEX survey is complete.

Stress analysis was often run in highly-unlikely "worst case scenarios". For example, FEA methods were run on components that modeled fasteners as infinitely stiff so that the model was constrained more rigidly than the real component is likely to be.

This helped identify areas of high stress under load since the stress-relieving effects of an elastic constraint/fastener were eliminated. This method also simplified the model and calculations. Another example would be the case of the struts. Some are in compression while others are in tension, so each strut was designed with the highest strut load determined by analysis, increased by the safety factor, and assumed to be acting in whichever direction was most detrimental to the design.

Finally, if some aspect of the design was questionable in feasibility, small scale tests were conducted for proof-of-concept or data gathering.

Implementation of off-the-shelf components

Oftentimes there are off-the-shelf components that require little to no modification to accomplish a functional requirement or operational desirement. Use of such an item drastically lowers cost on two fronts: engineering time and cost per item. Since the off-the-shelf component is likely mass produced by a company that specializes in this type of manufacture, the engineering and manufacturing costs are amortized over a much larger number of pieces than a part designed for use in this specific application. Off-the-shelf items were used wherever possible to help lower costs without affecting performance of the design. However, modifications to some of the off-the-shelf components were necessary, or changes to the basic design so as to accommodate the off-the-shelf components were made.

Examples of off-the-shelf items are the spherical bearings used in the strut ends, splined shaft used in the adjuster mechanism, and steel tubing used in the upper strut assembly. As with all items discussed in this chapter, more detail will be available in subsequent chapters.

Manufacturing methods

More often than not, certain design parameters that fulfill a functional requirement or operational desirement must be implemented using a specific manufacturing method otherwise performance suffers. The best examples of this in the PFIP support strut design are the slits in 10223-DT-459. Since they must be added after

the threading operation to ensure concentricity, they must be done in such a way that residual stresses in the material do not cause a flowering effect. The slitting operation must also leave no burrs in the threaded features otherwise the adjustment mechanism is at risk of binding or damaging the threads. Wire electrical-discharge machining, or Wire-EDM, is known to produce accurate cuts with no residual burr. Therefore this method was chosen as the manufacturing process by which to create the slits.

Manufacturing methods can also be determined by cost, however in such a specialized application of these parts, there is already in an inherent high cost due to low volume of components produced. MDO is interested more in overall component performance than maximizing the performance/cost ratio. Therefore if an exotic manufacturing process is required to achieve the desired performance they are unlikely to compromise performance in favor of reducing cost. There are a few exceptions to this, and they will be discussed as they arise in subsequent chapters. Despite the preceding statements, most components were designed with the lowest cost conventional manufacturing/machining methods available in mind.

Risk identification and mitigation

With each design parameter selected comes a risk, as discussed in the FRDPARRC system primer in the background section. Along with the discussion of the chosen design parameters associated risks will be identified and any necessary precautions or countermeasures will be implemented and described. These will be discussed in detail at the subcomponent level.

Chapter 4: The Strut-End Subassembly

DESCRIPTION OF SUBASSEMBLY

The strut end assembly is shown in Figure 2-6 in Chapter 2. This figure along with a list of components in the assembly are reprinted here for convenience.

The strut end consists of the following components:

A: Insert, p/n:10223-DT-458 (also valid for 10223-DT-454)

B: Retaining Ring, p/n: 10223-DT-422

C: H-COM 19 Ball

D: Modified H-COM 19 Bearing Race, p/n: 10223-DT-427

E: Strut Spacer, p/n: 10223-DT-466

F: Bear-lok BLM-05 Lock Nut

G: Upper/Lower Rho Block (10223-DT-015 or 10223-DT-083)

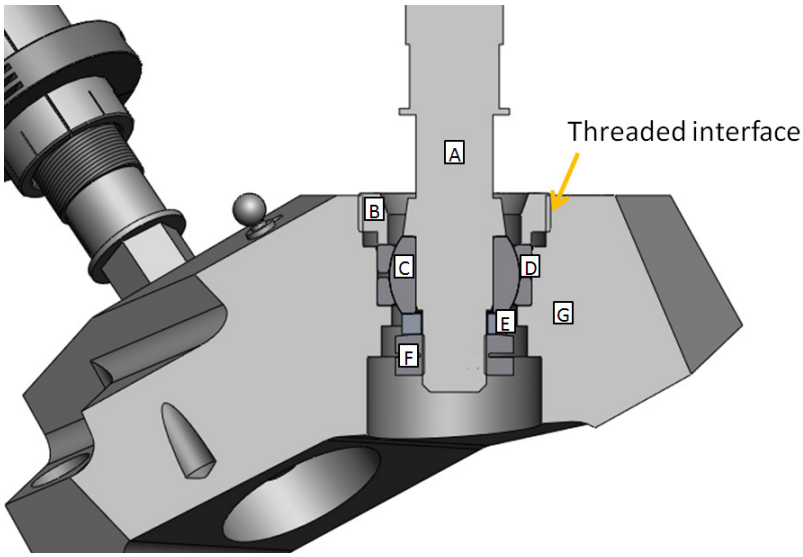

Figure 4-1: The strut-end subassembly [**24**].

It is important to remember that there are effectively two sets of strut end assemblies, those on the strongback and those on the Rho stage. Since the FRDPARRC breakdown for both of these subassemblies are nearly identical they will both be considered in this chapter. The main differences are the components labeled "A" and

"G" in Figure 4-1. When a significant difference exists between them, it will be explicitly identified and discussed.

FUNCTIONAL REQUIREMENTS AND OPERATIONAL DESIREMENTS

The FRDPARRC breakdown of the subassemblies and components in these assemblies follows. Primary or subassembly-level FRs and ODs will be designated with roman numerals while component-level FRs and ODs will be designated with lower-case letters for ease of designation.

FRs & ODs for the subassembly

The functional requirements and operational desirements of the strut end assemblies are:

I. to provide unconstrained pivoting action through the entire range of motion of the 6-6^{p} GSP formed by the PFIP support structure and the +/- 19 mm strut travel.

II. to resist motion due to either tension or compression in the struts that contain these strut-end assemblies.

III. to lock fully when not being adjusted/serviced by a technician.

IV. to conform to the overarching functional requirements listed in Chapter 3.

FRs, ODs, and description of subassembly components

Each component shown in Figure 4-1 above serves its own set of FRs and ODs it must perform within the subassembly to be able to accomplish the subassembly level requirements. How these affected the design of each component follows.

10223-DT-458 and 10223-DT-454

These components interface with the H-COM 19 bearing ball and the strut-side of the strut-end assembly. Although they are vastly different in geometry due to their necessary functions with regards to their interactions with other components, the geometry at the nut-side of the assemblies are identical. Therefore their FRDPARRC breakdown (with regards to the strut-end subassembly) is identical.

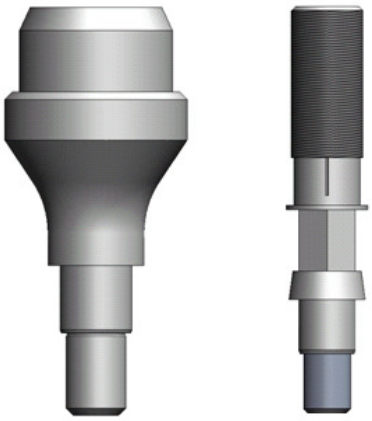

Figure 4-2: Components 10223-DT-454 (left) and 10223-DT-458 (right) are shown [**24**]. Identical geometries on the lower, nut-side, can be seen.

FRs & ODs

Functional requirements and operational desirements of 10223-DT-458 and 10223-DT-454 are as follows:

a. Interface with the H-COM 19 ball with high concentricity

b. Conform to subassembly requirements I-IV at the subassembly level

Implications of the high concentricity FR are the need for high precision machining and tight tolerancing and GD&T practices in component technical drawings. To provide pivoting with adequate clearance means paying attention to geometric issues that may arise during design development not only of this component but of other components in the subassembly. Resistance to design loads means paying attention to stress analysis and choosing suitable materials.

Design Parameters

To meet the FRs/ODs a few design parameters were established. First, a locational clearance fit would be ideal for this situation if concentricity were the only concern, but an interference fit capable of supporting the maximum design load of 12 kN specified for the interface between the 10223-DT-454 or 10223-DT-458 and the H-COM 19 would take care of concentricity as well as the load-supporting FRs. As an added measure of redundancy for this particular assembly, a lock-nut and spacer were used to

ensure that the strut is never pulled loose from the H-COM 19 ball. Threaded features are needed to support these items. This leaves the ability to use both the interference and the locational-clearance fits as the extremes of a range of acceptable fits.

Additionally, to give the components a black finish, they were to be case-hardened by nitrocarburization [**35**] using a process called Nitreg-C + ONC created by the Nitrex Corperation. These processes boast increased corrosion resistance, no dimensional distortion, and a black surface finish [**36**]. Because of these features, this process was specified for numerous components in the PFIP support strut assembly.

Implementation of DPs

Typically components that interface with a bearing are machined with a high quality surface finish [**37**]. Additionally, fits are determined by either a "shaft basis" or a "hole basis" depending on which parameter is out of the engineer's control. Since the H-COM 19 ball is a purchased item, the hole size is set from the factory—only the tolerance band can be specified by the purchaser. It would be best to determine the fit on a hole basis. So a surface finish of 0.8 Ra and a fit of 0.0062 mm loose (locational clearance) to 0.0151 mm tight (interference) were implemented. Additionally a lead-in chamfer of 20° was added to aid in assembly of this component and the H-COM 19 ball.

Additionally, to ensure maximum contact area, the bearing shoulder feature was made to the full diameter of the machined flat on the H-COM 19 ball. Not only does this give effective contact between the components, but it acts as a built-in squaring mechanism to ensure proper seating and concentricity.

To accommodate the spacer and BLM-05 locknut, a length of M25 X 1.5 thread with the appropriate thread relief and tolerance per manufacturer's recommendation were added as well. See Figure 4-3 for details.

Effects of stresses on design

Since the only loads of consequence on the struts are the axial design loads [**16**] [**29**] of 12 kN in either tension or compression, external loading analysis is quite simple. Additional loading on this component comes from pressure due to the interference fit with the H-COM 19 bearing (see Appendix 1, Section 2, Part 2) and tensile loads arising

from preloading the BLM-05 (see Appendix 1, Section 2, Part 1). FEA on the strut ends revealed that so long as material strength was sufficient to withstand these stresses, other factors such as machinability rating, cost, and other design parameters should determine material choice. For this reason, and to allow for the use of the specified Nitreg nitrocarburization process, low alloy steels—namely 4140 and 4340—were used for the 10223-DT-454 and 10223-DT-458 respectively. The reason for the use of higher strength 4340 in 10223-DT-458 is discussed along with the adjustment mechanism.

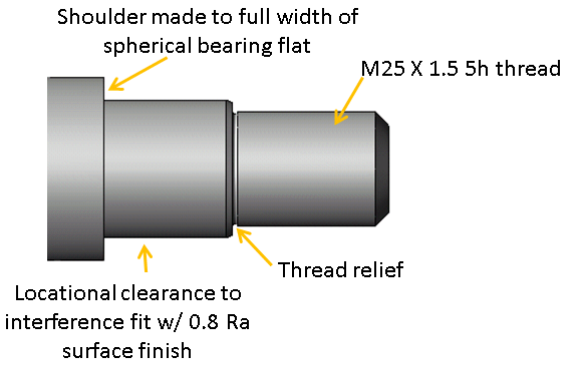

Figure 4-3: Design parameters of the nut-side of 10223-DT-458 and 10223-DT-454 are shown [**24**].

Manufacturing processes

There are no features on these components that require anything beyond conventional machining processes, namely turning and threading operations on a lathe. The machinist is free to add any provisions for live/dead centers they deem necessary to hold the tolerances necessary to accomplish FRs and ODs.

The Nitreg-C + ONC case hardening process satisfies assembly-level FR #5 regarding non-reflective components. It also acts as a corrosion resistant layer to add protection that would otherwise be missing from a low-alloy steel. Finally it acts as an anti-galling measure to prevent any possible adverse reactions within the threads on each of these components. Despite the increased brittleness, the case-hardening of these components in this particular case is of no consequence—neither desirable nor detrimental to the performance of these components.

Risks and risk mitigation

The only real risk in these components is the possibility of them becoming separated from the H-COM 19 ball. The countermeasure, as discussed above, is the addition of the BLM-05 nut to act as a retainer. With proper preload (see Appendix 1, Section 2, Part 1), this is no longer a possibility.

However, the addition of the BLM-05 creates a problem that may violate sub-assembly FR I regarding unconstrained pivoting action. At the extremes of the H-COM 19 Ball +/- 8.5° tilt capability, the BLM-05 is at risk of running into the bores in the Rho blocks. The introduction of the spacer, 10223-DT-466 (see Figure 4-1), and a minor change in the geometry of the bores in the Rho blocks acts as a countermeasure.

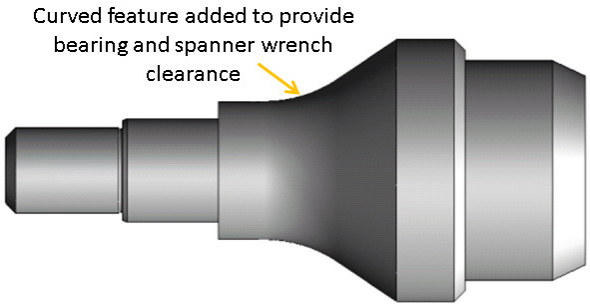

Figure 4-4: 10223-DT-454 is shown with the modified profile added for clearance [**24**].

A risk exclusive to 10223-DT-454 is the possibility of running into 10223-DT-422 at the extremes of the bearing +/- 8.5° tilt capability. Additionally, the spanner wrench needed to install and preload 10223-DT-422 requires adequate clearance. To mitigate this risk, a curved feature was added to the outer profile (see Figure 4-4) slightly complicating the manufacture of this component. The only other effect of this geometry was a negligible decrease in component axial stiffness.

10223-DT-422

This component is responsible for preloading the strut end so that the bearing does not pull out of the block during use. It also imparts a force on the modified bearing race that in turn locks the H-COM 19 ball after the adjustment procedure is performed.

FRs & ODs

The functional requirements and operational desirements of 10223-DT-422 are as follows:

a. Ensure free rotation of the H-COM 19 ball during the adjustment procedure
b. Lock H-COM 19 bearing at end of adjustment procedure
c. Prevent bearing pull-out during both adjustment and telescope use
d. Conform to subassembly requirements I-IV

To perform FR/ODs *a*, *b,* and *c*, the 10223-DT-422 must act in concert with the Rho blocks. Ensuring free rotation has implications on two fronts: geometric interference throughout the H-COM 19 ball range of motion and adequate clearance between the two 10223-DT-427 to allow the ball to move. Recall that this entire assembly must be manually adjustable, so the locking/unlocking procedure cannot require a prohibitively large amount of torque. To prevent pull-out, 10223-DT-422 must be capable of resisting maximum axial loads at all times.

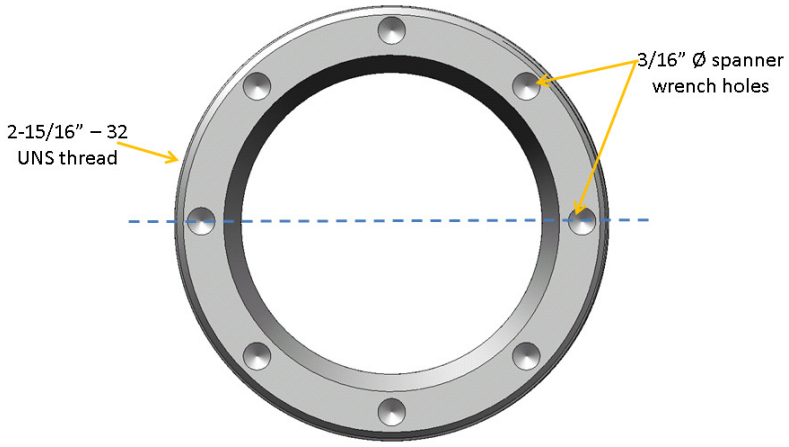

Figure 4-5: A top view of 10223-DT-422 is shown [**24**].

There is a balancing act to the adjustment procedure. There must not be so much play in the bearing strut-end assembly that it begins to disturb the adjustment procedure. At the same time, however, the assembly must be capable of removing all clearance or "locking down" at the end of adjustment and remaining locked for extended lengths of

time. Design parameters for 10223-DT-422 must address this conflict as its role is crucial to the performance of the entire strut-end subassembly.

Design Parameters and their implementation

There are a number of functional requirements that are met by the design parameters of 10223-DT-422. To meet functional requirement *a* the component must be able to accommodate the geometries of 10223-DT-458 and 10223-DT-454 through the entire range of expected motion of the H-COM 19 ball. Since at this point in the design process the exact range of motion of the ball is not known, the best practice is to assume the entire range is necessary and design to meet that requirement. This is accomplished by using CAD to determine the maximum travel and using this data to create a large chamfer in the inner diameter of the 10223-DT-422 (see Figure 4-6).

Part-level functional requirements *b* and *c* are accomplished using a fine thread on the outer diameter of 10223-DT-422. The thread is a 2-15/16"-32 UNS thread. This odd thread size was chosen for a number of reasons. First to ensure adequate thread engagement at all times that the part is in contact with the bearing. As per best practice [**37**] an engagement of at least 4 threads is used. There is 19 mm of thread on the Rho blocks; this makes for approximately 24 threads engaged at full depth. Secondly, this thread requires multiple turns for advancement in lead. The more turns required, the more precise the technician can be during the adjustment process. With the small axial advancement to angle of rotation ratio the technician is allowed more room for error. A full rotation of 10223-DT-422 advances or retracts the thread only about 0.8 mm. The thread can be seen Figure 4-6, which is a section-view along the dashed line of Figure 4-5. Finally, early concepts of this component looked at the possibility of using taps and dies to create the threads required. This thread size was one of the few available from preferred suppliers in the appropriate diameter range. While the use of taps and dies was abandoned, the thread size remained.

The bottom of 10223-DT-422 is machined flat in order to contact 10223-DT-427 as squarely as possible. This feature facilitates proper preload by evenly distributing the axial force generated by the tightening procedure.

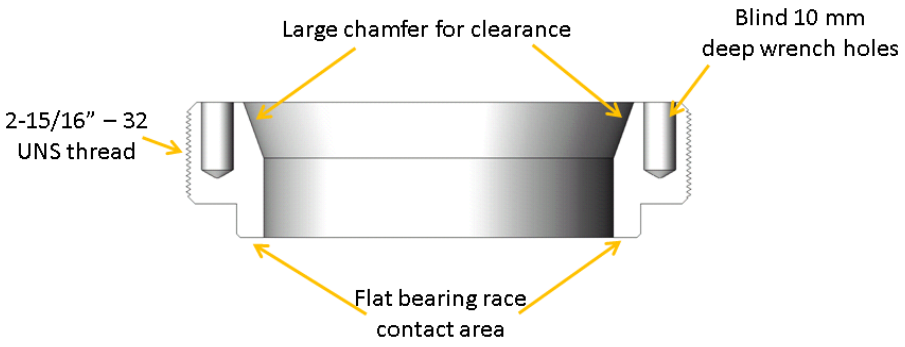

Figure 4-6: A section-view of 10223-DT-422 along the dashed line of Figure 2-5 is shown. Design parameters are identified [**24**].

Early concepts included multiple external fasteners and dedicated locking mechanisms. However, multiple fasteners would add tedium to the tightening process as each fastener would have to be accurately torqued to ensure proper preload. Additionally, loose fasteners at altitude pose a threat to the mirrors below should they fall while the telescope is being adjusted or serviced. By eliminating the fasteners and locking mechanism the part count is reduced, the design is simplified, and the adjustment process is streamlined.

Tightening 10223-DT-422 is accomplished through use of a spanner wrench designed for this component. There are eight 3/16" blind holes 10 mm deep. The spanner contacts 3 holes at any given time so that the pressure from torquing the locknut to the high preload is distributed over multiple features.

Chamfers are added to aid in assembly and reduce the possibility of damaging the threads. Also, to prevent any galling that may occur, 10223-DT-422 is nitrocarburized using the same Nitreg-C + ONC process used and described earlier. These features act in concert to create a component that only requires one hand to tighten/loosen (given adequate leverage with the torque wrench and spanner), advance by small amounts per turn to give clearance but not excess play that could hinder the effectiveness of the adjustment procedure, and ensure proper preload to lock and retain the strut-end and bearing assembly.

Effects of stresses on design

This component will see axial loads determined by the preload necessary to lock down the bearing assembly in a worst-case scenario. This preload is between 19,500 – 23,500 N and is calculated in detail in Appendix 1 Section 2 Part 3. However, these loads were very safe for this geometry. These axial loads are well below the compressive strength of this material, so they are of no real concern.

The stresses of greatest concern are in the thread. It is necessary to investigate the effects of these loads on the design. A spreadsheet using equations for bending, shear, bearing, and axial stresses in the threads and thread roots was created. These stresses were combined into a Von-Mises equivalent stress by the methods shown in [**37**]. They are summarized in Table 4-1 below. A detailed view of the spreadsheet is available in Tables A1-4 in Appendix 1.

Preload [N]	Avg Eq. Stress [MPa]	Percent of Yield Strength	Safety Factor
19500	129.3	13%	7.7
22000	145.6	15%	6.9
23500	155.9	16%	6.4

Table 4-1: Average Von-Mises thread stresses as a function of bearing preload are shown and compared to total 4340 normalized steel yield strength.

To keep permanent deformation from occurring in the threads, AISI 4340 low-alloy steel in the normalized condition was chosen as the material for 10223-DT-422. This material has a yield strength of approximately 1 GPa [**38**]. AISI 4340 also takes nitrocarburizing treatment well [**35**] [**36**].

Other areas of concern are the holes for the spanner wrench pins. However, these stresses were also shown to be well below the 4340 normalized yield strength.

Manufacturing processes

This component can be easily manufactured using conventional machining processes, namely turning and threading operations on a lathe and drilling on a mill. The machinist is free to add any provisions for live/dead centers they deem necessary to hold the tolerances given in technical prints.

While the component was originally designed for use with a die, the low production run did not justify the high cost of tap, die, and go/no-go gauge sets at 2-15/16"-32 UNS as the cost was not well amortized over the number of units produced. Therefore all threads on 10223-DT-422 are single-point turned. There is no need for extremely high precision machining on these components as they are only used for applying a preload and not for alignment.

Risks and risk mitigation

A risk involved with this component is the possibility of cross-threading which was addressed using sufficient chamfers in order to aid in the alignment of the internal and external threads.

The risk of thread galling or seizing is addressed with the case hardening.

The risk of damage to 10223-DT-422 by use/misuse of the spanner wrench is mitigated by using a high-strength steel and ensuring that all three holes are used to torque the component at any given time instead of only two.

The fine thread addresses the risks associated with loosening the ring too much (creating bearing slack/misalignment during the adjustment process) or over-tightening the ring by providing the built-in buffer of a low axial advancement-to-turn ratio.

10223-DT-015

The 10223-DT-015 is the lower Rho block that houses the lower strut-end assembly and sets the position of the origins of the bearings at a fixed distance from the strongback to create the 6-6^p GSP "base" plane. This exact distance occurs automatically given the geometry and features used to satisfy other functional requirements. In this way, the role of the Rho struts is multi-tiered.

FRs & ODs

The functional requirements and operational desirements for 10223-DT-015 are as follows:

a. House the strut-end assembly
b. Ensure free rotation of the H-COM 19 ball through its range of motion
c. Aid in locking and unlocking the modified H-COM 19 bearing
d. Interface with the strongback to form fixed ends of the 6-6 GSP
e. Set nominal bearing angle/strut length
f. Function as an anchor point for attachment of work platforms

Given the appropriate geometry (i.e. bores) to house components of the strut-end, many of these functional requirements are achieved by default. However, there are important subtleties in the geometries that make this component worth dissecting.

Functional requirement *f* was added much later in the design process once the part was nearing final approval prior to manufacture. Had MDO made this requirement of the block known earlier in the process, design parameters that better met the requirement could have been implemented.

Design Parameters and their implementation

Because of the multi-tiered nature of the functional requirements, the design parameters can be broken up into groups: the strut-end housing, the compound angle surfaces (or overall part shape), and the fastener locations. The first one dissected is the strut-end housing. Recall the design features of 10223-DT-015 seen in Figure 2-3 in Chapter 2. Figures and discussion in this chapter will focus on aspects of the design and will therefore have close-up views. Refer to Figure 2-3 for orientation.

The strut-end geometry has only one main design parameter with regards to setting the nominal bearing position/strut length. That is: bores must be perpendicular to the compound angled surface. The position of the bores on the compound surface will be discussed later in the chapter. A section-view taken through the center of the holes perpendicular to the compound surface is shown in Figure 4-7.

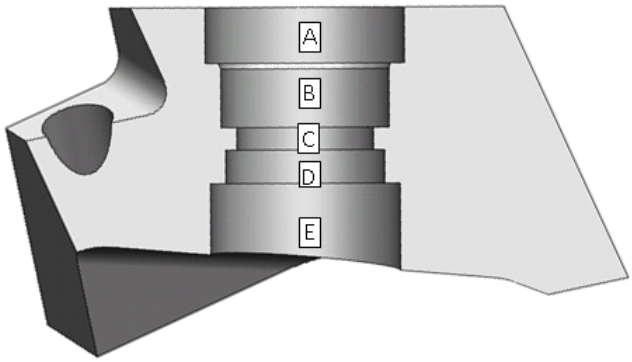

Figure 4-7: A section-view through the center axis of the bores in 10223-DT-015 [**30**].

The bores are labeled as follows:

A: 2-15/16”-32 internal threaded bore for 10223-DT-422

B: Bore for housing modified H-COM 19 bearing assembly

C: Load bearing shoulder bore

D: BLM-05 clearance bore

E: Through bore

Bore A is the 2-15/16”-32 UNS internal threaded bore that accommodates 10223-DT-422 to lock and unlock the bearing during adjustment. It measures 19 mm deep and is threaded as deep as possible using single-point mill technology. However, threading to the bottom shoulder is not necessary since there is a protruding surface at the bottom of 10223-DT-422 that extends downward to contact the upper 10223-DT-427. This part of the block must be capable of withstanding the stresses shown in Table 4-1.

Bore B houses the modified H-COM 19 bearing assembly. As touched on earlier, the H-COM 19 bearing is an off-the-shelf component that is modified for use in the PFIP support structure. It will be discussed later in detail in the “Existing Technologies and Solutions” section of this chapter. To function properly, the bearing bore surface must be extremely smooth as well as provide a small amount of clearance for the outer diameter of 10223-DT-427. Therefore the bearing is cut to -0.000”, +0.001” clearance with a surface finish of 0.8 Ra. Once assembled this allows the bearing halves to move axially as 10223-DT-422 is tightened or loosened to either give clearance to or clamp down on

the H-COM 19 ball. The surface finish along with a small amount of lithium grease ensures smooth motion without binding. A considerable chamfer is added to the strut-side of bore B. This aids in bearing assembly installation [**37**].

Bore C provides the shoulder that essentially supports the entire PFIP. The shoulder created by bore C and the bottom of bore B bears the axial load transmitted to bearing assembly through the strut structure. It is of great importance to the strength of the structure and sets stiffnesses and deformations under load. Because much of the motion in the telescope is very slow, it approaches a quasi-static state. Analysis in Appendix 1 referenced later in this chapter will operate under this assumption and examine loads on the block in the region of the bores. This shoulder must be capable of not only bearing the strut design load but the entire preload applied by 10223-DT-422 on the modified bearing assembly. The strut spacer 10223-DT-466 was added to make this shoulder as thick as necessary to support the strut; it measures 8 mm thick.

Bore D is primarily a clearance feature. It allows the strut end to pivot around the center of the H-COM 19 ball without having the BLM-05 run into the bore sidewall. It measures 57 mm in diameter. This is 8 mm larger than the BLM-05 outer diameter. This was done to accommodate the specialized socket tool that is used to preload the BLM-05 to 70-95 lb-ft. Additionally, by making the diameter of bore D different from that of bore B a non-ideal shear geometry, one which would put the walls of bores B and D in line with each other and the axial load thus creating two sharp corners at the same diametral distance from the load axis, is avoided.

Bore E is quite simply a bore that is made wide enough to allow access to the nut-side of the strut-end during the assembly process. It is made as wide as reasonably possible to help lighten the weight of the component.

Ideally, bores A, B, and C would be manufactured as concentric as possible with some tolerance for the remaining bores.

A look at Figure 2-3 will show two compound angled surfaces into which the bearing housing features are bored. The compound angle surfaces along with the location of the bearing bores set the nominal position of the bearing at nominal elongation. Recall

that each strut has +/- 19 mm of travel and that each bearing has a range of motion of 8.5°. These surfaces were designed to set the angle of the bearing to 0.0° at the center of strut travel to be able to get the most travel out of the bearing should it be necessary during the adjustment process. The way this was accomplished was through heavy use of CAD modeling. This zeroing action automatically happens by ensuring that the angled surfaces are parallel when the Rho stage is at nominal height then projecting a circle such that it lands towards the center of the plane formed by the surface.

Figure 4-8 below shows a simplified PFIP support structure in the earlier stages of design. It has the two complementary compound-angled surfaces highlighted with a measurement dialog box showing that the surfaces are parallel and distance measurements between them.

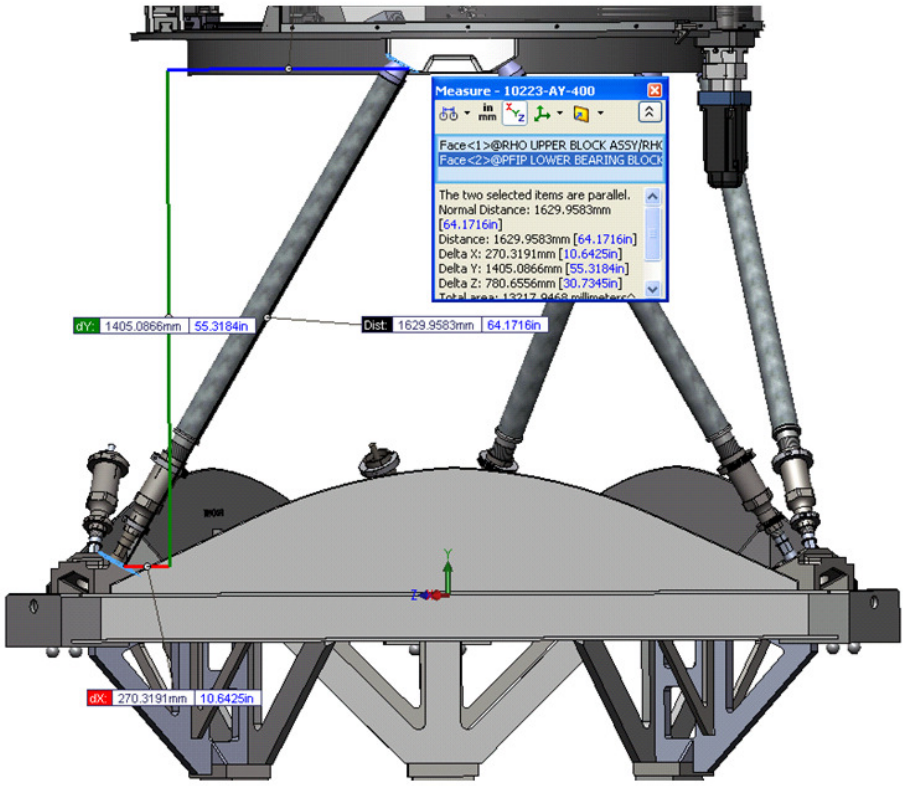

Figure 4-8: A profile view of an earlier PFIP support structure design [**24**]. Compound angles on complementary Rho blocks are parallel at nominal strut length.

Figure 2-2 shows the 2,307.5 mm circle made by the origins of the H-COM 19 balls. As demonstrated by the description of the design process, these dimensions essentially happen automatically by satisfying the functional requirements.

It is important to note that a design change in the strongback shifted the lower Rho blocks upwards a small amount. This disturbs the planned nominal strut length and offsets the bearing at around 0.1° at nominal. Later motion analysis showed that this was inconsequential as total bearing displacement at maximum elongation was under 1°, and it never even approaches the 8.5° limit. The conservative design worked in its favor; this will be discussed more in Chapter 7.

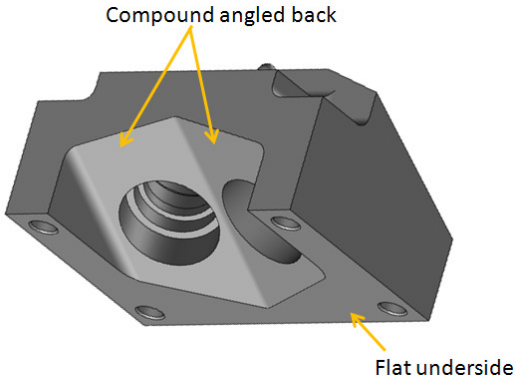

Figure 4-9: A view of the underside of 10223-DT-015 is shown [**30**].

In addition to the compound-angled surfaces on the strut-side of the block there are compound-angled surfaces on the nut-side or far-side. While they are not dimensioned as tight or as intricately as the strut-side flats are, they are still important in being able to access the BLM-05 for preloading during the assembly process. The underside features also control how far apart the bores are on the underside. A higher cut makes the bores seem further apart since they are angled. A shallower cut will make the bores appear closer from the backside. If the cut is shallow enough it will have occur where the bores would intersect. Its depth was carefully chosen to allow access to all the nut-side strut end features plus keep material between the bores to resist any forces that act between strut-ends (see Figures 2-2 and 4-9).

The part "thickness"—meaning the amount of material between the upper and lower compound-angled surfaces on 10223-DT-015—plays a small role in determining deformation of the block under the axial strut load. However, this deformation is mostly determined by material selection and the 8 mm shoulder formed by bores B and C above. This thickness is also a dimension that automatically arises from having the blocks placed correctly with all of the bearing geometry in place. Bore E is a feature whose depth could be adjusted without affecting part performance. This sacrificial buffer feature proved useful in determining depth of underside cut that rendered the proper dimensions to achieve the functional requirements.

Effects of stresses on design

There are two distinct areas of interests regarding stresses in 10223-DT-015 when examining the strut-end. These are the threaded feature that interfaces with 10223-DT-422 and the shoulder that supports the H-COM 19 bearing assembly and consequently supports the entire PFIP structure.

The 2-15/16" – 32 thread stresses, which are summarized in Table A1-4 in Appendix 1, are shown to be below the yield stresses of most common structural low-alloy steels [**38**]. Therefore, 4000s series low-alloy steel is a good material choice.

In addressing the load bearing shoulder, however, a different approach was taken that employed SolidWorks' FEA analysis to find the highest stresses. This approach is outlined in detail in Appendix 2. A maximum stress under load of 83 MPa was found using this method. Since deformation analysis was also done using an elasticity modulus characteristic of low alloy steel all loads and deformations calculated by using this FEA method are accurate for most common forms of alloy steel, namely the readily available 4000 series.

Since stresses and deformations of 10223-DT-015 similar for all low alloy steels and are well below the yield points of any 4000 series low alloy steel, the only real property driving the choice of one over the other is price. For this reason 4130 steel was chosen for 10223-DT-015 (and 10223-DT-083) Rho blocks.

Manufacturing processes

All features on 10223-DT-015 can be created using conventional machining, namely a multi-axis vertical or horizontal milling machine [**35**]. While none of the features require unconventional machining methods, the complicated compound angled surfaces and the subsequent bores and threaded features normal to these surfaces require either complicated fixtures, double sine-plates, or fully automated 3 or more axis CNC machining. The technical drawing for this block and others like it on the HETDEX program include provisions for a precision tooling ball that can be used to aid in machining, programming, and quality inspection of the compound angled components. The bores on the back-side, meaning the bores on the nut-side (as established in Figure A1-2) of the load bearing shoulder, may have to be machined in a separate process from those on the strut-side. The exact method of manufacture for this block is left to the discretion of the vendor.

Since the 10223-DT-427 modified bearing races are kept loose circumferentially in order to allow the axial clamping action that occurs by tightening 10223-DT-422 to the proper preload, Bore B as established by Figure 4-7 must be machined smooth and slightly oversize. This bore is therefore specified at 0.8 micron Ra surface roughness (equivalent to 32 RMS in the English system) and is oversized by up to 0.001". This feature will also be lubricated with a light coat of lithium grease to prevent corrosion and lubricate the sliding surfaces during the adjustment and locking processes.

To satisfy FR #3 regarding reflection, the entirety of the block will also be subjected to the Nitreg-C + ONC proprietary process to give the component a dull black finish. The case hardening effect of this treatment is merely a side-effect in this particular case and neither aids nor hinders performance.

Risks and risk mitigation

There are a number of risks involved with this particular component. The primary risk is that components mounted in the bores could come into contact with the sidewalls of the bores. To prevent this, the bores were carefully designed using CAD software to model the full range of motion of the bearings. Equally careful tolerances were applied

to the engineering drawings supplied to the vendors responsible for these blocks. With the current specified geometries, only a severely out-of-specification manufacture of these block or other subcomponents in this assembly could cause this condition.

The tooling ball was added to give an additional layer of accuracy to the final product. Because of the complex nature of the angled feature on this block, additional risk of error on the manufacturing side—instead of the design side—is incurred. Appropriate 'design for manufacture' techniques were then employed in the design phase of these blocks to help avoid these errors. An additional layer of protection is added when the bearing range of motion of +/- 8.5° is considered. The predicted maximum travel of the bearing from nominal height is around +/- 1.8° in the absolute worst case. So errors in the angle, and subsequently the bores, are more tolerable when viewed as an assembly rather than at the component level.

In a similar vein, the four M16 X 2.0 mounting holes pose a potential problem when considering their placement with respect to load-bearing shoulder bores on the 10223-DT-015 angled surfaces. The processes that are used to create these features are likely to be three separate machining processes occurring in three separate planes with three separate set-up operations if no multi-axis CNC machine is used to manufacture this component. Again the tooling ball and the additional angular headroom in the bearings act to reduce the effects of this risk. While relying on the additional angular capabilities of the bearing will ensure an operational support strut in spite of the aforementioned geometric issues, any dimensional inaccuracies will affect the ability to model the true behavior of the GSP formed by these struts. The true positions of the centers of the twelve H-COM 19 balls will not be known, so a given change in strut length will cause the platform to move in a different manner than what a 6-6^p GSP model would predict. Aside from careful dimensioning and tolerancing, there are no ways to mitigate this risk.

10223-DT-083

On the other end of the strut is the 10223-DT-083 upper Rho block. This block features many of the same design parameters and is subject to many of the same

functional requirements/operational desirements as does 10223-DT-015. Because of this only major design and manufacturing differences will be highlighted in this section.

FRs & ODs

The FR/ODs of 10223-DT-083 mirror those of 10223-DT-015 except for serving as an attachment point for work platforms. There are no such platforms at the upper Rho block location. However, 10223-DT-083 must serve an additional FR/OD on top of those enumerated in the section on 10223-DT-015. The full list is as follows with the additional item labeled 'f.'

a. House the strut-end assembly
b. Ensure free rotation of the H-COM 19 ball through its range of motion
c. Aid in locking and unlocking the modified H-COM bearing
d. Interface with the strongback to form fixed ends of the 6-6 GSP
e. Set nominal bearing angle/strut length
f. Conform to Rho platform geometry with adequate clearance

It is important to recall overarching FR/OD #6, which is that all removable PFIP components use repeatable mounts to aid in reassembly. Because the plane formed by the underside of these blocks serves as the attachment point for the Rho platform, and not the other way around as with 10223-DT-015 and the strongback, this attachment point is critical for alignment. Talks with MDO have shown that it is unlikely the PFIP support structure would ever come apart more than removing the Rho platform [**39**]. Therefore ensuring repeatability at this junction would aid in reassembly and simplify any adjustments required to reestablish optimal optical alignment.

Design Parameters and their implementation

Discussion of the first 5 component-level FR/ODs is already done in detail for 10223-DT-015. Geometries for the bore are nearly identical, so all FRDPARRC commentary applies to 10223-DT-083 as well.

Design parameters for fitting the Rho platform are simply related to geometric fit. Figure 2-4 in Chapter 2 shows the clearance left by the design choice. The inner radius

of the Rho platform sidewall measures 731.35 mm and the outer radius measures 868.65 mm. The inner and outer radii on the contours of 10223-DT-083 measure 750 mm and 850 mm respectively. As seen in Figure 2-4. This leaves adequate clearance for fitting the part, leaves room for any design changes that may have come along in the Rho platform itself, and gives the machinist a round number with which to work.

To satisfy overarching FR/OD #6, the flat backside/Rho platform mounting point is equipped with four M16 X 2.0 blind tapped holes as well as a set of ball and slot alignment features. These mounts work by adequately constraining each block with respect to transverse and rotational motion along the plane created by the flat back-side of the block. Combined with the socket-head cap screws, the block is fully constrained when installed. Therefore once the struts are locked using 10223-DT-422, the fasteners that hold the Rho platform to the three 10223-DT-083s can be removed and the Rho platform can be uninstalled and reinstalled without disturbing alignment between the platform and the strongback.

Effects of stresses on design

Analysis efforts on 10223-DT-083 that serve to determine the effects of predicted loads on the performance of the part are detailed in Appendix 3 of this thesis. The methods and results are very similar to the methods outlined for 10223-DT-015 as these parts are loaded nearly identically. At maximum worst-case load the block FEA model showed 50 MPa maximum Von Mises stress in the bore,and a maximum of 11 microns of equivalent displacement.

These results lead to the same conclusion arrived at in the analysis of 10223-DT-015; that is all low-alloy steels would perform satisfactorily when used in these components. The factors once again are cost and availability. Therefore 4130 low alloy steel in the normalized condition was recommended to the vendor.

Manufacturing processes

Like the 10223-DT-015, the 10223-DT-083 can also be manufactured using conventional multi-axis milling machines. The same caveat about a complex fixture or a multi-axis CNC capability to achieve the compound angles applies. However, there are a

few features on 10223-DT-083 that were added solely to help the manufacturer produce the part.

The most notable is the presence to two flats on the inner diameter that provide the machinist with a 90° angle from which to indicate their tooling that would otherwise have not existed. These flats serve no function other than to aid in production and quality assurance. Secondly, like the 10223-DT-015, a tooling ball at the horizontal center of the block is precisely located to give both the machinist and the quality assurance technician an object that can be referenced at most any relevant canted angle.

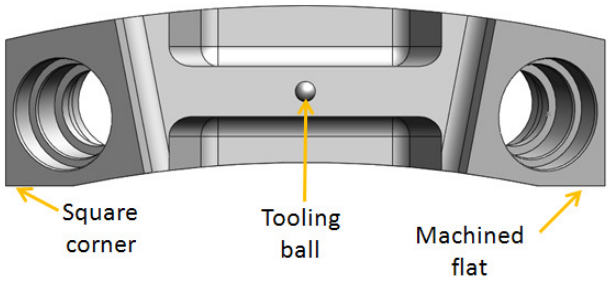

Figure 4-10: Features added to aid in manufacturing of 10223-DT-083 are shown [**32**].

All surface roughness specifications, case hardening treatments, and material choice are the same as 10223-DT-015.

Risks and risk mitigation

Risks on this component mirror those on 10223-DT-015. See the "Risk and risk mitigation" section under the 10223-DT-015 description for details.

10223-DT-466

Although this component is small and simple, it serves a vital role in the performance of the strut-end. Here is a brief FRDPARRC analysis.

FRs & ODs

a. Provide spacing to prevent collision of components of the strut-end assembly throughout the entire range of motion of the H-COM 19 ball
b. Effectively transmit axial load from the BLM-05 nut to strut-end
c. Resist corrosion in situ.

The 10223-DT-466, called a spacer, must essentially act as both a spacer and a washer. Reference Figure 4-1 component E for a solid model depiction of where this component lies. There is a direct relationship between the depth (and therefore maximum load capability) of the load bearing shoulder bore in 10223-DT-015 and 10223-DT-083 and the thickness of 10223-DT-466. It serves to lower the position of the BLM-05 locknut that sets the preload on the strut end in order to avoid collision with the sidewalls of the bore through the 8.5° range of motion of the spherical bearing, and it must also transmit the preload established by BLM-05.

Design Parameters and their implementation

Establishing the thickness of the spacer is a two-step process. The first is to find a depth for the shoulder in the Rho blocks that would adequately support the load with plenty of margin while not requiring significant changes to the general design of the blocks. This number was established using iterations of the FEA techniques established in Appendices 2 and 3. A depth of 8 mm proved sufficient.

The next step is to use a CAD model of the assembly using the proposed dimensions with a bearing free to move the full 8.5°. This allows the engineer to run spacers of multiple thicknesses and check for collision with the sidewalls of the bores in the Rho block. Because the final bore on the backside of the block was intentionally left oversized to accommodate tooling, this dimension was also modified to allow the full range of bearing motion without any interference. This method kept the spacer thickness and bore depth the same, 8 mm.

To effectively transfer the load, the outer diameter of the spacer should be large enough to overlap the outer diameter of the flat surface of the H-COM 19 ball while the inner diameter is kept as small as possible to make sure the inner surface is also contacted while also allowing clearance for the M25 X 1.5 thread. The chamfered lead-in to the bore in the center of the H-COM 19 ball aids in accomplishing this goal. Additionally, the spacer must contact the flat surface of the BLM-05 locknut as well. These parameters have dictated the geometry of the spacer to be 8 mm thick with an inner diameter of 26 mm and an outer diameter of 41 mm.

Also related to load, a material of high hardness and yield strength is recommended by [**37**] for use in washer applications.

Design parameters to aid in corrosion resistance would be to either treat 10223-DT-466 using the Nitreg-C + ONC process used on other components or to make it from corrosion resistant material.

Effects of stresses on design

In this particular case, there is no real analysis beyond checking for failure by compressive stresses induced by torquing BLM-05 to the proper torque to achieve the 19.6 kN axial preload as calculated in Appendix 1, Section 2, Part 1. If failure does not occur, then geometric factors dominate the design. When using a hardened steel or stainless steel these stresses pose no danger of yielding.

Manufacturing processes

This component can be made using very basic lathe operations. The tolerances are not tight. Final material choice was 17-4PH stainless steel since this component is fully enclosed in the Rho blocks and is therefore not required to be black to reduce reflection, and this material meets the high hardness, high yield strength criteria.

EXISTING TECHNOLOGIES AND SOLUTIONS

This section deals with off-the-shelf components or other existing technologies/solutions that were used in the strut-end subassembly. These can be implemented as intended by the manufacturer or modified to meet FRs, ODs, and even DPs established in the previous sections. With regards to the FRDPARRC design theory, this functions as one use of the "References" to help achieve the desired design outcome. For the strut-end assembly both a stock and a modified off-the-shelf solution are used; these are the BLM-05 Bear-lok nut and the H-COM 19 spherical bearing respectively.

Whittet-Higgins Bear-lok BLM-05 locknut

Component Description

The BLM-05 locknut features an internal M25 X 1.5 thread with a 5h tolerance for precision applications, and it's capable of imparting a maximum axial load of 101 kN [**40**]. This is far in excess of the 19.6 kN (as determined in Appendix 1, Section 2, Part 1) required of it in the strut-end assembly.

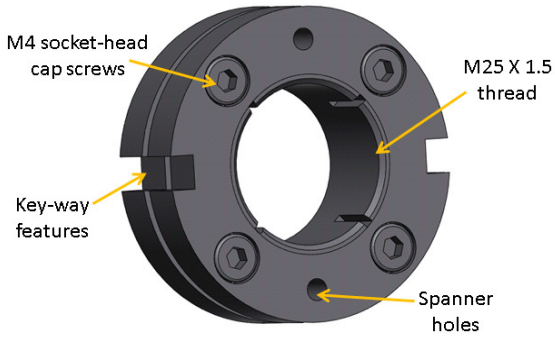

Figure 4-11: The BLM-05 model is shown with unique features identified [**40**].

Instead of relying only on the friction and elastic deformation that occurs in the threads during the course of torquing a nut onto a thread, the BLM-05 incorporates four M4 socket head cap screws that, when properly tightened, apply additional axial loading in the internal threads that increase elastic deformation. This increases the BLM-05's ability to maintain a sufficient preload over longer periods of time than a standard nut—thus creating a more reliable joint.

Additionally, the BLM-05 has holes in the surface that accommodate a spanner wrench or keyways along the side that accommodate a specialty socket. Both of these tools are proprietary Whittet-Higgins installation tools that can be attached to a standard torque wrench for accurate measurement of the applied preload.

In use on the HETDEX strut-end subassembly, the BLM-05 threads onto the M25 X 1.5 thread on either 10223-DT-458 or 10223-DT-454 after the 10223-DT-466 spacer is applied. A section-view of this configuration can be seen in Figure 4-1. No modifications to this existing technology were needed in this case.

Aurora Bearing Company H-COM 19 spherical bearing

Component Description

The H-COM 19 bearing was selected to give the struts the pivoting action required in a 6-6^p GSP arrangement. It features a carbon steel race with a corrosion resistant coating and a hardened alloy steel ball with a hard chrome plating. It is rated for a maximum static radial load of 448 kN and a maximum static axial load of 90 kN when used as received. Its outer race diameter is nominally 2.375 inches and it accepts shafts that are nominally 1.1875 inches in diameter. Its most pertinent feature in this design is its maximum misalignment angle of 8.5° before the flattened shoulder dips below the race [**33**].

Figure 4-12: An image of the H-COM 19 depicting a stock bearing [**33**].

Modifications

Because of the locking requirement of the strut ends, a full spherical bearing would require an external brake or locking device of sorts. The design set forth in this chapter and analyzed in detail in Appendix 1 instead uses an axial load on the H-COM 19 race to clamp down on the H-COM 19 ball. However, the race must be split with some gap for this design to work without repeatedly causing permanent damage to the race or the ball.

A cross-sectional view of the bearing is shown in Figure 4-13. A lubrication channel can be seen at the approximate center height-wise of the H-COM 19 race. This channel provides clearance for cutting the H-COM 19 race in two without risking damage to the ball. Since the amount of axial motion occurring during the tightening and

loosening process is on a order of a few thousands of an inch, the width of the tool used to cut the race is likely large enough to provide adequate space between the split race. However, a set split width was enumerated in engineering drawings to ensure that there is adequate clearance and for the aesthetic appeal of symmetric components. It should be noted that the lubrication channel functionality not lost as the bore will be coated with grease, and the split will act as a reservoir.

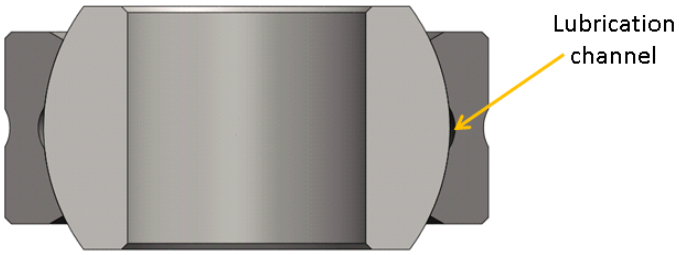

Figure 4-13: A cross-sectional view of the H-COM 19 reveals a lubrication channel at the center of the race [**33**].

Although split race bearing technology does currently exist, it is aimed at splitting the race in such a way that when fully assembled it behaves like a full bearing. In this case, the split acts only to aid in an otherwise difficult installation. However, this technology was not adequate for use in the strut-end subassembly design as the braking or clamping functionality is a prime requirement in order to secure the bearings once the alignment process has taken place.

Figure 4-14: A solid model of the modified H-COM 19 bearing [**33**].

Chapter 5: The Adjustment Mechanism

DESCRIPTION OF SUBASSEMBLY

The adjustment mechanism is shown in Figure 2-7 in Chapter 2. This figure is reprinted here for convenience.

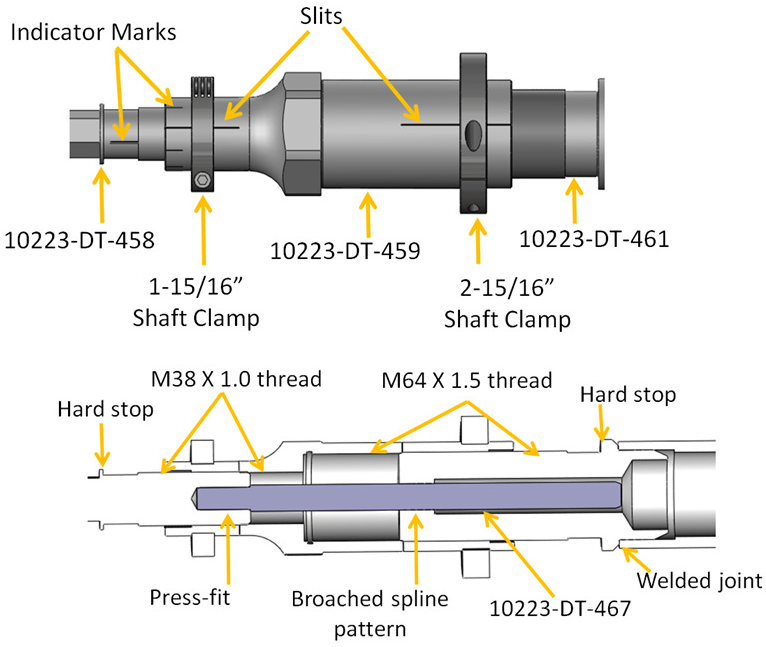

Figure 5-1: The adjustment mechanism is shown.

A brief description of how it works: 10223-DT-458 is held stationary while the technician applies an input torque to 10223-DT-459 to rotate it. Depending on the direction the collar is rotated the strut it either lengthened or shortened by the difference between the two thread pitches. The threaded inserts, 10223-DT-458 and 10223-DT-461, are coupled by the spline of 10223-DT-467. By holding the lower insert stationary, the technician ensures that only the collar is rotating. The 10223-DT-467 and 10223-DT-461 are free to move axially with respect to each other to accommodate any lengthening or shortening of the strut arising from adjusting 10223-DT-459. A detailed description of the functionality of the adjustment mechanism is given in Chapter 2.

FUNCTIONAL REQUIREMENTS AND OPERATIONAL DESIREMENTS

Recall the functional requirements set for by MDO:

1. The adjustment mechanism must be manually adjustable, and
2. feature a differential thread pitch mechanism.

All other over-arching FRs/ODs must be adhered to as well.

FRs & ODs for the subassembly

The functional requirements and operational desirements of the adjustment mechanism are as follows:

I. Allow adjustment of each strut by +/- 19 mm.
II. Lock to prevent accidental adjustment and preserve set-up.
III. Allow for increments of 50 microns.
IV. Transition strut to strut-end geometries

FRs, ODs, and description of components within subassembly

10223DT-459

The 10223-DT-459 is the centerpiece of the adjustment mechanism. It is the point of interaction for the technician and essentially couples the upper-strut subassembly with the strut-end subassembly. It also contains a primitive dial that reads changes in strut length in 50 micron increments. Its FRDPARRC analysis follows.

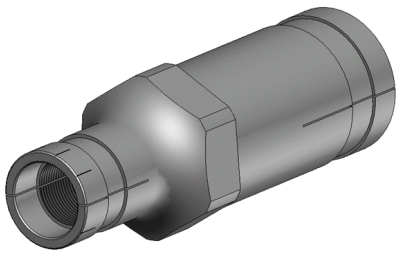

Figure 5-2: An isometric view of 10223-DT-459 is shown [**41**].

FRs & ODs

The FRs and ODs specific to the performance of 10223-DT-459 are as follows:

a. accommodate enough thread to allow a differential thread mechanism to adjust +/- 19 mm
b. clamp to threads to aid in locking
c. support expected strut design loads

Design Parameters

To accommodate the differential pitch mechanism, the thread diameter and pitch must be selected. M64 x 1.5 and M38 X 1.0 were originally selected since they produce the requisite 500 micron per revolution adjustment and were available from vendors in bottoming tap sizes. While this manufacturing technique was eventually abandoned, the sizes remained as they proved sufficient in early analysis.

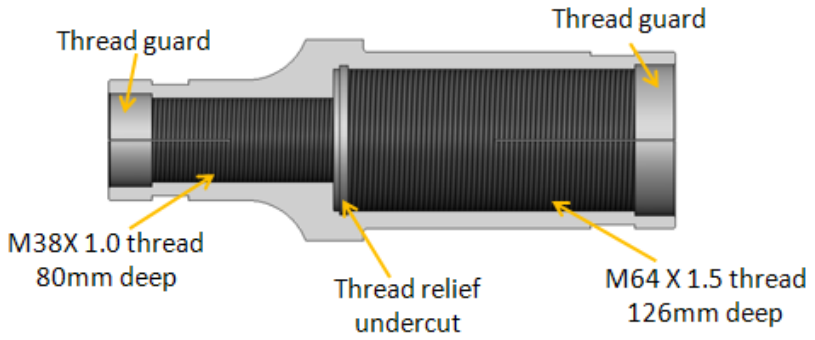

Figure 5-3: A section-view of 10223-DT-459 reveals the threaded interior features that accommodate the differential thread pitch mechanism [**41**].

If the goal was strictly to achieve +/-19 mm adjustment, there would be 80 mm of M38 X 1.0 thread and 120 mm of M64 X 1.5. However, the collar must be able to hold the load at the extremes of travel. To ensure it does there must be some minimum thread engagement. Here is where the geometry of the part is used to create 'virtual thread'. According to [**37**], there must be a minimum of 3 – 4 threads engaged for proper load transfer. During assembly 10223-DT-459 is drawn down until it reaches the hard stop on 10223-DT-458. This leaves the first four threads of 10223-DT-458 protruding past the end of the M38 thread. Only then is 10223-DT-461 threaded in, effectively retreating these threads to make 10223-DT-458 flush with the bottom of the M64 bore when at

minimum engagement. These four threads translate to 6 mm worth of thread at the M64 side. After four revolutions the minimum thread engagement has been fulfilled with minimal added material/weight. The collar can then be advanced to its nominal center position. More details regarding this process are available in Chapter 6. The thread relief serves a dual purpose as a relief to aid the machinist and to act as a buffer layer should a small amount of additional thread be needed for any reason at the bottom of travel.

For accuracy both internal and external threads of both sizes were given a class 4 tolerance with no allowance (or fundamental deviation as it is known in inch thread sizes). This is known as a 4H4h tolerance class [**42**]. For long lengths of engagement this arrangement is not typically recommended as achieving these tolerances can drive the price of the components of up considerably, and they raise the risk of problems within the thread such as fit or galling. However, the accuracy produced by this arrangement is required in this application, so these risks will have to be addressed. One redeeming feature of this arrangement is that as one thread engagement lengthens the other shortens, so the effects of the tight tolerance are somewhat balanced.

The collar also features lips that protrude the terminations of the thread. These act as guards that will work to prevent damage to the male threads closest to the threaded bores. These act in lieu of a full guard to prevent damage and preserve the ability to adjust by at least the amount of threads they cover.

To clamp to the threads, narrow slits have been cut into the threaded region. In conjunction with the off-the-shelf shaft clamps shown in Figure 5-1, these slits will allow the 10223-DT-459 to clamp or release the threads. Because accidental adjustment is highly unlikely during telescope use, these clamps are more of an added layer of protection for the technicians and peace of mind for the scientists using the telescope with regards to the stability of the structure and the longevity of their set-up. The hoop strength that is lost by adding these slits is restored and even surpassed by the addition of these clamps. These slits will also aid in reducing the risk of binding that is introduced with such a tight thread tolerance.

The 10223-DT-459 will be made from low alloy 4000 series steel, with the specific alloy to be determined by the stresses shown in the "Effects of stresses on design" section. It must bear not only the 12 kN axial design load but the stresses that arise during adjustment as a result of the input torque and the stresses within the threads themselves as well.

So that the mechanism can be "manually adjustable" as per FR #1, the input torque required to adjust the collar will need to be low enough that a person can actually turn it at altitude without putting themselves at risk. While this is at odds with the high precision/tight tolerance needed for the sake of accuracy, it is the prime focus of this mechanism and must be realized. The technicians must also have a method to measure incremental changes in length based on revolutions. A dial-type of mechanism is employed here and discussed in further detail in the next section.

A look at 10223-DT-459 shows it is an ideal location to transition the strut geometry from that of the strut, approximately 3 inches in diameter, to that of the strut-end that interfaces with the H-COM 19 ball. The component is a natural point that can be exploited to transition in both a functional and aesthetically pleasing way.

Finally, to adhere to the low-reflectivity requirement (FR #3) 10223-DT-459 will be nitrocarburized using the previously discussed Nitreg-C + ONC process.

Implementation of DPs

Effectively implementing the tight tolerance threads along such a deep bore will require precision machining with very stiff threading fixtures and boring bars. Whether these threads are to be ground or not is left for to the vendor to decide. So long as the precision is preserved, the method of manufacture is of no consequence (within financial reason). However, it must first be shown that this mechanism is adjustable by a person. A spreadsheet was employed for this, and a worst-case input torque of 110 ft-lbs was the result. Details can be seen in Appendix 4, Section 2, Part 1. The actual expected input torque is one third of this value. While 110 ft-lbs is quite high for a person, it is possible to achieve with the proper tools.

Adding the slits to the threaded regions puts the integrity of the threads at risk. However if a wire-EDM is used, there will be no burrs on the part after the machining process [**35**]. This is an ideal use for an EDM as it preserves the thread while achieving the desired feature

To aid in clamping this assembly employs two shaft clamps. The 10223-DT-459 contains two channels in its outer surface that retain these clamps. This allows the technician to loosen the screw that shuts the clamps without having to remove it entirely. This also eliminates the risk of dropping the clamp onto the mirrors below. These channels can be seen in Figure 5-2.

Since input torque is of the utmost importance, proper lubrication of the threads is paramount. The use of Everlube Products' Lubri-Bond A dry lubricant significantly reduced the coefficient of friction present in the threads compared to grease [**43**] (see Appendix 4). This guarantees an input torque lower than the high but manageable 110 ft-lbs predicted using values representative of greased threads. Additionally, the use of nitrocarburized 4140 is hardened material that further discourages thread galling. Lubri-Bond A also acts as a long term anti-seize [**43**].

The 10223-DT-459 acts as a transitional component that takes the rather large but hollow 3 inch strut diameter into a smaller geometry that can interface with the H-COM 19 ball and strut-end. Since the differential pitch mechanism is already a desirement expressed by MDO, this is the natural point in which to transition these geometries. This is accomplished through use of two significantly different pitch diameters and strategic tapering of the 10223-DT-459. Figure 5-3 is a section-view of 10223-DT-459; it shows the amount of material that reinforces the transition point. The threaded inserts never come in contact with each other and are not axially coupled, so the load must transfer through 10223-DT-459 to the mating insert.

To give the technician a reading of incremental length adjustment as a function of revolution, the external surface of the M38 thread guard feature is engraved with 10 precisely placed marks every 36° along its circumference. These correspond to a mark that is on 10223-DT-458, which is held stationary during the adjustment process,

showing adjustments with a 50 micron resolution. Should higher resolution be sought, all that has to be done is to place additional marks at the circumference.

Finally, to support the expected loads, 4140 low allow steel is used as the material from which this component will be made. It will be hardened between 28-32 Rockwell C scale in preparation for the Nitreg-C + ONC treatment that is used as an anti-galling and anti-reflection measure.

Effects of stresses on design

Analysis using axial loads was performed to determine how 10223-DT-459 would perform. The only change in design this brought about was the addition of some material and a tapered radius underneath the wrench flats on the M38 side. This material also aided in expected loads from the input torque required to adjust the collar. Both the axial 12 kN and torsional 150 N-m loads are relatively low for a high strength steel like 4140.

The stress that posed the greatest risk to structural integrity is the stress between the threads. These values are summarized in Appendix 4 in the last column of Tables A4-1 and A4-2. Again, these stresses were low compared to the yield strength of 4140.

Manufacturing processes

In this component, more so than previous components, manufacturing processes have a direct correlation on the performance of the component. This is especially true of the threaded features and the slits that run across them. Because this is a high-precision component the threads have a tight tolerance as well as a high concentricity requirement. Precision machining is required for most lathe operations on this component, namely boring and threading. The threads may be single-point turned if the vendor is confident enough in their machine, set-up, and ability to hold the required tolerances. Grinding the threads is also a viable option. For a while CEM considered lapping these threads to create a zero slack set of threads that would make each strut unique but later ruled it out as unnecessary and too expensive [**39**].

The technical prints of 10223-DT-459 specifically call for the use of a wire EDM machine to add the slot features to the threads. This is because the EDM process leaves no burrs in the remaining material. This leaves the threads intact with additional risk of

binding due to burrs. However, it introduces the need to thoroughly wash the parts to remove any particles that have settled from the EDM fluid into the extra fine threads. Also, since the Nitreg process is being used as an anti-corrosion measure as well, the slits must be put in 10223-DT-459 prior to the nitrocarburization process.

Risks and risk mitigation

There are a number of risks associated with the design parameters of 10223-DT-459. The first of which is the risk of binding or galling of threads with such a fine pitch and tolerance. The binding is mitigated by careful tolerancing and realizing the care that is needed in manufacturing this component. Galling is more of a material interaction phenomenon. This is addressed by the use of hardened low alloy steel with a nitrocarburized case hardening treatment on the threads and the MoS_2 in the Lubri-Bond A lubricant. In fact the only reason why any components on the entire PFIP support strut assembly have this treatment is because it was investigated and approved for use on this component to prevent galling within the adjustment mechanism threads.

There is another risk imposed by the Nitreg-C + ONC process. Typically case-hardened steel becomes brittle since the process essentially trades ductility for yield strength [**35**]. Since the threads are so fine, there is the possibility of through-hardening the thread which would severely embrittle the threads. The risk mitigation countermeasure comes from the process itself. The Nitreg-C + ONC process is a potential controlled process that allows for precise case depth and white layer generation [**36**]. By specifying a maximum case depth that poses no risk of through hardening the M38 X 1.0 thread this risk is completely avoided.

The slits pose their own set of risks. Their existence essentially eliminates any hoop strength the adjustment collar had. A very worst case scenario of this weakened collar was investigated and shown that the M64 threaded side is in danger of flowering and allowing the 10223-DT-461 to jump threads. However the shaft clamps that are used for the tightening feature restore this hoop strength. Additionally, with the way the collars are set-up it is possible to loosen them to allow for adjustment without removing or even allowing excess slack. A light backing off of the tightening screw has been

shown to be all that is needed on a prototype made at CEM. Any other manufacturing method to create the slits besides EDM will leave burrs and deform the immediate area surrounding the slits. This may cause hang-ups in operation. Therefore EDM is explicitly called out in the technical print.

The final risk also comes from the threads but in a way that only arises during the assembly process. A remnant of the threading operation is typically a partial thread at the start and end of the thread; that is a thread whose cross-section is not the full 60° triangular profile defined in [**42**]. This thread is weaker than the full threads in terms of its resistance to axial load. During the assembly process it is also the first thread to make contact. This critical point in the assembly process poses the risk of damaging this fragile first thread which could prevent the two threads from mating or cause physical damage to all of the threads that come in contact with this damaged thread. It should be noted that the partial thread is likely present on both the male and female components. The way to avoid this is using a process called "thread blocking" whereby the first thread is milled off to the root diameter until a full thread profile is reached [**44**]. This process is popular in oil rigs and other applications where a damaged thread could potentially bring production to a stop or cause an unsafe working condition and where reliability is paramount. An added complexity is the brittle nature of case-hardened steel that would render this first thread especially fragile. Thread blocking was therefore selected for use on all threaded components in the adjustment mechanism.

10223DT-458

The 10223-DT-458 threaded insert was discussed from the point of view of the strut-end in the previous chapter. It serves as the piece that interfaces both with the H-COM 19 ball in the strut-end and the 10223-DT-459 adjustable collar. It is the smaller diameter lower piece that contains the M38 X 1.0 external thread. Since the functional requirements of this component with respect to the strut-end were already discussed, this chapter will focus only on its role in the adjustment mechanism.

FRs & ODs

The 10223-DT-458 lower strut threaded insert is to:

a. accommodate enough M38 X 1.0 thread to allow a differential thread mechanism to adjust +/- 19 mm
b. provide safeguards against improper installation or adjusting too far such as to allow the adjustment mechanism components to separate
c. accommodate 10223-DT-467 (spline shaft) and ensure it does not rotate during the adjustment process
d. act as an indicator to give the technician feedback as to the amount of strut-length adjustment as a function of rotation
e. provide a suitable surface to interface with the H-COM 19 ball
f. accommodate the tooling required to properly operate the adjustment mechanism
g. withstand expected worst-case design loads

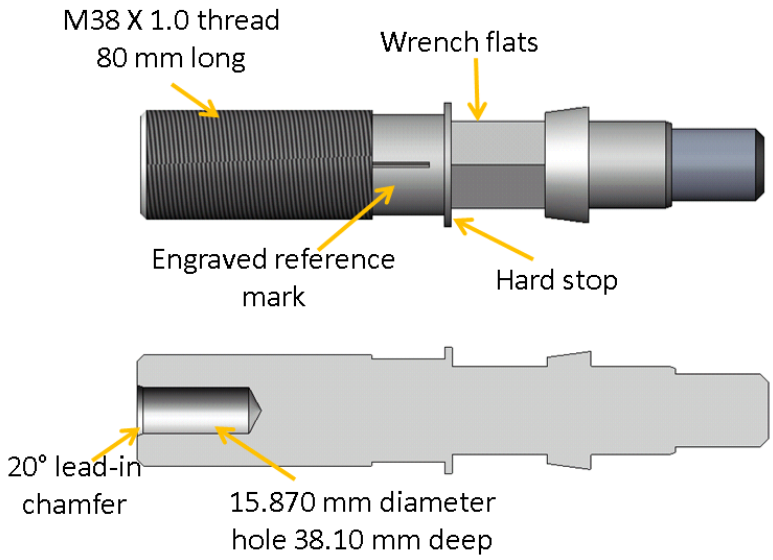

Figure 5-4: Profile and section-views of 10223-DT-458 are shown with design parameters identified [**45**].

Design Parameters

From the design of 10223-DT-459 and the assembly process laid out above only 80 mm of thread is required to give the +/- 19 mm of travel required from the differential pitch ratio. Just like in 10223-DT-459 the threads are given a grade 4 tolerance with no allowance to assure accuracy.

A hard stop acts as a safeguard against adjusting too far. This also aids in assembly. Figure 5-4 shows where this hard stop is located, 25 mm from the last M38 thread. It is meant to serve also as an indicator during the assembly process. The technician is to draw down 10223-DT-459 until it contacts the hard stop feature. This feature is located in such a way that the first four threads protrude from the bottom of the M64 bore in preparation for mating 10223-DT-461 to the collar. The hard stop also serves as a visual indicator to let the technician know if they are near the end of travel.

A function of 10223-DT-458 that has not been detailed yet in this thesis is its role in retaining the spline shaft (10223-DT-467) shown in Figure 5-4. The spline serves as the angular coupling device to make sure the threaded inserts undergo the same angular rotation for precise differential thread pitch functionality. It is installed with a tight press fit that prevents relative angular motion under the input torsional loads required to overcome resistance forces in the threads. Details regarding exact sizing of the fit and analysis used to arrive at this information are discussed in Appendix 4.

There is a small tick mark shown on the upper model in Figure 5-4. It exists on the rounded section on 10223-DT-458 between the threads and the hard stop feature. This engraved mark works in conjunction with the 10 precisely located marks on the circumference of the M38 thread guard feature on 10223-DT-459. Since 10223-DT-458 is held stationary by the technician during the adjustment process, the 10 tick marks on 10223-DT-459 indicate a rotation of 36° or an axial strut elongation or contraction of 50 microns: one-tenth of the thread pitch difference.

A stable shoulder that contacts as much of the flattened shoulder on the H-COM 19 ball as possible is needed. Additionally, a full depth shaft is required for maximum contact area to resist relative motion between the ball bore and 10223-DT-458.

Most likely an adjustable wrench will be used to keep 10223-DT-458 stationary during the adjustment process. Wrench flats below the hard stop features are added so that this can be accomplished.

Analysis and material selection will determine the component's ability to withstand the design loads. Any red flags that come to light through analysis will warrant a change in design.

Implementation of DPs

Implementation of DPs related to the threads are exactly as those listed in 10223-DT-459. These threads require a tight tolerance and precision machining. The same goes for the placement of the hard stop. The only important requirement of the hard stop is that it exceeds the inner diameter of the thread guard lip on 10223-DT-459. It is not meant to be load bearing, but only to serve as a visual and tactile stop.

To implement the bore required for the press fit that secures 10223-DT-467 such that it will remain stationary despite the loads required to adjust the mechanism a few pieces of information are required: the expected input torque, the friction present between the two materials, and the amount of pressure required to resist the torsional load. Once this data is made available (see Appendix 4) then a minimum interference can be specified. This feature will also require precision machining as the acceptable bore diameters fall within a 6 micron window to prevent an over-tight fit condition. Additionally, the bore features a high quality surface finish, 0.8 Ra, and a generous 20° lead-in chamfer to aid in assembly.

The engraved reference point and milled wrench flats work together to give the technician a visual indication of the amount of axial displacement that occurs during the adjustment process. Likewise, the wrench flats and spline work to keep the male threaded inserts stationary as 10223-DT-459 is rotated during adjustment. The location of the engraved mark is not important as it does not rotate like the collar does.

A tapered feature that terminates in a shoulder below the wrench flats provides the support for the H-COM 19 ball under load. Analysis that is not included in the

appendices was used to determine if the taper angle is sufficient to withstand the axial strut loads that are seen in operation.

Effects of stresses on design

Since the thread is much finer as well as the cross-sectional area being smaller than other places in the strut, a higher strength low alloy steel—AISI 4340—was selected for this application. The finer 1.0 mm thread pitch incurs a higher stress in the threads than the larger 1.5 mm (see Tables A4-1-8 in Appendix 4). While AISI 4140 would have been sufficient [**38**], this alloy provides for a more robust component.

Manufacturing processes

The features on 10223-DT-458 can all be manufactured using basic mill and lathe operations. Multiple set-ups will be required however, especially with the mill features—wrench flats and engraved indicator marks. However since the relative angular position of these features is not important the set ups are significantly simplified. Drill points remaining from the initial bore to create the press-fit features are acceptable since the shoulder of the splined shaft will provide any downward axial resistance required during installation, since the spline exhibits no axial loading during use.

Risks and risk mitigation

Of utmost importance is making sure this component is not subject to failure since it has the smallest cross-sectional area of all axial load bearing components of the strut assembly. To make sure this does not happen, analysis using worst case shear/torsion and bending loads were run. Since the geometry/design of the component was not impacted by the results of the analysis (the geometry shown was found to adequately resist these loads based on the model used) the analysis was not included in this thesis.

Other risks are the same as the 10223-DT-459 with regards to problems within the thread, and the countermeasures are identical as well: high strength steel with case hardening and solid film lubricant.

10223DT-461 & Upper strut assembly

This component is essentially the complement of 10223-DT-458. It serves to accept the spline and fits into the M64 side of 10223-DT-459. Because of the manufacturing methods involved making this component it will be described in conjunction with the entire upper strut assembly which incorporates 10223-DT-461, 10223-DT-454, and 10223-DT-449 which comprise assembly model: 10223-AY-450.

FRs & ODs

The 10223-DT-461 upper strut threaded insert is to:

a. accommodate enough M38 X 1.0 thread to allow a differential thread mechanism to adjust +/- 19 mm
b. interface with the spline to angularly couple 10223-DT-461 and 10223-DT-458
c. provide a support for 10223-DT-449 (strut tube)
d. ensure accurate strut adjustment as a function of rotation
e. support all expected design loads in the strut (applies to 10223-DT-454 and 10223-DT-449 as well)

Design Parameters

To ensure full +/- 19 mm strut length adjustment, there are 120 mm of M64 X 1.5 thread on 10223-DT-461. No additional threads are required on this component since the extra 6 mm of internal thread on 10223-DT-459 serve to eliminate their need.

The spline that is used in the adjustment mechanism (which will be discussed further in the "Existing Technologies and Solutions" section) is a Grob Inc. #0687 spline profile. The section-view in Figure 5-5 shows where this pattern is with respect to the rest of the component. There are also oversized clearance bores on the back end of the spline pattern; these aid in the broaching process as well as accommodate excess spline length during the adjustment process.

There is a hard-stop feature in the area just above the thread relief. It serves two purposes: 1) preventing the component from being drawn down far enough to push 10223-DT-458 out of the bottom of 10223-DT-459, and 2) provide a solid shoulder on which 10223-DT-449 mounts. The inner diameter of 10223-DT-449 is precision

machined to a few microns tolerance as is the precision outer diameter highlighted in the figure above. These two diameters form a locational clearance fit that ensures concentricity between the threads, the spline, and the bearing surface on 10223-DT-454 on which the H-COM 19 ball mounts. Therefore these two features, precision OD and hard stop acts to ensure accurate adjustment and provide support for 10223-DT-449.

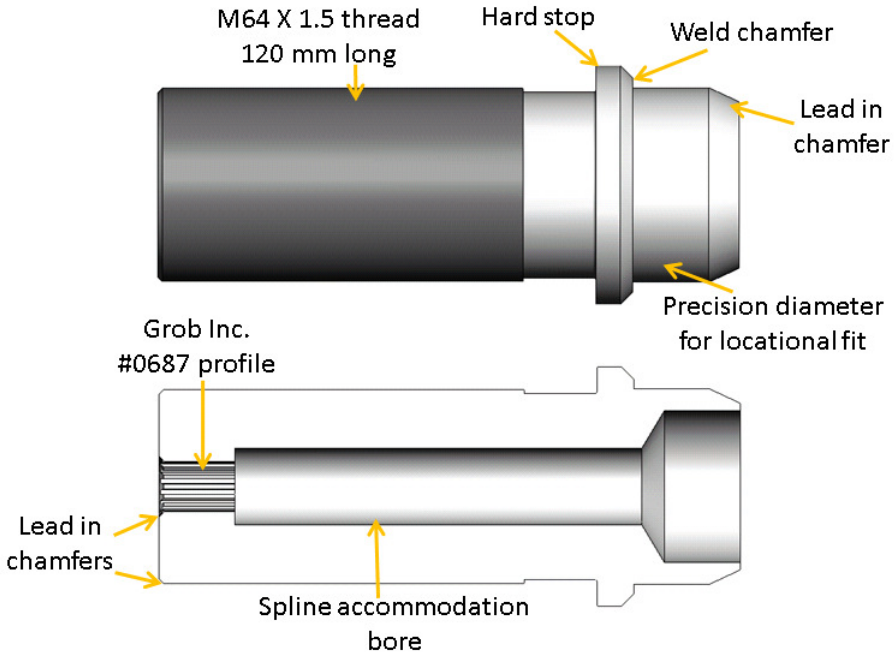

Figure 5-5: Profile and section-views of 10223-DT-461 with design parameters identified.

On the top side of the hard stop/shoulder there is a rather large chamfer. This chamfer accommodates weld material used in the assembly process of 10223-AY-450 to join 10223-DT-461 and 10223-DT-449.

As with other components in the strut assembly, analysis performed and material selection will determine if the design can support the expected loads. If the component cannot, design changes will be made so that it can.

Implementation of DPs

As noted in the introduction of 10223-DT-461, it has a unique manufacturing process in that it is manufactured as part of an assembly: 10223-AY-450. Also, unlike

the other components of the strut assembly, CEM decided not to subject this component to the Nitreg-C + ONC process for case hardening/ blackening. Therefore achieving overall FR # 3 regarding non-reflective components will be achieved through a CEM paint specification [**46**]. Therefore information that has normally been discussed in this section in discussions of other components will be discussed in the "Manufacturing processes" section in subsequent pages.

Effects of stresses on design

Analysis to find the stresses within the threads was performed and is summarized in Appendix 4, Table A4-1. Analysis not featured in the appendix included spline profile analysis, which showed this arrangement to be adequate for transmitting/resisting expected design torsional loads. Shear, bending, and axial load analysis also showed this configuration in an AISI 4140 heat-treated to 28-32 on the Rockwell C hardness scale to be adequate for use in all 3 components of the 10223-AY-450 subassembly.

Manufacturing processes

This section covers the manufacture of each component in the 10223-AY-450 subassembly, 10223-DT-461, 10223-DT-449, and 10223-DT-454. It also contains information on the assembly procedure/ weld procedure in creating this subassembly. Therefore the upper strut assembly weldment can be considered one component at the end of this process. Figure 2-8 shows the 10223-AY-450 subassembly, and it is reprinted here for convenience.

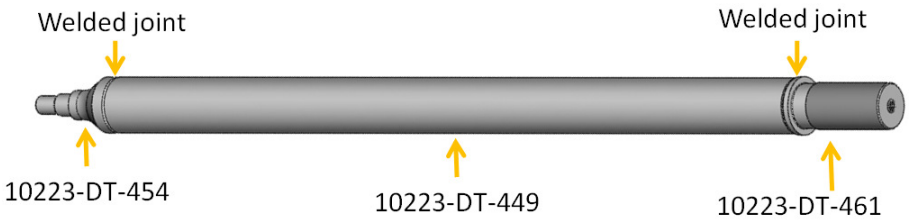

Figure 5-6: The 10223-AY-450 subassembly is shown with its components identified.

First off is 10223-DT-449. It is made from heat treated AISI 4140 tube stock with a 2 3/8" nominal inner diameter and a 3 1/8" nominal outer diameter and 1159.5 mm long. The tube stock is prepared by machining the inner diameters 40 mm deep and

within a concentricity of 0.1mm at 64.25 mm on one end and 64.025 mm on the other end. The former diameter accommodates 10223-DT-454 and the latter accommodates 10223-DT-461. The reason for the tighter fit with 10223-DT-461 is to ensure concentricity between the threads, the splined feature, and the spherical bearing mount on 10223-DT-454. The full length of the inner diameter of the tube is cleaned with a wire brush to remove scale and corrosion that may be present in the as-received material. Finally the ends of the tube are cut parallel to each other within 0.1 mm to each other to ensure each of the inserts remain along the center axis of the tube.

Next a piece of 3 1/8" round heat treated AISI 4140 is used to make a blank that will become 10223-DT-461. A 16.56 mm pilot hole for the broach that will be used to create the spline profile is bored in the center of the round blank. The blank is then turned around and bored at 25 mm diameter until only 25 mm of depth remain of the pilot hole. Then a large 50 mm diameter hole is bored 25 mm into the back end of the part to decrease its weight and aid in the thermal phenomena that occur during the weld process. Finally the back 35 mm of the diameter are turned at 64 mm with a 12 micron tolerance and a 10 mm 25° lead-in chamfer (see Figure 5-5). The shoulder formed by this process is chamfered at 5 mm and 45° to accommodate the weld metal used later in fabrication. These blanks are then sent to Grob Incorporated for broaching with the #0687 profile. Note no threads are cut until after the weld process. The vendor is given the freedom to rough turn the remainder of the part so long as adequate stock is left for final machining.

A similar process is applied to the stock used to create 10223-DT-454. The only differences are the tolerance on 64 mm OD are loosened to 0.1 mm and there is no boring of the stock except for the 50 mm hole that extends 25 mm from the back face. At this point no features besides those that interface with the tube have been added. Beyond the weld chamfer 10223-DT-454 still just round stock.

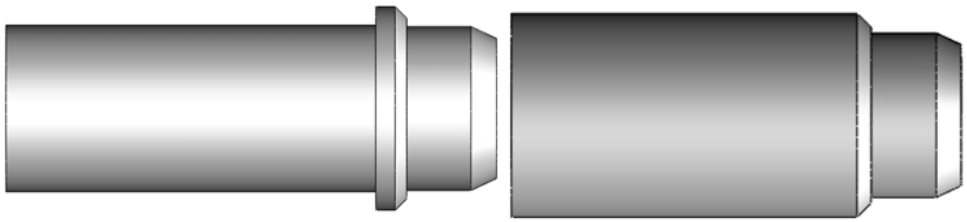

Figure 5-7: Rough machined blanks of 10223-DT-461 (left) and 10223-DT-454 (right) are shown.

Once the insert blanks are complete they are mated to the tube in preparation for welding. Recall that the fit between 10223-DT-461 and 10223-DT-449 is a precision fit that may require a rubber mallet or other soft headed hammer to fit. AISI 4140 steel is classified as a heat-treatable low-alloy (HTLA) steel that lies in Zone III of the Graville diagram, that is it is susceptible to hydrogen-assisted cold cracking after welding because of it high carbon content and high hardenability [**47**]. Measures to reduce thermal shock and hydrogen content must be taken to avoid an overly brittle joint. The exact procedure recommended for the welding process is as follows:

- Preheat assembly to 290C – 340C
- Maintain interpass temperature of 290C minimum
- Perform full-penetration welds using gas metal, shielded metal, or flux-cored arc welding processes according to best practices using a low hydrogen wire (ex. E7018)
- Perform thermal stress relieving immediately after welding while keeping the assembly vertical
- Slow cool at 65C per hour maximum using a furnace, sand, or insulated fire blankets until assembly reaches 90C then air cool
- Perform weld inspection using fluorescent penetrate or magnetic particle techniques

This procedure reduces the effects of thermal shock by preheating the entire assembly and maintaining and interpass temperatures. The use of E7018 or similar wire keeps introduction of hydrogen low while keeping the relative high-strength properties of

the AISI 4140 intact. Performing thermal stress relieving immediately after welding encourages hydrogen diffusion out of the heat affected zone while keeping thermal shock effects to a minimum. The slow cooling also helps in this regard.

Once cool, the component is to go into a lathe for detail machining. The bearing mount features are cut on the 10223-DT-454 side of the strut, and then M64 X 1.5 threads are cut on the 10223-DT-461 side of the strut. This sequence allows the machinist to keep the required 0.1 mm concentricity between the bearing mounting surface and the M64 X 1.5 threads/broached spline feature. This process also hides the weld seam.

Finally the full 10223-AY-450 assembly is to be painted except on the threaded portions and the H-COM 19 ball mounting surface. This is performed by preparation with an acetone wash, applying a 4-6 mil layer of PPG Spectracron 531/532 High Build 2K Epoxy Primer, and applying a 2-3 mil layer of PPG Pitthane High Build Semi-Gloss paint with a flattening agent added [**46**].

At of time of this writing, one full 10223-AY-450 assembly has been produced using this manufacturing technique. The vendor was able to successfully hold and even exceed the required concentricity and length call outs in the technical print.

Risks and risk mitigation

A number of the risks and countermeasures involved with the creation of this assembly have already been discussed. The entire manufacturing process was driven by risk reduction: be they material influenced (cold cracking) or dimensional (concentricity tolerances). One risk not addressed before but implied with the process is the dimensional distortion in the broached spline feature during the welding process and its associated heating processes. This was one of the reasons a heat treated material was used in the first place. By using quenched and tempered AISI 4140 the vendor is afforded more dimensional stability than an 4140 in the normalized or annealed condition with regard to effects of relatively low (compared to the quench/temper temperatures) thermal processes such as preheating and thermal stress relieving. The other reason was to have a Nitreg-C ready material without having to subject the finished weld assembly to

a high temperature hardening process as steels used are pre-hardened to 28 - 32 on the Rockwell C scale (optimal hardness to accept the nitrocaruburizing treatment).

In the earlier design phases the female spline that is currently broached on 10223-DT-461 was a separate piece that pressed into the threaded insert. However, uncertainties with how the deformation processes that occur within the splined insert and 10223-DT-461 raised questions about the ability to keep smooth axial motion along the spline and the ability to keep the tight 4H tolerance in the M64 thread. Additionally, imperfections in the concentricity would be compounded by errors in the press fit hole and errors on the insert itself. By directly broaching the component prior to assembly all of these risks are avoided with the added benefit of a reduced part count.

EXISTING TECHNOLOGIES AND SOLUTIONS

The adjustment mechanism features three off-the-shelf components: the 2-15/16" and 1-15/16" shaft clamps used to lock 10223-DT-459 after adjustment, and the Grob Inc #0687 spline profile shaft.

McMaster-Carr hinged one-piece shaft clamps

Component Description

The shaft clamps used to clamp the split ends of 10223-DT-459 are of a straightforward design. They feature an interweaved hinge on one end and a tapped hole/counter bored feature for a socket-head cap screw on the other. Besides geometric differences the two sizes used are of the same design.

Figure 5-8: Pictures of a hinged one-piece shaft clamp in the closed and open configurations are shown [**48**].

The clamp on the M38 side of 10223-DT-459 has an inner diameter of 1-15/16”, an outer diameter of 3-1/4”, and a width of 5/8”. It is clamped by tightening a 5/16”-24 socket head cap screw. The clamp on the M64 side has an inner diameter of 2-15/16”, an outer diameter of 4-1/2”, and a width of 3/4". It is clamped by tightening a 3/8”-24 socket head cap screw. The difference in fastener size is an unfortunate, but unavoidable, occurrence when ‘design for assembly’ is considered. This means the technician will require two separate hexagonal wrenches to adjust the fasteners on the same assembly. Both clamps feature a black-oxide finish that requires no additional preparation for use on the telescope and compliance with FR #3 regarding low reflectivity.

Grob Inc. #0687-16-2 stainless steel spline shaft

Component Description

Grob Inc provided the spline shaft shown in Figure 5-1 in a single 6 foot length made of 316L stainless steel. The decision to use a stainless steel was made because it bypasses the need for a corrosion resistant treatment or an oil film on the component. An oil film could potentially run and interact negatively with the dry film lubrication on the internal threads of 10223-DT-459 or any of the threaded inserts with which it interfaces.

Modifications

Minor modifications were performed to get the shaft ready for uses in this subassembly. A 38 mm length at the end of the shaft was precision machined to 15.875 mm for a minimum 5 micron interference with the bore on 10223-DT-458. The opposite end was given a generous chamfer to aid in alignment of the shaft with the broached feature on 10223-DT-461 during the main assembly process. Finally, the shaft was acetone washed and sprayed with Lubri-Bond A dry film lubricant for a reduction of friction in operation.

Chapter 6: Assembly Procedure

There were a number of "design for assembly" aspects involved in the component design process. These ranged from making sure adequate space was left for tooling to specifying counterbore depths that allow for a single fastener type to be used on an assembly. To illustrate these concepts in practice a brief outline of the assembly process of the PFIP support structure will be discussed.

There are two main categories that the assembly falls into: 1) assembly on the ground and 2) assembly at elevation. What this means is that prior to the final assembly at elevation in the observatory some subassemblies can be made on the ground to reduce the number of steps that must be performed at elevation and to reduce the risk of accidentally dropping tools, fasteners, etc. onto the expensive mirror array below.

ASSEMBLY ON THE GROUND

PFIP Lower Bi-Pod Assembly

This assembly consists of the strut end and a number of components of the adjustment mechanism assembly. This assembly attaches directly to the strongback using four fasteners, and it is responsible for setting the position of the base plane of the 6-6^{p} GSP that the support structure forms.

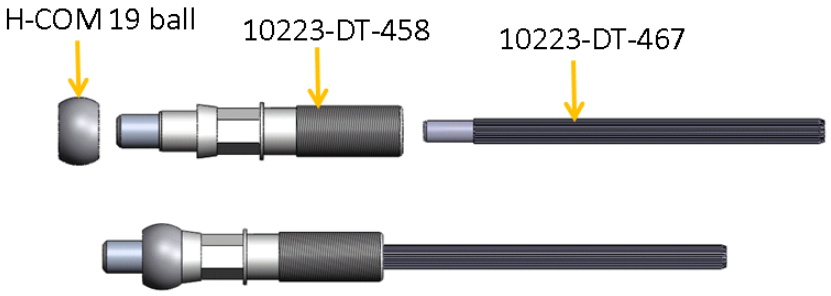

Figure 6-1: The first two steps in assembling the lower bi-pod assembly are shown [**24**].

The first thing that happens is the H-COM 19 ball, taken after the splitting of a stock H-COM 19 spherical bearing , is pressed onto 10223-DT-458. After these two components are mated, 10223-DT-467 is pressed into the opposite end of 10223-DT-458

(see Figure 6-1). The flat ends of 10223-DT-458 provide the required surface for restraining 10223-DT-458 during the fitting. A light coat of lithium grease is then applied to the ball surface. A light coat of Lubri-Bond A dry film lubricant is sprayed on the threads and spline and allowed to cure 24 hours.

Next, one of the modified H-COM 19 races is coated with lithium grease and placed in the bearing bore on 10223-DT-015 and the subassembly pictured in the lower portion of Figure 6-1is lowered onto this race. The complementary 10223-DT-427 is put onto the opposite side of the H-COM 19 ball. Then 10223-DT-422 is put in place and threaded into the 2-15/16”-32 thread on 10223-DT-015 until the joint stiffens somewhat. This step requires a specialty spanner wrench that CEM has fabricated specifically for this purpose. It features a 1/2” square drive for use with a torque wrench to accurately torque 10223-DT-422 to 138-165 ft-lbs per Appendix 1.The 10223-DT-466 is put onto the M25 X 1.5 thread that protrudes on 10223-DT-458 that protrudes the H-COM 19 ball. Next the BLM-05 Bear-lok nut is hand tightened onto the thread (see Figure 6-2).

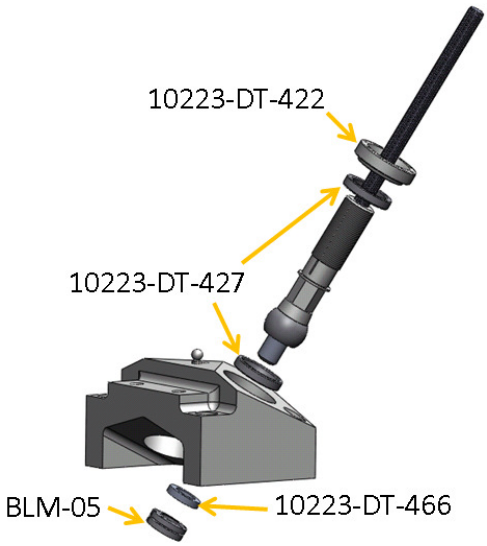

Figure 6-2: The strut-end assembly components are added on. 10223-DT-422 threads into 10223-DT-015 to capture the H-COM 19 ball between its split race. The spacer and BLM-05 go on the backside [**24**].

Once the BLM-05 is in place a second specialty tool created by CEM, a 1/2” drive socket that fits over the BLM-05, is used in conjunction with a torque wrench and an

adjustable wrench on the flats of 10223-DT-458 to properly torque the assembly to 70-95 ft-lbs (Appendix 1). The BLM-05 is then locked per the manufacturer's directions [**49**].

Finally, 10223-DT-459 is threaded onto 10223-DT-458 until it bottoms out at the hard stop. The shaft clamps can be put on 10223-DT-459 prior to assembly so long as they are not fully tightened (see Figure 6-3).

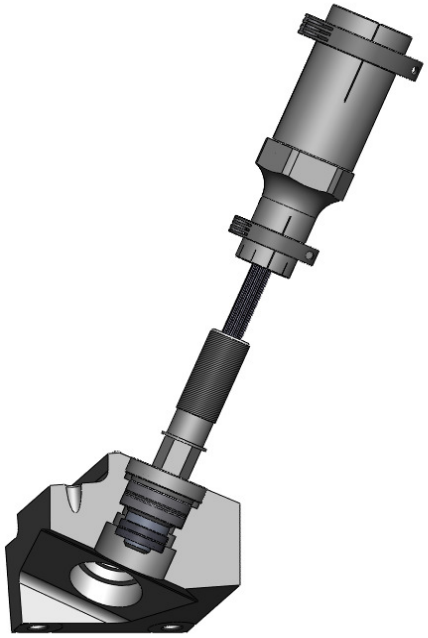

Figure 6-3: 10223-DT-459 is threaded onto 10223-DT-458 as shown. 10223-DT-015 is sectioned such as to show the fully assembled and properly preloaded bearing assembly [**24**].

This same procedure is repeated for the other set of bores. When completed the bi-pod subassembly is properly preloaded and ready to be lifted up onto the strongback. The assembly should look as shown in Figure 6-4. The lifting eye feature on 10223-DT-015 discussed earlier in this thesis is used once the bi-pod is assembled to lift the entirety onto the strongback during final assembly at the McDonald Observatory.

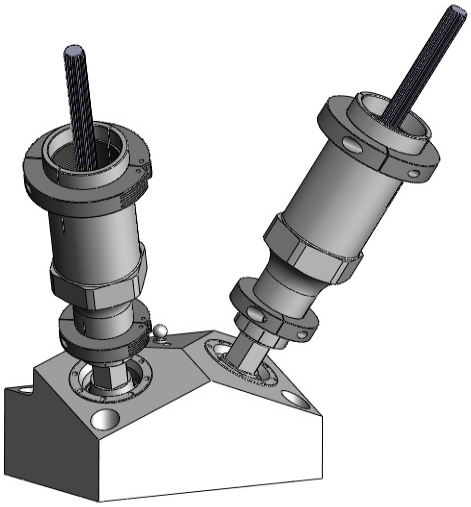

Figure 6-4: The completed lower bi-pod assembly is shown [**24**].

Upper Bi-Pod Assembly

The upper bi-pod assembly is very similar with regards to the strut-end portion save one important difference outlined below.

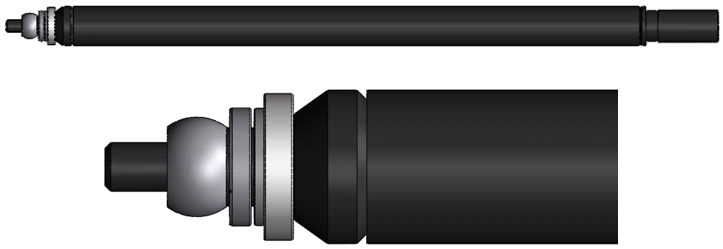

Figure 6-5: A profile view of the entire upper strut assembly (top) and a close-up of the strut-end (bottom) where the H-COM 19 ball traps 10223-DT-427 and 10223-DT-422 [**24**]. Note: black coloration is used for contrast and clarity in the figure.

When the H-COM 19 ball is pressed onto 10223-DT-454 in the upper strut assembly it must trap one 10223-DT-427 and 10223-DT-422 so that they can be properly placed prior to assembling the strut-end in 10223-DT-083. A graphical representation of this is shown in Figure 6-5. The geometry of 10223-DT-454 was tweaked during the design process to allow not only for accommodating these two components without

negative effects to assembly but also to allow spanner wrench access once the assembly is mated to 10223-DT-083.

The remainder of the assembly process is very similar to that of the lower bi-pod assembly. A full upper bi-pod assembly should appear as follows when fully assembled.

Figure 6-6: The completed upper bi-pod assembly is shown [**24**].

There are three each of the upper and lower bi-pod assemblies. Once these ground-based assemblies have been completed the rest of the support structure can be put in place.

ASSEMBLY AT ELEVATION

The basic strategy is to place all three lower bi-pod assemblies securely in place on the strongback, lift each upper bi-pod one-at-a-time and mate the M64 threads until all three are in place. Finally, lift the Rho platform and use the ball and slot mounts that are already in place to align the upper Rho blocks. The upper blocks are then secured with 4 M16 fasteners each.

Lower Bi-Pod Placement

Each lower bi-pod assembly is lifted using lifting eyes attached to the threaded into 10223-DT-015 and a crane at the observatory. The telescope is assembled up to the strongback at this point. Once at height, the blocks are secured to the strongback using 4 M16 X 2.0 socket-head cap screws 80 mm in length.

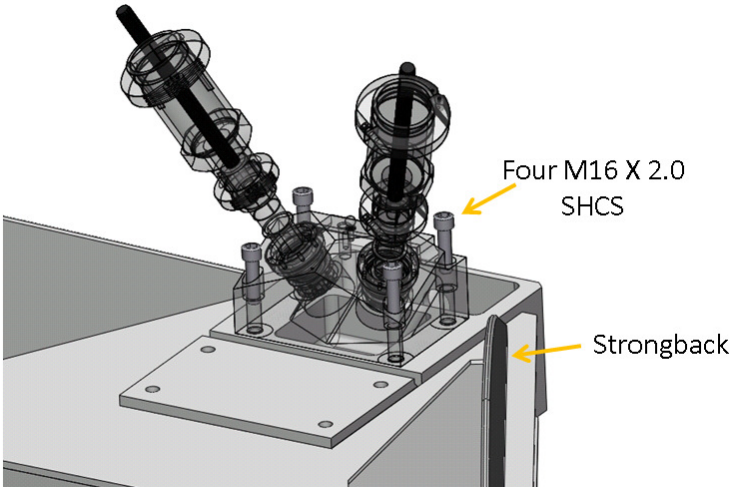

Figure 6-7: The installation of a lower bi-pod assembly onto the strongback at elevation is shown [**24**].

Since all of the shoulders created by the counterbores for the socket-head cap screws are at the same height, a single size cap screw is used to simplify the assembly. The fasteners are tightened to 90% proof load as established by ASTM A 574M-08 according to recommendations for permanent bolted joints [**37**]. The complete assembly atop the strongback should appear as in Figure 6-8. Note: the figure is simplified only to include the blocks and the strongback. None of the rest of the telescope is shown. At this point in the assembly process it is safe to attach any work platforms to 10223-DT-015 that are necessary. At the time of this writing MDO has yet to detail the exact procedure or sequence for this installation.

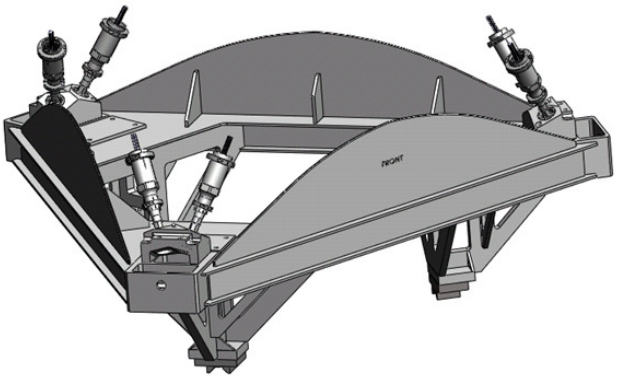

Figure 6-8: A model of the strongback with lower bi-pod assemblies attached [**24**].

Upper Bi-Pod Placement

Just prior to lifting the upper bi-pod assembly, 10223-DT-422 is tightened to remove some slack in the bearing and add stiffness to the structure. This is to comply with the MDO desirement that no "dangling hexapod struts" be present during assembly. The exposed threads at the base of the strut are also covered to prevent damage and to prevent the Lubri-Bond A on the threads from being removed prematurely.

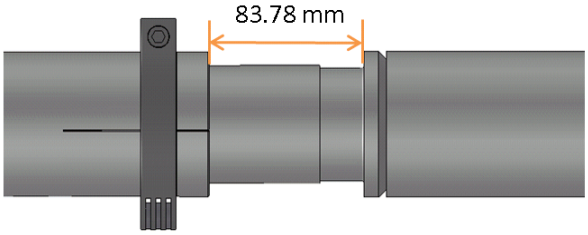

Figure 6-9: The proper gap measurement for approximate nominal length is shown [**24**].

Once an upper bi-pod set is lifted into position, the bearings are loosened just enough to allow the strut to be manipulated. The bearings in the lower bi-pod assembly are also loosened. The exposed spline is slid into the broached feature in the bottom of the upper strut assembly until the threads of the strut and collar come in contact. Then with a pair of wrenches—one on the flats on 10223-DT-458 and the other on the flats on 10223-DT-459—the collar is rotated until the threads mate. At this point rotation of the collar continues and the M64 thread should be advancing into the collar while the M38

thread retreats out the bottom. A set of dial calipers is used to measure the distance between the top of the collar and the bottom of the hard stop; the strut is approximately at nominal length when this distance is 83.78 mm (see Figure 6-9).

The shaft clamps on 10223-DT-459 are locked once the proper gap is achieved. This process is repeated for the remaining strut and the two remaining upper bi-pod assemblies. When complete the structure should appear as shown in Figure 6-10.

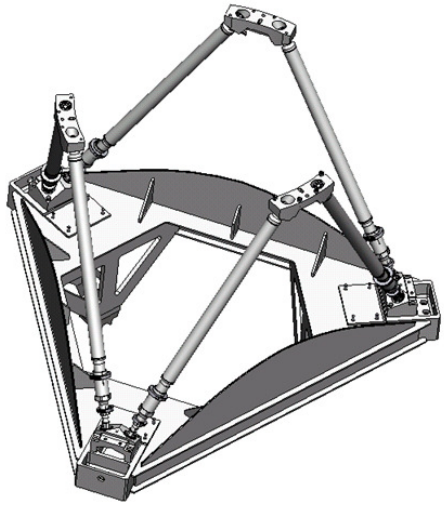

Figure 6-10: A model of the strongback with upper and lower bi-pod assemblies installed [**24**].

Next the Rho platform assembly is lifted and positioned above the upper Rho blocks. Despite what is depicted in Figure 6-10 the flat upper portion of the Rho blocks will likely not form a plane, so the bearings are left loose enough to allow manipulation of the location of the blocks. The ball and slot features on the blocks are then mated to the ball and cylinder on the underside of the Rho platform assembly. Once a block is in place on the platform four M16 X 2.0 socket-head cap screws are fastened through the top of the Rho platform to secure the platform to the block.

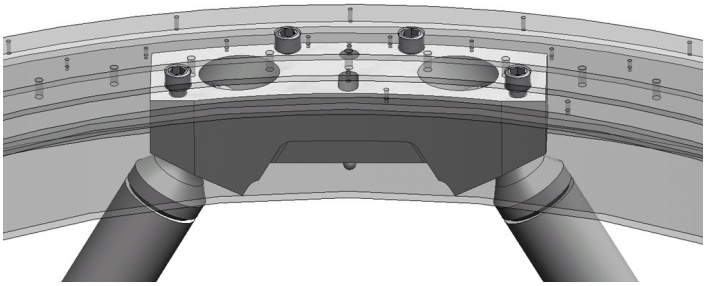

Figure 6-11: An upper bi-pod assembly is secured to the Rho platform with 4 fasteners. The platform is made transparent to show the fasteners and ball/slot alignment features [**24**].

These fasteners are tightened to 75% of proof load as established by ASTM A 574M-08 since this was requested by MDO to be a temporary joint. Both the fasteners and the blocks will have corrosion resistant outer layers, but anti-seize compound is still recommended to facilitate future disassembly.

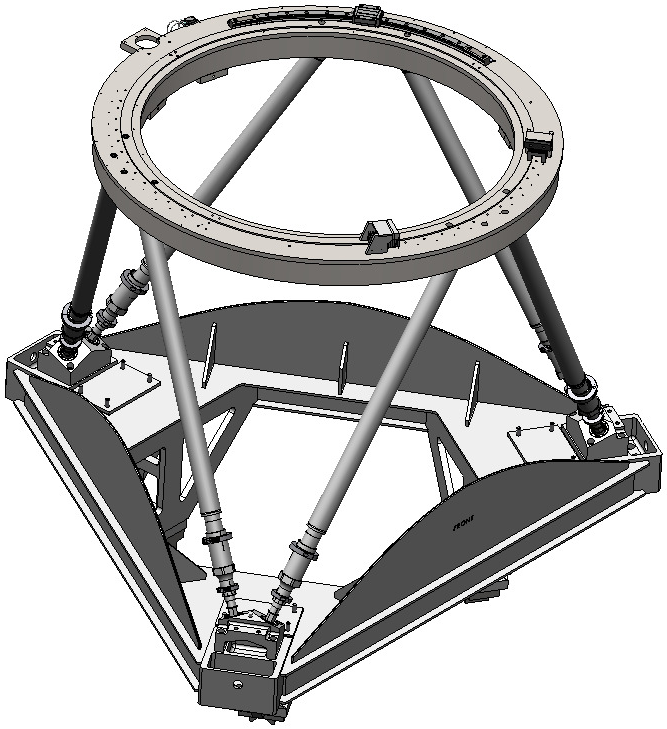

Figure 6-12: A model of the completed PFIP support assembly is shown [**24**].

If the previous steps have been followed properly the full PFIP support assembly should appear as shown in Figure 6-12. The struts are approximately at nominal length. At this point the bearings can be locked by torquing 10223-DT-422 to 138-165 ft-lbs as discussed in Appendix 1 to continue with installation of components that mount to the Rho platform. However, MDO may decide to adjust the platform first.

Chapter 7: Design and Design Process Evaluation

CHAPTER SCOPE

This chapter will evaluate the overall completed design and the FRDPARRC design methodology. The design itself will be examined to establish whether or not the finished product adheres to the FRs and ODs, how well the design is expected to perform, the effective reduction in associated risks, and any shortcomings of the design. The design process will then be evaluated based on this analysis. Finally, the process itself will be evaluated from a more abstract viewpoint.

DESIGN EVALUATION

Performance

As of the time of this writing the actual performance of the physical system has not been realized since it is still under manufacture. However, computer aided modeling concepts were used to estimate the expected performance of the system.

strut length [mm]	*plane distance [mm]*	*bearing angle [deg]*	*strut condition*
1598.447	1542.149	0.772	minimum length
1617.447	1564.365	0.372	nominal length
1636.447	1586.400	0.397	maximum length

Table 7-1: Predicted displacement with minimum and maximum strut lengths.

Table 7-1 shows the predicted distance between the top of the strongback and the bottom of the Rho platform and the angular displacement from the axis though the cent of the bore of the spherical bearing at minimum, nominal, and maximum strut length conditions. The total optical axis displacement is +21.765 mm and -22.486 mm for a total adjustment capability of 44.251 mm at this given nominal length. Note that the bearing angle is an absolute angular displacement from the axis through the bore. This means that even though the nominal and maximum length conditions show similar displacements the bearing actually rotates 0.769° between these two conditions and a total of 1.169° between minimum and maximum heights.

These numbers are valid only for this nominal condition. The kinematics of the 6-6^p GSP would dictate a different amount of optical axis displacement and bearing rotation with respect to the bore axis for the same +/- 19 mm strut length change centered about a different nominal strut length. This detail highlights one of the difficulties in accurately modeling the behavior of a real 6-6^p GSP-based system. The symmetry and exact locations of the bearing origins (and the likely non-planar configuration these origins form) required for analysis are nearly impossible to obtain from a manufacturing and metrology standpoint. The actual strut length will vary for each strut based on unavoidable variances in manufacturing tolerances in nearly every component in the system despite being adjusted to the same gap as established in Chapter 6. Indeed there may not even be an actual plane though either set of 6 origins to create a reliable "base" or "platform" geometry. While the difficulties in modeling the actual configuration and its effects on the adjustment capabilities and procedure are beyond the scope of this thesis, they are worth mentioning in a discussion about system performance.

Adherence to FRs & ODs

All system-level functional requirements and operational desirements expressed by MDO and listed in Chapter 3 were met or exceeded with some combination of design parameters, manufacturing techniques, or assembly procedures. One feature of the FRDPARRC design process is that it can be applied both at the system and subassembly/component levels. Its consistent use throughout the design ensures that not only each component serves its function reliably but that the system requirements are also met almost by default.

Remaining risks and design shortcomings

As discussed in the "Performance" section of this chapter the biggest design shortcoming is the inability to accurately predict its behavior. This poses challenges in the adjustment since the movement of a GSP is not intuitive and that most platform movements require all 6 struts to be adjusted to some degree. However, MDO has only requested 50 micron resolution of the adjustment mechanism. This implies that finer

adjustment may be possible within the instrumentation that will be mounted on this PFIP support structure. With the application of careful tolerancing in the technical prints for the manufacture of these components and internal adjustment higher precision is likely possible. While this does not address the difficulties in accurately modeling the system it may mean that a mathematical model created using the figures given in Chapter 2 for the bearing origin locations and the relative platform/base locations within the ideal computer model of this system may prove accurate enough for this purpose.

MDO added the functional requirement of having 10223-DT-015 serve as the mounting point for electronics boxes and work platforms very late in the design process while technical prints for this component were being finalized. While analysis run at the time showed that these components could serve this new purpose without harm to the system or significant sacrifice to accuracy/stability, this component was not designed with the intent of supporting this additional load. Since this functional requirement escaped inclusion in the FRDPARRC process used in designing the blocks they are no longer the best design for the job. Had this functional requirement been known during the initial detail design the blocks would likely have had design parameters that specifically address this type of load and would act to isolate the effects of the work platform loads and the strut loads so that one load would not affect the performance of the block in supporting the other load.

DESIGN PROCESS EVALUATION

FRDPARRC's iterative nature

An impression of the hindsight view of the components (with respect to the FRDPARRC design process that is presented in this thesis) is that the process immediately led to the final design shown in the figures. This is most definitely not the case. The iterative nature of the process is lost in a post-mortem analysis, but it is a very important aspect of the system itself as these iterations led to the final design. In actuality the FRDPARRC process is highly iterative and time consuming, but this is part of what makes it a powerful design tool. The engineer can devise many design

parameters to satisfy a functional requirement of a system or component and use the remaining steps as a metric by which to compare the possible solutions. Comparison to other solutions invariably leads to strengthening of the best suited design by identifying its shortcomings or by incorporating aspects of what would have been a completely different design solution to the problem.

One example of using iterative processes to devise a superior solution is that which occurred during the course of designing the mechanism that couples the two threaded inserts, 10223-DT-458 and 10223-DT-461, in the adjustment assembly. While all solutions featured a splined shaft of sorts to transmit the torque, the terminations were all different. One design featured an expensive precision ball-spline to keep friction from axial motion to an absolute minimum, but it required significant material removal from the threaded insert and increased the cost dramatically. Other solutions consisted of pinned or press-fit inserts that had the spline profile cut into it. These posed problems of their own like deforming the threaded insert too much or not being strong enough to withstand the design loads. Eventually, after applying Occam's razor to design per Professor Slocum's recommendation [**21**], the idea to simply cut the spline into the insert was born. While this seems like an obvious and simple solution—and it is precisely that by design—the FRDPARRC methodology assisted in arrival at this conclusion. That is not to say that it is the only way this idea would have occurred.

FRDPARRC requires clear goals

As alluded to in the discussion on the shortcomings of the design, there were a few times where functional requirements and operational desirements were made known only after the design had progressed to a certain level. This illustrated one possible weakness of this design methodology—all functional requirements must be clearly defined at the start. This weakness is common to most any design methodology as it is impossible to create a solution when the problem itself is not clearly defined. However, a change in the functional requirements of a system occurred with surprising regularity on this project [**34**] [**39**]. Much of this occurred because of the parallel design process that

MDO and CEM both participated in to help cut delivery time, but it is not exclusive to this project.

Often during the design process a functional requirement of a design, or one with which it interfaces, is not known until detailed design is undertaken. While these are often minor tweaks such as geometric changes or changing fastener locations, should the case be that the functional requirement is more significant it could potentially render the design inadequate. This is especially apparent in FRDPARRC which is a sort of funnel system that takes a broad—but well defined—problem and creates an application specific solution to this problem. However, if a basic functional requirement of a design is radically changed it is likely to require a redesign no matter which design methodology was used.

FRDPARRC and resources

In reading through the FRDPARRC analysis of the component in Chapters 4 and 5 one thing is made clear, a very broad knowledge of engineering, manufacturing, and physical principles is required to successfully implement this design methodology. The designs in this thesis included aspects of manufacturing from machining to case hardening, aspects of engineering from material properties to computer aided modeling, aspects of mathematics from simple algebra to calculus, and much more. A wealth of engineering knowledge is required, and when the engineer does not have this knowledge they must have the resources to attain it through research.

An example of using research to effectively implement FRDPARRC is seen in the modification of the H-COM 19 bearing for use as a clutch mechanism. Originally the strut-end assembly featured to method to constrain the spherical bearing itself. The references mentioned in Chapter 1 posited that in a GSP arrangement the bearing is constrained automatically by fixing all 6 strut lengths. While this is true in theory, the small clearance built into the bearing between the ball and the race would always be present. Since the bearing was going to be preloaded anyway the idea became apparent

to use the preload not only to secure the bearing race but as a way to constrain the ball from rotating and eliminate the slack in the bearings during telescope operation.

This idea arrived from examining clutch mechanisms and devising a way to install a spherical bearing that would likely have to trap its retaining ring on the strut (as illustrated in Chapter 6). During the course of research into bearing arrangements, I was handed a catalog for split-race bearings that mimic full race bearings when installed by a colleague at CEM. While this solution helped with the problem of installation, it also spurred the idea to combine the split-race feature with a clutch mechanism. After the initial feasibility analysis was performed (which eventually led to analysis shown in Appendix 1), the idea was detailed and incorporated.

The engineer must be very knowledgeable of their craft and willing to research extensively if they are to implement FRDPARRC properly and with success. While this can be taxing on the engineer, it provides the benefit of serving as a method of continuous learning. Each time the engineer must research something outside the scope of their knowledge, that scope is expanded. Consistent use of the FRDPARRC system on various design projects should force the engineer to research ideas and concepts that will only strengthen their design abilities and allow them to refine their ideas from points of view not previously possible. Not only does this give the ideas generated by this engineer a competitive edge, but the competitive advantage also goes to the engineer. Much like the continuously improving design solutions afforded by FRDPARRC's iterative nature, the engineer is continuously improving in their ability to innovate.

Chapter 8: Contributions and Conclusion

SUMMARY

Professor Alex Slocum's FRDPARRC design methodology was applied to the concept and detail design phases of each component and subassembly in the PFIP support strut assembly for the HETDEX telescope. The PFIP support structure consists of the strongback, the adjustable strut assembly, and the Rho platform. This configuration forms a special symmetric type of Gough-Stewart platform called the 6-6^p GSP. Advantages of this configuration include the ability to move the platform in six degrees of freedom to at least some extent, but the kinematics of such a structure require all six support struts be adjusted even to accommodate simple translation.

The FRDPARRC design methodology was originally meant to serve as a tool to help the engineer organize their thoughts and focus their efforts on solving a specific problem. It starts with an abstract understanding and philosophy of the problem and its possible solutions. Then, through iteration and comparison, the engineer is able to evaluate possible design solutions to the problem at hand while improving/refining their optimal solution at the same time. By defining goals independent of each other, the system inherently leads the engineer to create a modular design. So while the original intent of the design methodology was more based in abstract philosophy, a practical application of the method at the detail design level enabled the engineer to innovate new solutions to the design problem at hand.

Because analysis and research are part of the design process itself, the engineer is forced to be proactive in continuing their education as they tackle each new design problem. In this way the engineer is constantly improving as a designer and enhancing their pool of knowledge from which they can generate ideas. This will enhance the engineer's ability to innovate and give their solutions a competitive edge.

However, to fit the FRDPARRC methodology to this specific application (the HETDEX PFIP support strut assembly), some modifications were necessary. Since the users of this telescope (meaning the scientists, technicians, and astronomers at MDO) had previous experience with the HET prior to this upgrade effort, they had specific operational "desirements" they wanted incorporated in CEMs upgraded design. Therefore the first step of the system, identifying the Functional Requirements of a component or subassembly, was added to included these Operational Desirements, expressly requested by a technically advanced customer. In Slocum's book the FRDPARRC system is described in the context of a means to accomplish a goal. To some extent the aspect of product design or end-user input is not emphasized as much. Therefore to apply his design methodology more broadly to product design as a whole, a modification such as the one proposed in this thesis is necessary. User feedback and customer profiling is typical in product design and marketing surveys, so this modification to the original methodology helps ensure that the customer requests are specifically addressed in the design phase of any product to which this method is applied.

Also, in the original text modularity of a design and the design parameters that are incorporated are closely coupled—meaning that a sort of one-feature-per-functional-requirement type of design is encouraged. While this is important, aspects of the design should also include 'design for assembly' and 'design for manufacture' provisions as well. These assemblies, assembly procedures, and manufacturing techniques act as additional layers that allow functional requirements to be met. This is especially true if there are specific operational desirements in the assembly process itself, as was the case with MDO.

With these modifications and added layers to the original FRDPARRC philosophy in mind, the components and subassemblies that comprise the PFIP support

strut assembly were designed. This thesis then takes a hindsight view of each component and highlights how each step of the process helped shape the component into its eventual final form. Innovative solutions to design problems are shown through explicit detailing of design parameters and their incorporation into the final design. And since analysis and risk identification/mitigation are parts of the process, there are innovations in these areas as well that arrive either through necessity (analyzing a design that has not either been done before or ever analyzed previously by the engineer) or the research component built into the FRDPARRC system.

'Design for assembly' and 'design for manufacture' techniques that were applied to the components and subassemblies within the PFIP support are also discussed. A proposed assembly procedure is detailed whereby specific design parameters that address 'design for assembly' are identified and discussed.

Finally the effectiveness of the FRDPARRC design methodology and its ability to drive innovation within the context of the design of the PFIP support strut assembly is discussed. Aspects of the FRDPARRC system and its effects on the engineer and their designs are identified. Specific examples of innovative design solutions that arose during the course of detailing the design in the body of this thesis are cited as evidence. This leads to the conclusion that this system does indeed drive innovation.

CONTRIBUTIONS

Aside from contributions that will indirectly occur because of the use of the design detailed in this thesis within the fields of astronomy, cosmology, and physics that the study of dark energy will lead to, there are a number of contributions to existing literature that can be found in this thesis.

The first is the proposed modification of a design philosophy, the FRDPARRC method, to incorporate customer input and features desired by the end-user. By widening the original scope of the method, the engineer is able to specifically address these concerns in the both the concept and detail level designs.

The second is that this thesis serves as both a companion to and a case study of application of Slocum's FRDPARRC design methodology. Would-be designers looking to become more familiar with design philosophies but needing a more tangible example of its use can find the information given in the post-mortem analysis of the PFIP strut assembly design useful. This thesis explains in detail how all aspects of a design, from its shape to how it's made, serve to accomplish its functionality. Because it is a hindsight view of components (meaning the iterations and failed design solutions that went into improving the final design) it also serves as a reverse engineering exercise by the actual designer of the system. This eliminates the guesswork normally present in reverse engineering since the original design intent and the purpose of design parameters are preserved and conveyed by the designer rather than interpreted by a third party.

Finally, since some of the design parameters that are incorporated in the PFIP support strut assembly are innovative, they require innovative analysis techniques. Some of this analysis can be found in the appendix. The most applicable example is the analysis of the H-COM 19 bearing that was modified to act as a clutch-style locking mechanism presented in Appendix 1.

FUTURE WORK

One of the drawbacks of the hindsight view of components is that the iterative nature of the FRDPARRC system is lost. This is an important aspect that also serves to drive innovation in improving and eliminating risk in what eventually becomes the final

design. Perhaps a design diary that shows the evolution of a design through the use of the FRDPARRC system (and incorporating modifications proposed in this thesis) would serve as a useful tool.

With regards to this specific design, a method for monitoring real-time adjustment of each strut would be suitable. It would work hand-in-hand with an adjustment procedure that allows for accurate prediction of the kinematic behavior of the PFIP support assembly.

Appendix 1

STRUT END ANALYSIS

Section 1: Summary of loads

There are a variety of loads on the strut end assembly and each must be taken into account when completing the analysis. The goals of the analysis are four-fold:

- To verify stresses are safely below the yield threshold
- To determine assembly values (namely component torque values)
- To determine maximum clamping force in the bearing assembly
- To verify/investigate the effects of all component analysis

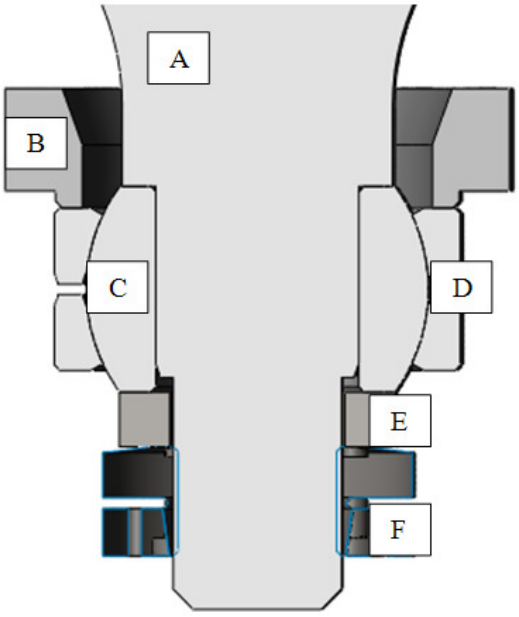

Figure A1-1: A vertical section-view of the strut end is shown [**24**].

A section-view of the strut-end is shown in Figure A1-1. It consists of the following components:

A: Insert, p/n:10223-DT-458 (also valid for 10223-DT-454)

B: Retaining Ring, p/n: 10223-DT-422

C: H-COM 19 Ball

D: Modified H-COM 19 Bearing Race, p/n: 10223-DT-427

E: Strut Spacer, p/n: 10223-DT-466

F: Bear-lok BLM-05 Lock Nut

For the purposes of this analysis, all component parts will henceforth be referred to by their CEM part number. Figure A1-2 shows a planar section-view of the bearing assembly complete with arrows indicating forces on the bearing. This simplified assembly functions as a load map that summarizes the effects and locations of the applied loads. NOTE: constraints are not currently shown—only loads.

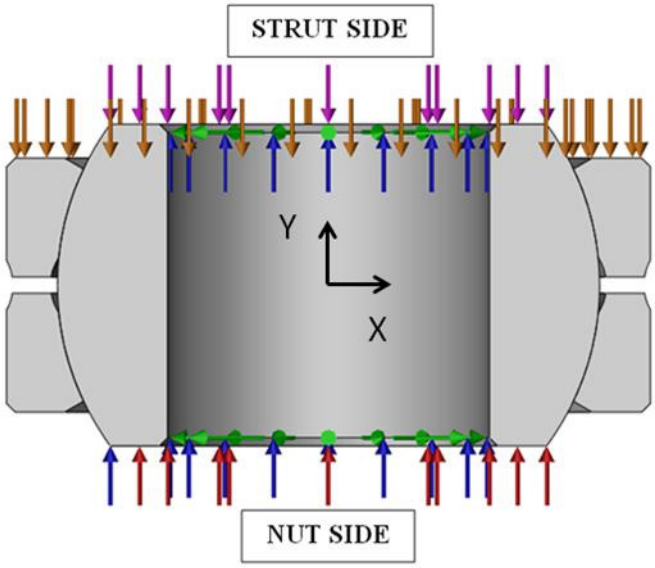

Figure A1-2: A vertical section-view of the spherical bearing sub-assembly with loads represented by arrows shown [**33**].

The arrows are color-coded as follows:

Orange: Force (preload) from 10223-DT-422 on strut-side face of 10223-DT-427.

Blue: Force from tensile loading in the strut. This force acts on the outboard face of the bearing shoulder (due to tensile forces pulling in BLM-05 and compressing 10223-DT-466) and as a shear force at the inner diameter of the H-COM 19 ball—this is a press-fit interface.

Red: Force (preload) from BLM-05 compression on 10223-DT-466.

Purple: Resultant force from BLM-05 preload.

Green: Radial stress from press-fit with 10223-DT-454.

Section 2: Calculation of individual loads

Part 1: Determining BLM-05 preload

The effects of the BLM-05 preload are represented by red and purple arrows in Figure A1-2. They arise from tension introduced to 10223-DT-454 by tightening BLM-05. Because of this, the stack of A, C, E, & F in Figure A1-1 is analyzed as a bolted joint where 10223-DT-455 is treated as a shoulder bolt. All dimensions shown are known; numberical values can be found in Table A1-1.

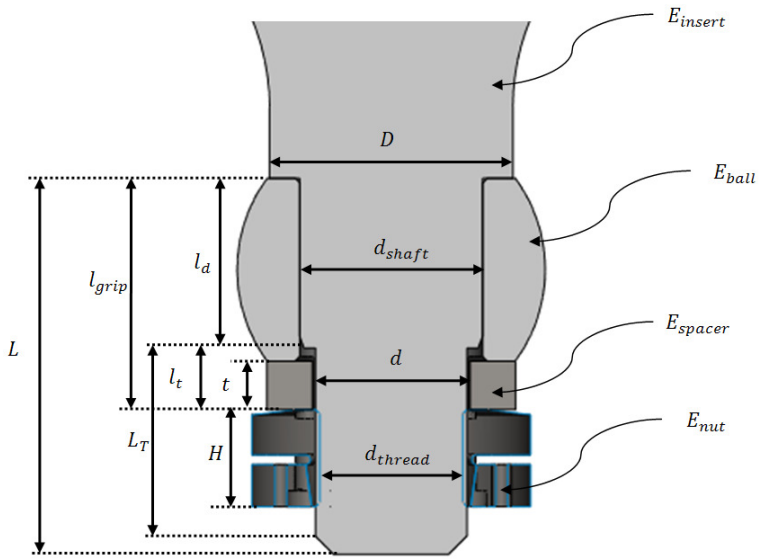

Figure A1-3: A vertical section-view of the components used in the bolted joint approximation analysis [**24**].

Variable	Numerical Value	Unit	Variable	Numerical Value	Unit
E_{insert}	205	N/mm^2	d_{thread}	23.16	mm
E_{ball}	210	N/mm^3	H	28.85	mm
E_{spacer}	204	N/mm^4	l	38.15	mm
E_{nut}	200	N/mm^5	L	62	mm
l_d	28	mm	l_T	10.15	mm
t	8	mm	d_{shaft}	30.1625	mm
d	25	mm	D	40.16	mm
L_T	34	mm	-	-	-

Table A1-1: Numerical values for dimensions used in bolted joint approximation of strut end preload.

The strategy for analysis is as follows:

- Determine the stiffness values of each member in the joint as well as an overall equivalent stiffness
- Using the calculated stiffness values, determine load fractions for the members and the threaded component
- Find an upper limit to the preload
- Apply a reasonable safety factor against joint seperation and determine the corresponding preload
- Compare calculated preload to upper-limit to verify yielding does not occur
- Use verified preload to determine tightening torque of BLM-05

Stiffnesses are calculated using the following relations [**37**]:

$$k_{insert} = \frac{A_d A_t E_{insert}}{A_d l_T + A_t l_d} \qquad \textit{Eq A1-1}$$

where:

$A_t = {\pi d_{thread}^2}/{4}$ and $A_d = {\pi d^2}/{4}$

$$k_{ball} = \frac{0.5774 \pi E_{ball} d_{shaft}}{ln\left\{\frac{\left(1.155 t_{ball} + D - d_{shaft}\right)\left(D + d_{shaft}\right)}{\left(1.155 t_{ball} + D + d_{shaft}\right)\left(D - d_{shaft}\right)}\right\}} \qquad \textit{Eq A1-2}$$

where: $t_{ball} = l - t$

$$k_{spacer} = \frac{0.5774\pi E_{spacer} d}{ln\left\{\frac{(1.155t + D - d)(D + d)}{(1.155t + D + d)(D - d)}\right\}} \qquad \textit{Eq A1-3}$$

$$k_{eq} = \left(\frac{1}{k_{ball}} + \frac{1}{k_{spacer}}\right)^{-1} \qquad \textit{Eq A1-4}$$

Table A1-2 below summarizes the values calculated from the equations above.

Variable	Numerical Value	Unit
k_{insert}	2,880	N/mm
k_{ball}	10,460	N/mm
k_{spacer}	39,990	N/mm
k_{eq}	8,290	N/mm

Table A1-2: A summary of stiffness values of the components of the bolted-joint approximation obtained by using Eqs A1-1 through A1-4

The load fraction in the threaded feature, C, is determined by the following relation [**37**]:

$$C = \frac{k_{insert}}{k_{eq} + k_{insert}} \qquad \textit{Eq A1-5}$$

Despite the maximum load per strut, either tensile or compressive, being published at 4 kN [**39**], loads were later found to be just under 8 kN [**29**]. A safety factor of 1.5 was applied, and it was treated to as if the load applied in the direction which would cause joint separation at BLM-05 whether or not it actually applied in this direction. This would ensure that under all likely conditions, the calculation would specify a preload—and therefore an assembly torque value—that proved adequate.

The following relation is used to determine the maximum preload, $F_{i_{max}}$, for a material given its thread geometry [**37**]:

$$F_{i_{max}} = 0.75A_t(0.85\sigma_y) \qquad \textit{Eq A1-6}$$

The published yield strength for AISI 4140 steel in the annealed condition is around 685 MPa [**38**], so the corresponding maximum preload on the insert is 184 kN. However, it is not necessary to use this maximum value. A lower value would make assembly easier and still provide the requisite preload to prevent joint separation. To determine this value, a safety factor against joint separation, n_d, of 2.2 was chosen and used in the following relation [**37**]:

$$F_i = n_d P(1 - C) \qquad \textit{Eq A1-7}$$

where F_i is the minimum preload and P is the 12 kN design load acting to separate the joint. The calculated minimum preload is found to be 19.6 kN which is safely below the maximum preload calculated above. Since P and F_i are now known, they can be added to the model shown in Figure A1-2 as the absolute values of the vectors represented by the blue and red/purple arrows.

A spreadsheet that contains formulae and relations essential for determining assembly torque and maximum thread stresses as a function of thread geometry, friction coefficient, and preload is used to determine the assembly torque. This was run at the minimum preload value and at a value just below the yielding threshold at the base of the first thread. The reason for this is to keep the stresses below what would cause permanent deformation in the threads so that this strut can be disassembled, serviced, and reassembled without having to make a new strut or re-order a BLM-05. This window creates an assembly torque between 70 and 95 ft-lbs, assuming a coefficient of friction of 0.13 in the lubricated threads at minimum preload and a coefficient of friction of 0.11 in the case just below yielding in the threads. Note: after tightening the BLM-05 to its designated assembly torque, it is to be locked in place by tightening four screws. This does not pose a problem for the first thread engaged on the insert because the threads loaded most by this are those nearest the split in the BLM-05. The effects of the loading from locking will taper off with almost no load effects beyond the seventh thread [**37**].

M25x1.5	Total Torque Req'd [ft-lbf]	Preload [N]	lead (pitch) [inch]	major diameter [inch]	mean diameter (inch)	friction coeff	1/2 thread angle (alpha)	Axial Stress [psi]	Nominal shear stress [psi]	Nom. bearing stress (5 T) [psi]	Thread root bending stress (5T) [psi]	Thread root shear stress (5T) [psi]	Von Mises Stress (5T) [psi]
	64.6	19600	0.05906	0.976	0.9449	0.11	30.0	6738	5200	-10053	31230	15615	36225
	69.6	19600	0.05906	0.976	0.9449	0.12	30.0	6738	5598	-10053	31230	15615	36403
	74.6	19600	0.05906	0.976	0.9449	0.13	30.0	6738	5997	-10053	31230	15615	36593
	79.5	19600	0.05906	0.976	0.9449	0.14	30.0	6738	6395	-10053	31230	15615	36795
	84.5	19600	0.05906	0.976	0.9449	0.15	30.0	6738	6794	-10053	31230	15615	37008
	89.4	19600	0.05906	0.976	0.9449	0.16	30.0	6738	7192	-10053	31230	15615	37233
	94.4	19600	0.05906	0.976	0.9449	0.17	30.0	6738	7591	-10053	31230	15615	37470
single thread max	64.6		0.05906	0.976	0.9449	0.11		2560	5200	-19101	59337	29669	61323
	79.5		0.05906	0.976	0.9449	0.14		2560	6395	-19101	59337	29669	61661
	94.4		0.05906	0.976	0.9449	0.17		2560	7591	-19101	59337	29669	62067

M25x1.5	Total Torque Req'd [ft-lbf]	Preload [N]	lead (pitch) [inch]	major diameter [inch]	mean diameter (inch)	friction coeff	1/2 thread angle (alpha)	Axial Stress [psi]	Nominal shear stress [psi]	Nom. bearing stress (5 T) [psi]	Thread root bending stress (5T) [psi]	Thread root shear stress (5T) [psi]	Von Mises Stress (5T) [psi]
	95.7	29000	0.05906	0.976	0.9449	0.11	30.0	9969	7694	-14875	46208	23104	53599
	103.0	29000	0.05906	0.976	0.9449	0.12	30.0	9969	8283	-14875	46208	23104	53861
	110.3	29000	0.05906	0.976	0.9449	0.13	30.0	9969	8873	-14875	46208	23104	54142
	117.6	29000	0.05906	0.976	0.9449	0.14	30.0	9969	9462	-14875	46208	23104	54441
	125.0	29000	0.05906	0.976	0.9449	0.15	30.0	9969	10052	-14875	46208	23104	54757
	132.3	29000	0.05906	0.976	0.9449	0.16	30.0	9969	10641	-14875	46208	23104	55090
	139.6	29000	0.05906	0.976	0.9449	0.17	30.0	9969	11231	-14875	46208	23104	55440
single thread max stress values	95.7		0.05906	0.976	0.9449	0.11		3788	7694	-28262	87795	43898	89128
	117.6		0.05906	0.976	0.9449	0.14		3788	9462	-28262	87795	43898	89637
	139.6		0.05906	0.976	0.9449	0.17		3788	11231	-28262	87795	43898	90248

Table A1-3: Spreadsheet calculations for the required assembly torque of the BLM-05 nut onto the threaded insert at minimum preload and at the yielding threshold at the first thread are shown. The assembly torque is calculated as a function of thread geometry, preload, and friction coefficient.

Part 2: Determining press-fit stresses at HCOM-19 bore

The threaded insert, 10223-DT-454/458, is designed with a transitional fit. This gives rise to the possibility of an interference fit with the HCOM-19 ball. If this were two concentric cylinders, the governing equation for a simplified case is [**37**]:

$$p_{max} = \frac{E_{steel}\delta}{2d_{shaft}}\left[1 - \frac{d_{shaft}^2}{d_O^2}\right] \qquad \textit{Eq A1-8}$$

where E_{steel} is a generic elastic modulus for steel of 205 GPa [**38**], δ is the anticipated maximum interference on the diameter, d_{shaft} is as defined by Figure A1-3, and d_O is the outer diameter of the bored cylinder. However, the 'outer cylinder' in this case is actually a sphere, so the calculated pressure would be inadequate. It is therefore necessary to find a non-uniform pressure distribution that can represent the physical reality more accurately.

For ease of calculation, the following analysis will apply only to the X-Y plane where Z=0, and the Y axis is aligned with the center axis of the bore. See Figure A1-2 for orientation. This essentially simplifies the problem to a 2D problem, allowing for a pressure distribution that depends on X and Y only. Since:

$$x^2 + y^2 = r^2 \qquad \textit{Eq A1-9}$$

for any circle, this can be rearranged and substituted in for d_O in the following manner:

$$p(x,y) = \frac{E_{steel}\delta}{2d_{shaft}}\left[1 - \frac{d_{shaft}^2}{4x^2}\right] = \frac{E_{steel}\delta}{2d_{shaft}}\left[1 - \frac{d_{shaft}^2}{4(r^2 - y^2)}\right] \qquad \textit{Eq A1-10}$$

The radius of the HCOM-19 ball and the y-coordinates of the surface of the bore are known values. This equation gives the exact pressure distribution using an equivalent outer diameter of a cylinder at any given point, y, on the sphere. The ultimate goal of finding each of these loads is to use it in the SolidWorks 2010 FEA package. It can only process non-uniform pressure distributions of the following form:

$$p(x,y) = P_{nominal}(A + Bx + Cy + Dxy + Ex^2 + Fy^2) \qquad \textit{Eq A1-11}$$

so Eq A1-10 must be converted to this form. This requires a curve-fit approximation of the pressure distribution. An Excel plot of Eq A1-10 is shown in Figure A1-4 below.

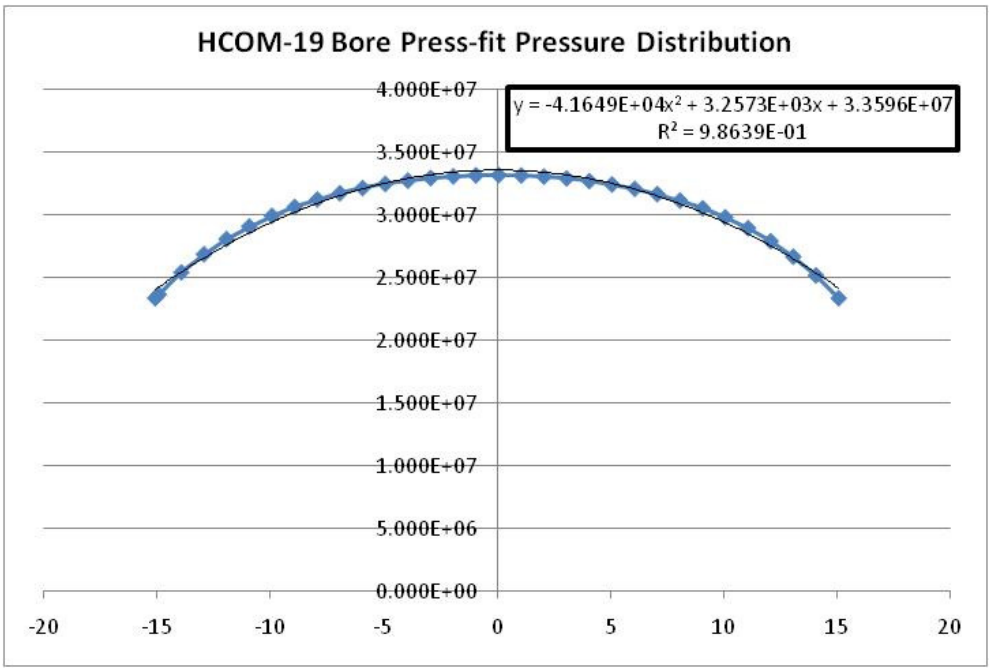

Figure A1-4: A plot of non-uniform pressure distribution due to press fit at bore face of the H-COM 19 ball at Z=0 is shown. The abscissa (labeled 'x' automatically by MS Excel) is the y-coordinate at the face of the bore, and the ordinate (labeled 'y' automatically by MS Excel) is the corresponding pressure at that point. A curve-fit is also shown using the maximum order available to SolidWorks Simulation. It shows adequate correlation with a coefficient of determination of 0.9864.

The curve-fit equation shown in Figure A1-4 has a coefficient of determination of 0.9864. Increasing the order of the equation would improve the fit, but it would no longer conform to the designated format. This analysis is merely an estimate using the assumption that the dual-concentric cylinders equation, Eq A1-8, still holds true for this case. Normalizing the curve-fit equation and formatting it per Eq A1-11 yields the following equation that can be used as an input directly into SolidWorks Simulation:

$$p(y) = 3.3596 * 10^7 Pa\,[1 + (9.6955 * 10^{-5})y - (1.2397 * 10^{-3})y^2] \quad \textit{Eq A1-12}$$

Notice that Eq A1-12 only depends on y. This is ideal for SolidWorks Simulation as it merely takes the y value associated with the nodes on the bore of the H-COM 19 ball and determines the pressure at that node. Also, since Z is nowhere to be found in this equation, the results from the FEA analysis are only valid at Z=0 in the model. However, these results are valid for all diametric cross-sections on the actual assembly.

Part 3: Determining Bearing Retainer Load/ Installation Torque

The process of finding the clamping force and bearing retainer preload is relatively straightforward. The results are needed to run an FEA model to solve for the contact pressure at the surface of the H-COM 19 ball in contact with the split-race pair, 10223-DT-427. The preload provided by 10223-DT-422 must at least prevent the upper bearing race from moving under maximum tensile load. Therefore a safety factor of 1.6 was applied to the design load, and then rounded to the nearest 500 N. This rendered a preload of 19,500 N. By using the following relation [**37**]:

$$T_{preload} = \frac{F_{preload} * d_{nominal}}{2}\left(\frac{l + \pi f d_{nominal} \sec\alpha}{\pi d_{nominal} - f l \sec\alpha}\right) + T_{friction} \quad \textit{Eq A1-13}$$

where $d_{nominal}$ is the 2-15/16" nominal diameter of the retaining ring, l is the 32 thread per inch pitch, f is the friction factor (0.11-0.20 for lubricated steel-on-steel contact), α is the 60° thread angle, and $T_{friction}$ is as defined below [**37**]:

$$T_{friction} = \frac{F_{preload} f d_{contact}}{2} \quad \textit{Eq A1-14}$$

where $d_{contact}$ is the average diameter at the point of contact between 10223-DT-427 and 10223-DT-422, (see Figure A1-1 for graphic). A spreadsheet containing the resultant total assembly loads and the corresponding thread stresses as a function of friction factor, thread geometry, and preload is on the following page. To determine the maximum assembly torque, these components were not analyzed—instead the spanner wrench used

to tighten 10223-DT-422 was analyzed. The maximum torque before failure at the base of the pins in the spanner (with some safety margin added) corresponded to a 23,500 N preload—thus giving a preload window from 19 kN to 23.5 kN. The results of a 22,000 N "middle" preload are also shown for completeness.

Since the friction factor has both a large range and physical effect, the maximum torque value that the spanner wrench can safely transmit is chosen as the maximum torque value. The variability of the friction factor makes this input torque correspond to more than one preload. Therefore, a range of acceptable torque values is specified. The range was chosen at $f = 0.12$, so it spans between 138-165 ft-lbs. This range prevents over tightening of the wrench that could cause failure and ensures adequate preload to prevent bearing pull-out is in place. However, the question still remains as to what the clamping force on the H-COM 19 ball is.

2 15/16 - 32	Total Torque Req'd [ft-lbf]	Preload [N]	lead (pitch) [inch]	major diameter [inch]	mean diameter (inch)	friction coeff	1/2 thread angle (alpha)	Axial Stress [psi]	Nominal shear stress [psi]	Nom. bearing stress (5 T) [psi]	Thread root bending stress (5T) [psi]	Thread root shear stress (5T) [psi]	Von Mises Stress (5T) [psi]
	128.1	19500	0.03125	2.938	2.9240	0.11	30.0	659	317	-6109	18411	9205	18757
	138.2	19500	0.03125	2.938	2.9240	0.12	30.0	659	343	-6109	18411	9205	18758
	148.3	19500	0.03125	2.938	2.9240	0.13	30.0	659	368	-6109	18411	9205	18760
	158.4	19500	0.03125	2.938	2.9240	0.14	30.0	659	393	-6109	18411	9205	18761
	168.6	19500	0.03125	2.938	2.9240	0.15	30.0	659	418	-6109	18411	9205	18763
	178.7	19500	0.03125	2.938	2.9240	0.16	30.0	659	443	-6109	18411	9205	18765
	188.8	19500	0.03125	2.938	2.9240	0.17	30.0	659	468	-6109	18411	9205	18766

2 15/16 - 32	Total Torque Req'd [ft-lbf]	Preload [N]	lead (pitch) [inch]	major diameter [inch]	mean diameter (inch)	friction coeff	1/2 thread angle (alpha)	Axial Stress [psi]	Nominal shear stress [psi]	Nom. bearing stress (5 T) [psi]	Thread root bending stress (5T) [psi]	Thread root shear stress (5T) [psi]	Von Mises Stress (5T) [psi]
	144.5	22000	0.03125	2.938	2.9240	0.11	30.0	743	358	-6892	20771	10386	21117
	155.9	22000	0.03125	2.938	2.9240	0.12	30.0	743	386	-6892	20771	10386	21119
	167.3	22000	0.03125	2.938	2.9240	0.13	30.0	743	415	-6892	20771	10386	21121
	178.8	22000	0.03125	2.938	2.9240	0.14	30.0	743	443	-6892	20771	10386	21122
	190.2	22000	0.03125	2.938	2.9240	0.15	30.0	743	471	-6892	20771	10386	21124
	201.6	22000	0.03125	2.938	2.9240	0.16	30.0	743	500	-6892	20771	10386	21126
	213.0	22000	0.03125	2.938	2.9240	0.17	30.0	743	528	-6892	20771	10386	21128

2 15/16 - 32	Total Torque Req'd [ft-lbf]	Preload [N]	lead (pitch) [inch]	major diameter [inch]	mean diameter (inch)	friction coeff	1/2 thread angle (alpha)	Axial Stress [psi]	Nominal shear stress [psi]	Nom. bearing stress (5 T) [psi]	Thread root bending stress (5T) [psi]	Thread root shear stress (5T) [psi]	Von Mises Stress (5T) [psi]
	154.3	23500	0.03125	2.938	2.9240	0.11	30.0	794	383	-7362	22187	11094	22605
	166.5	23500	0.03125	2.938	2.9240	0.12	30.0	794	413	-7362	22187	11094	22606
	178.7	23500	0.03125	2.938	2.9240	0.13	30.0	794	443	-7362	22187	11094	22608
	190.9	23500	0.03125	2.938	2.9240	0.14	30.0	794	473	-7362	22187	11094	22610
	203.1	23500	0.03125	2.938	2.9240	0.15	30.0	794	504	-7362	22187	11094	22612
	215.4	23500	0.03125	2.938	2.9240	0.16	30.0	794	534	-7362	22187	11094	22614
	227.6	23500	0.03125	2.938	2.9240	0.17	30.0	794	564	-7362	22187	11094	22616

Table A1-4: Spreadsheet calculations for the required assembly torque of the 10223-DT-422 bearing retaining ring torque as a function of thread geometry, preload, and friction coefficient is shown. By choosing a friction coefficient of 0.12 as the nominal, an assembly torque range of 138 – 165 ft-lbs is chosen. Since the actual friction coefficient of the assembly may vary, this guarantees both adequate preload.

Part 4: Determining 10223-DT-427 Clamping Force at Calculated Locking Torque

Constraints:

Since all forces shown in Figure A1-2 are accounted for, the entire assembly can now be analyzed for clamping force and locking torque. All of the loads and their calculations have now been discussed in detail. The details of the FEA analysis remain. Since the bearing races are sitting in a bore with a "locational fit" of -0.000" +0.001", this essentially means both races are radially constrained. Additionally, since the bottom bearing ring rests at the bottom of the bore, it is axially constrained, preventing it from motion due to compression. The FEA was set to a "No penetration" global contact. This means that when components come into contact with each other, they deform but never penetrate each other, no matter what the load is. This contact set ensures that the bearing/race interactions are modeled as they occur in reality. Since the loads are low relative to the bearing rating [**33**], there is no danger of incorrectly modeling the interaction due to penetration or inelastic deformation.

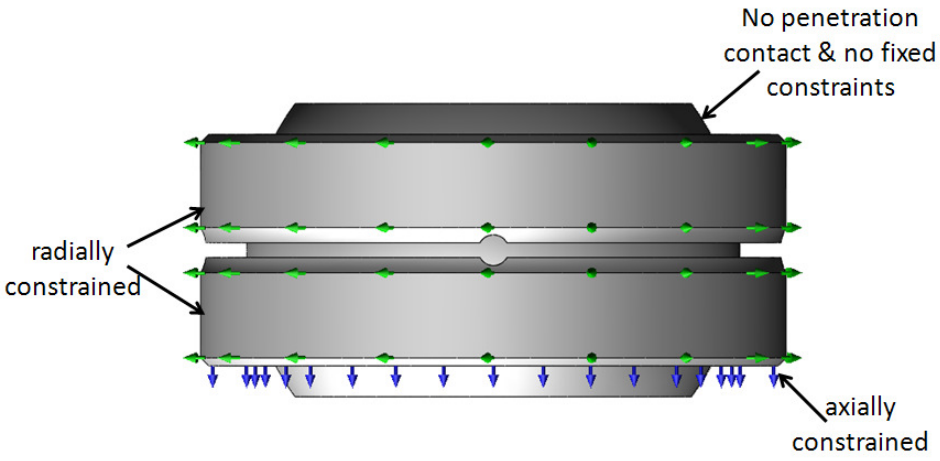

Figure A1-5: Constraints for FEA analysis are shown. Green arrows represent radial constraints, and blue arrows represent axial constraints. No constraints were applied to the H-COM 19 ball beyond the no-penetration contact condition. Note: Directions of the colored arrows are not important since they represent a fixed geometry i.e. a displacement of 0 mm.

Meshing & Mesh Control:

With the constraints and forces in order, what remains is the mesh. The prime area of concern is the interface between the outer H-COM 19 ball surface and the bearing surfaces of the 10223-DT-427 races, specifically in the area at which the X-Y plane bisects the assembly. Therefore a split-line was added to the surface of the H-COM 19 ball at precisely this location prior to meshing. This will ensure that enough nodes reside on the split-line to be able to probe this feature and provide a clear understanding of the behavior at the interfaces.

The mesh consists of two main types: the solid mesh, and the mesh controlled feature. The solid mesh needs only to be of fine enough detail to be able to gather an overall picture of what is happening, and it must not add too many nodes as this has a dramatic effect on the degrees of freedom and therefore calculation time. This mesh is applied to all surfaces/solids that are not the prime focus, i.e. not the ball/race interface. Conversely, the mesh control area, i.e. the ball/race interface, must have a large number of elements so that the detail of the contact pressure can be seen both visually and tracked numerically along the added split-line. Too few elements can cause an aliasing-like effect whereby significant portions of the behavior under load are lost due to the lack of adequate nodes in the vicinity.

The mesh parameters applied here are as follows:

SOLID MESH

- 0.5-2.5 mm tetrahedral element size
- Curvature based mesh (acts as an automatic mesh control on curved features to increase resolution)
- 1.6 element size growth ratio
- 8 elements minimum per circle

MESH CONTROL

- 0.95mm tetrahedral element size
- 1.5 element size growth ratio

The mesh network is shown visually in the figure below. The split-line detail is now visible as this view is a projection along the Y-Z plane, not the X-Y plane as all previous figures have been.

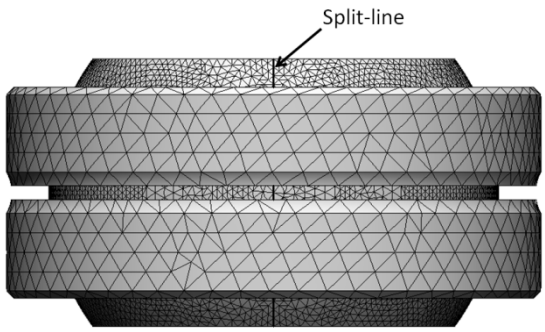

Figure A1-6: The meshed solid with mesh controls on the surface of the H-COM 19 ball and bearing surfaces is shown. The split-line feature has been made thicker graphically to emphasize its position. There are numerous nodes along the length of the split-line. When probed, these act as data sample points that indicate the behavior at the ball/race interface.

Three different 10223-DT-422 preload cases were run at: 19,500 kN, 22,000 kN, 23,000 kN. All other loads and constraints remained constant. The figure below shows the resultant behavior under load common to all 3 cases. No scale is shown because the magnitudes of the forces are not important for this illustration, only the behavior of the part under load and where the stress "hot spots" are located. What is shown is not a graph of the contact pressure (which is what is ultimately needed) but rather a Von Mises equivalent stress that captures general behavior.

The peak contact stress occurs where the sharp corners of the bearing surface are pressed into the surface of the H-COM 19 ball. The stress rapidly drops off along the added split-line feature. Figure A1-7 is merely a visual aid to understand the behavior of the components. No real results are shown.

Solidworks Simulation 2010 has the ability to use contact conditions and geometric constraints to calculate a contact pressure between 2 or more surfaces. This calculation along with the "probe" feature—which allows the user to get the geometric

location and stresses at specific nodes individually, or along a set path e.g. a split-line—were used to create Figure A1-8.

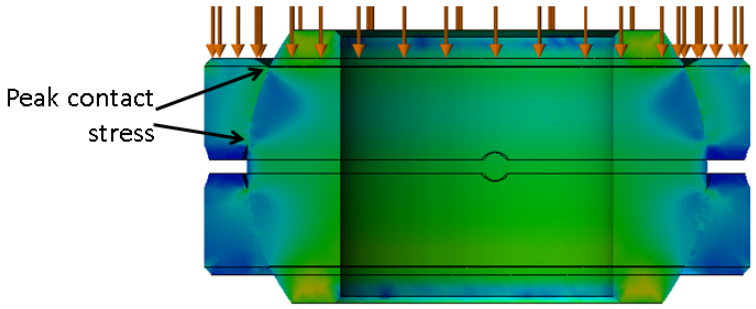

Figure A1-7: A cross-sectional stress plot at the X-Y plane. Peaks occur at the surface of the H-COM 19 ball where the sharp corners of the bearing surface of the 10223-DT-427 races come into contact. The stress rapidly drops off along the perimeter away from these contact points. However, a later 'contact pressure' study shows that in fact all of the bearing surface is in contact with the ball, but the largest stresses are at these locations.

The three preload cases discussed above were applied to the model while keeping all else constant. The contact pressure along the surface of the H-COM 19 ball surface in contact with the races on the positive X side (the model is assumed to be symmetric) is shown in Figure A1-8. Peak pressures that occur at the sharp contact surfaces behave almost as singularities. He slight changes in mesh height and number that occur randomly with mesh generation determine the resolution at this point. That is why the lowest preload appears to have the highest peak contact stress.

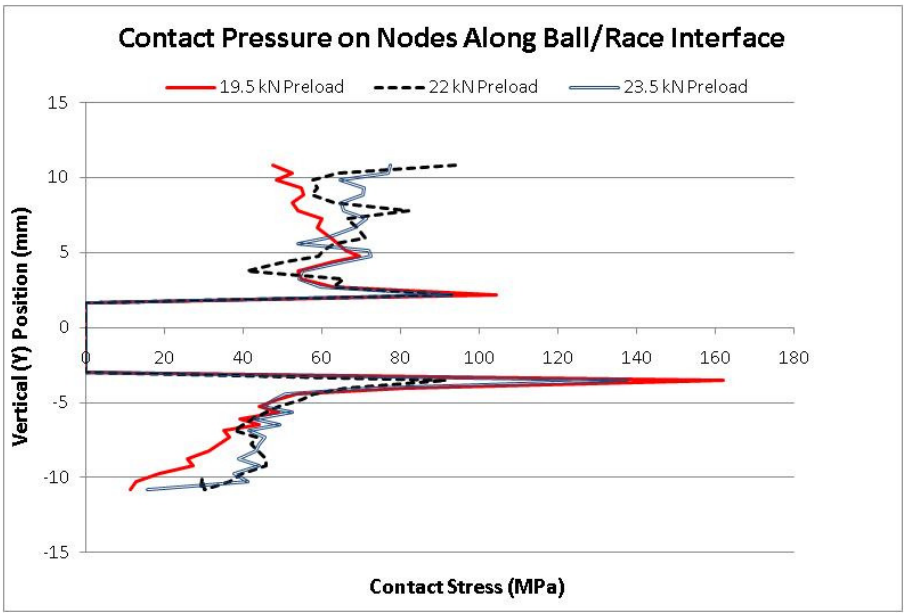

Figure A1-8: The contact pressures along the H-COM 19 ball surface at the ball/race interface for three cases of retaining ring preload (minimum recommended, maximum recommended, and intermediary) are shown. The peak stresses act almost as singularities at the areas of peak stress-as expected. These results are then averaged by case to determine the clamping force.

Since these numbers are of no real use at the nodal level, they are averaged first by hemi-sphere then in totality. These average contact pressures are then used to find a clamping force and holding torque of the clamped strut-end (see Table A1-5).

Contact Pressure Averages (in Mpa)			
	19.5 kN	*22.0 kN*	*23.5 kN*
Pos. Y	60.2	65.4	67.5
Neg. Y	44.3	45.8	49.9
Total	52.2	55.6	58.7

Table A1-5: Average contact pressures at the ball/race interface for three different retaining ring preloads are shown. They are averaged by hemisphere first to show the diminishing effect of the preload with distance, then totally to use this value in calculation of the clamping force and holding torque of each strut end.

These contact pressures are used with the following relation [**37**] to calculate maximum safe torque capacity of the clamped bearing assembly.

$$T_{capacity} = \frac{\pi f P_{contact_{minimum}} l d^2}{2} \qquad \textit{Eq A1-15}$$

where f is the minimum friction factor for lubricated steel-on-steel contact, $P_{contact_{minimum}}$ is the minimum average contact pressure shown in Table A1-5—52.2 MPa, l is the arc length of total contact—approximately 17 mm, and d is the diameter of the H-COM 19 ball—25.4 mm.

By the calculation above, the maximum torque that the locked bearing assembly can safely resist is 98.9 N-m (66.4 lbf-ft) per locking assembly.

Appendix 2

10223-DT-015 (LOWER RHO BLOCK) ANALYSIS

Section 1: Summary of loads

There are two distinct areas of loading in 10223-DT-015. The first is the shoulder that supports the H-COM 19 bearing assembly, and the second is the rear that acts as a support for the work platforms/electronics boxes that were added late in the design process by MDO.

The load on the shoulder consists of a superposition of the maximum axial design load of 12 kN through the strut and the maximum axial preload of 23 kN imposed by torquing 10223-DT-422 to specification. This comes out to a total axial load of 35 kN if taken to act in the worst-case direction. A non-trivial Von Mises stress of approximately 186 MPa is also induced in the threaded bore area by the preload on 10223-DT-422 as calculated in the final column of Table A1-4; however, this load is not included in the following FEA analysis.

The second load of concern in this analysis is the load on the flat surface on the rear of the Rho block. Threaded hole features accommodate the mounting hardware for work platforms that have electronics housing boxes attached to them. These are expected to impart a 6 kN load on the flat surfaces of each 10223-DT-015. This load consists of the weight of the platforms and electronics boxes themselves plus some additional allowance for the weight of a technician or two and any tools they may be carrying.

Section 2: Constraints and loads

The 10223-DT-015 are mounted to the strongback using four M16 x 2.0 socket-head cap screws tightened to 90% proof load as recommended by [**37**] for permanent joints. To approximate this type of arrangement, the frustum method described in [**37**] is employed to calculate the diameter of the circle at the bottom of the pressure cone created by the bolted joint. For this configuration, the frustum diameter is approximately 44 mm. This diameter is then inserted into the model and separated from the rest of the solid through the use of split lines. Then these circles are held fixed instead of holding the

entirety of the contact surface fixed to more realistically simulate the bolted joint constraint in the FEA analysis. However, this approximation essentially means that the effective bolt stiffness is infinite which cannot occur in actuality. By making this approximation, the stresses in the block are amplified slightly as what is actually an elastic interface is being held perfectly rigid. This will lead to overestimation of the stresses in the block and therefore error on the side of caution—which is desirable. So long as this analysis is not used to determine the proper bolt torque or any other examination of the mounting configuration, this approximation is not a problem.

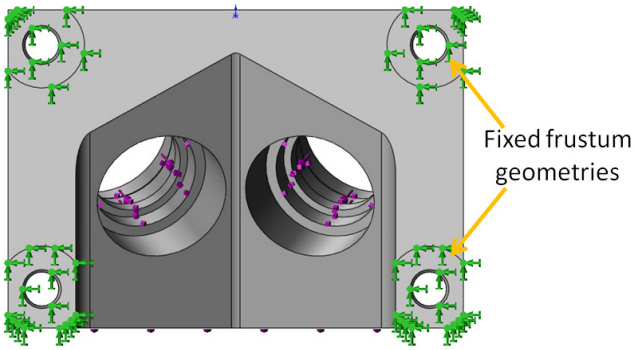

Figure A2-1: The flat underside of 10223-DT-015 is shown. Split lines were used to make the circular geometry that arises from the frustum method of analysis of bolted joints. These split geometries are held fixed to produce a more accurate model of the joint than merely holding the whole face fixed [**30**].

As discussed in the summary of loads, the load on the shoulder bore that support the bearing structure is a combination of maximum expected axial load, including a 50% safety margin, and the maximum expected load from the 10223-DT-422 retaining ring. This total load is 35 kN applied directly to the shoulder. This is likely an overestimate of the load, but it will provide sufficient data for examining stress concentrations and making sure the component is up to task of supporting these loads.

In actual service there are likely to be some off-axis loads arising from bending in the locked strut or components of the predominantly axial load that act off-axis. These loads were not examined as the worst-case loading scenario is the axial load applied directly to the normal face of the supporting shoulder within the bore.

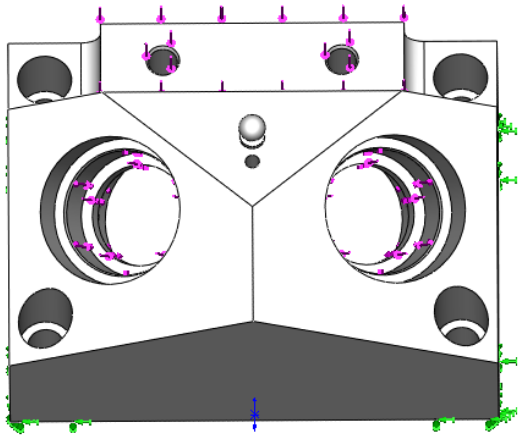

Figure A2-2: Load applied for FEA analysis on the bearing bore and work platform support plane are shown graphically [**30**].

In addition to the loads in the bore, there is also a 6 kN load on the rear upper surface of 10223-DT-015. This load is quite small and almost negligible with regards to examination of deformations and displacements of the shoulder within the bore and the overall strength of the component but is added here for completeness.

Section 3: Mesh parameters

The areas of interest in this analysis are within the bores, namely the internal corners of the bearing support shoulder bore, the mesh used must be of sufficient density to accurately model the physical phenomenon that is occurring in this area. However, a dense solid mesh applied to the entire model would unnecessarily increase the element and node count thus requiring more computation time and computer resources. Therefore a mesh control along with a curvature-based mesh was used to increase mesh density where needed but keep the computation time low enough to be reasonable without sacrificing to much accuracy.

First a curvature-based solid mesh was applied to the entire model. This type of mesh automatically increases the element and node count on rounded features so that more accurate results are obtained. The tetrahedral elements contained 4 Jacobian points and ranged from minimum 3.237 mm to 16.186 mm in size. The curvature sensitivity was set adjust element size to have to have a minimum of 8 elements in a given circle. The element size growth ratio was 1.6.

The mesh control was applied to all flat surfaces on the bored features of interest. These elements were set to 2.927 mm in size with an element ratio of 1.5. This allowed there to be at least 2 elements across the normal face of the shoulder and 4 elements across the depth. A graphical representation of the mesh overlaid on the solid model with these controls applied is shown in Figure A2-3 below.

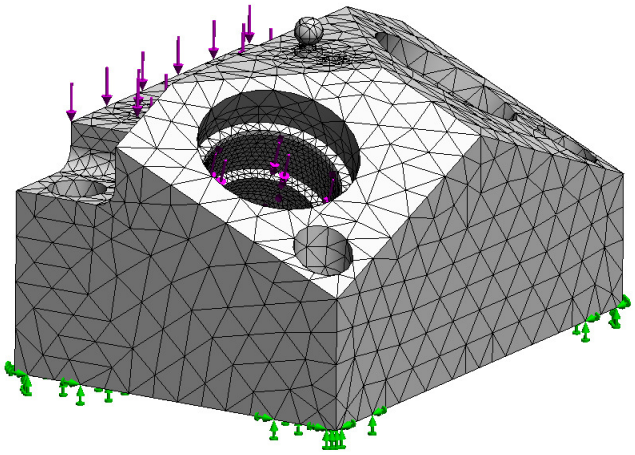

Figure A2-3: The solid mesh is shown overlaid on the solid model with constraints represented by green arrows and loads represented by purple arrows. The mesh control in the bore created a much denser mesh where needed while the overall mesh was coarse. Mesh density increases automatically around curved features due to the applied curvature-based mesh [**30**].

Section 4: FEA results

Ignoring the stress in the threads from the 10223-DT-422 retaining ring, the highest calculated Von Mises stress was 83 MPa in the corners of the bearing support shoulder with maximum equivalent displacement of around 14 microns at the innermost surface of the bearing support shoulder. Both of these numbers are very small and well

below the yield stress and maximum strain to plasticity. A shift of 14 microns in the bearing location is likely to impart a negligible bending moment into the strut. Aside from the stresses in bore corners, the FEA analysis revealed some stresses in the inner radius of the two support legs of around 50 MPa. Other significant stresses are due to the fixed geometry arising from the frustum method of constraint that should be disregarded since they are not indicative of reality. A section-view through one of the bearing bores showing the areas of highest stress is shown in Figure A2-4 below. For reference, Figure A2-4 is the same view as Figure 4-7 except this has the FEA stress map overlaid.

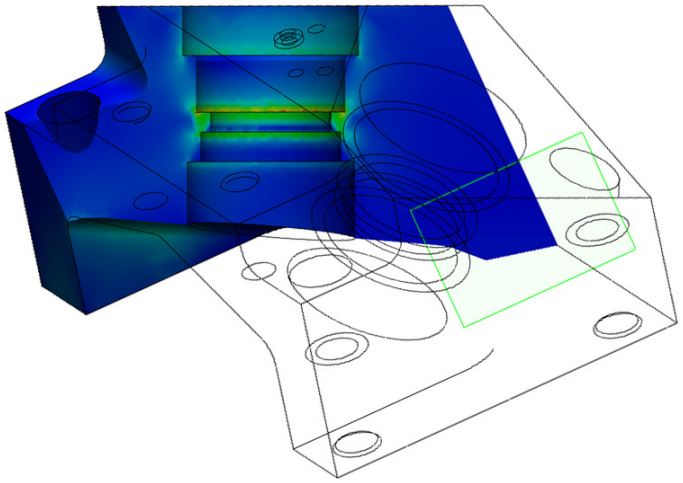

Figure A2-4: A section-view of 10223-DT-015 through a bearing bore at maximum load is shown [**30**].

Although these results were generated using the 10223-DT-015 Rho block stresses found using this FEA method are valid for the bored features on 10223-DT-083 block as well. Equivalent displacement values on the 10223-DT-083 block are somewhat lower since there is more material along the load axis and this material contacts the Rho stage. See Appendix 3 for more detail.

Appendix 3

10223-DT-083 (Upper Rho Block) Analysis

Section 1: Summary of loads

Unlike 10223-DT-015, there is only one primary area of loading in 10223-DT-083, and it is the shoulder that supports the H-COM 19 bearing assembly. This load also consists of a superposition of the maximum axial design load of 12 kN through the strut and the maximum axial preload of 23 kN imposed by torquing 10223-DT-422 to specification. This comes also out to a total axial load of 35 kN, and it is taken to act in the worst-case direction. A non-trivial Von Mises stress of approximately 186 MPa is also induced in the threaded bore area by the preload on 10223-DT-422 (see the last column of Table A1-4); however, this load is not included in the following FEA analysis.

Section 2: Constraints and loads

The 10223-DT-083 are mounted to the underside of the Rho stage using four M16 x 2.0 socket-head cap screws tightened to 75% proof load as recommended by [**37**] for removable joints. The frustum method in [**37**] is also used in this instance. In this case, the frustum diameter is approximately 19.6 mm. Aside from the difference in frustum diameter, there constraints are exactly like those listed in Appendix 2 for 10223-DT-015.

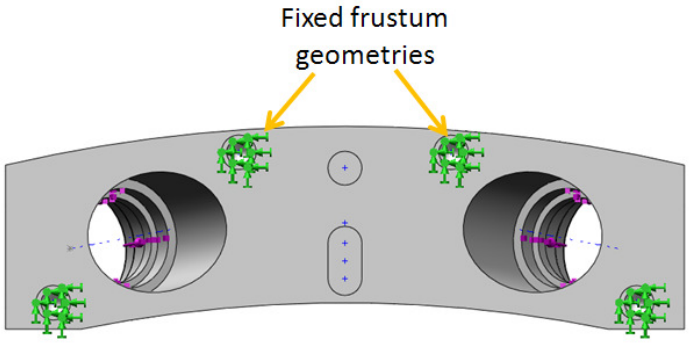

Figure A3-1: Fixed frustum geometries are shown on the underside of 10223-DT-083. These geometries act as perfectly rigid constraints to approximate a bolted joint [**32**].

Section 3: Mesh parameters

As with the 10223-DT-015, the areas of interest in this analysis are within the bores, namely the internal corners of the bearing support shoulder bore, the mesh used must be of sufficient density to accurately model the physical phenomenon that is occurring in this area. Because of the similarities, the exact same mesh parameters, controls, and element sizes as those used on 10223-DT-015 were employed. Please see Appendix 2, Section 3 for more details.

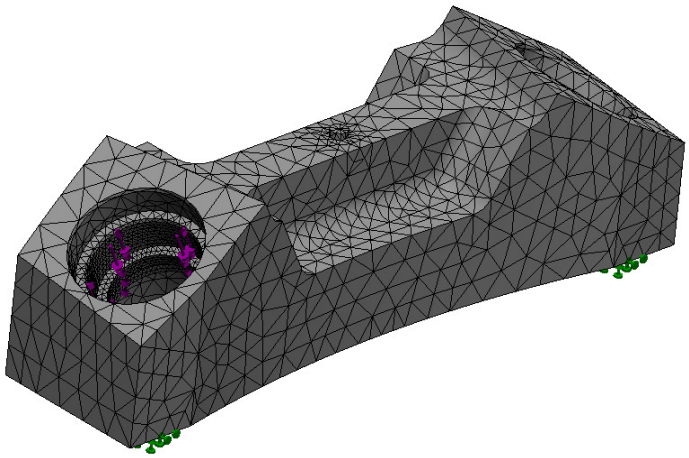

Figure A3-2: The solid curvature-based mesh with appropriate controls is shown overlaid on 10223-DT-083. Constraints are shown in green while loads are shown in purple arrows [**32**].

Section 4: FEA results

A section view through the center of the bore is shown in Figure A3-3. According to probes of nodes in the proximity of the loaded corner Von Mises stress levels remain below 50 MPa, and equivalent displacement is no greater than 11 microns. As discussed in Appendix 2, Section 4, these numbers are slightly lower than those calculated for 10223-DT-015 due to the contact of the nut-side of the bore with a flat surface and not raised as in the lower Rho block.

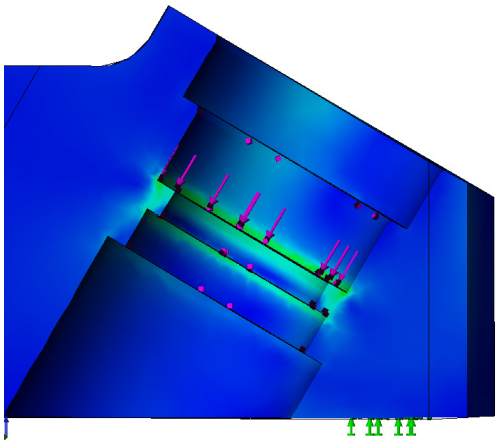

Figure A3-3: A section-view through the center of one loaded bearing bore geometry on 10223-DT-083 is shown.

Appendix 4

ADJUSTMENT MECHANISM ANALYSIS

Section 1: Summary of loads

As discussed in Appendix 1, the primary load on each strut is an axial load of 12 kN including a 50% safety margin in a worst-case scenario. The exact load is different for each strut, and it depends highly on the orientation of the platform. However, some degree of axial load is ever present within the strut and the adjustment mechanism. There are additional loads within the adjustment mechanism that arise due to either raising or lowering the load and only come into play during the adjustment process. It is these loads that will be addressed in this appendix.

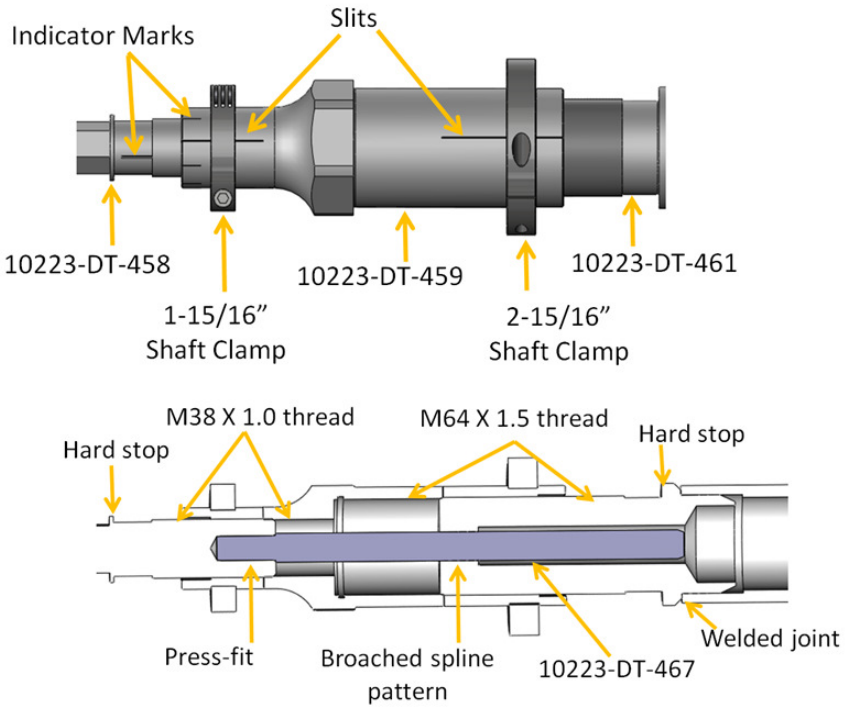

Figure A4-1: Figure 2-7 from Chapter 2 identifying components and features of the adjustment mechanism is reprinted here for reference.

The loads arising from raising or lowering the payload come from interactions in the threads when a torsional load is applied to 10223-DT-459 during adjustment. Despite there being motion, it is very slow, so the system will be treated as quasi-static. The loads to be identified then are as follows:

- Input torque required to raise and lower the load
- Resultant torsional loads on all components
- Minimum press fit required to transmit load along spline

Section 2: Calculation of loads

Part 1: Determining Torque to Raise/Lower Load

Resistance to raising or lowering the load comes from frictional intereactions within the thread and the axial load applied to the strut. There are two separate thread pitches to consider in the adjustment mechanism, M38 X 1.0 and M64 X 1.5.

To reiterate, the adjustment mechanism works by holding 10223-DT-458 stationary using the hexagonal flats just below the hard stop feature and applying a torsional load using a large wrench to the flats on the outer diameter of 10223-DT-459. The splined shaft along the length of the internal of the adjustment mechanism angularly couples 10223-DT-458 and 10223-DT-461 while allowing relative axial motion between the two parts. Because both threads are right handed, a clockwise rotation of 10223-DT-459 will advance the M64 X 1.5 thread and retreat the M38 X 1.0, and vice-versa for a counter-clockwise rotation. This means that while one thread is effectively lowering the load the other is raising it. Therefore in determining total torque required to rotate 10223-DT-459, it is necessary to determine the torque required to raise a 12 kN load with an M64 X 1.5 thread and lower the same load in an M38 X 1.0 and add them, then reverse the action for axial motion in the other direction.

The relations used to determine the torque required are similar in nature. They are as listed below [**37**]:

$$T_{raise} = \frac{F_{strut\ load} * d_{nominal}}{2}\left(\frac{l + \pi f d_{nominal} \sec\alpha}{\pi d_{nominal} - f l \sec\alpha}\right) \qquad \textit{Eq A4-1}$$

$$T_{lower} = \frac{F_{strut\ load} * d_{nominal}}{2}\left(\frac{\pi f d_{nominal} \sec\alpha - l}{\pi d_{nominal} + f l \sec\alpha}\right) \qquad \textit{Eq A4-2}$$

Based on these relations, torque is a function of the load on the strut, the nominal thread diameter, friction present, pitch, and lead angle. Each of the variables present in these relations are defined in Appendix 1.

Because friction plays such a dominant role, the first round of analysis was done with the threads treated as if they were lubricated with grease for a coefficient of friction between 0.11 and 0.17. The results of this analysis are shown in Table A4-1.

M64 x 1.5 Raising load	Total Torque Req'd [ft-lbf]	Friction Torque [ft-lbf]	Thread Torque [ft-lbf]	Preload [lbf]	lead (pitch) [inch]	friction coeff	Axial Stress [psi]	Nominal shear stress [psi]	Von Mises Stress (ST) [psi]
	69.6	17.33	52.24	2700	0.05906	0.11	1393	24	7086
	98.5	26.78	71.73	2700	0.05906	0.17	1393	33	7091
M38 x 1.0 Lowering load	Total Torque Req'd [ft-lbf]	Friction Torque [ft-lbf]	Thread Torque [ft-lbf]	Preload [lbf]	lead (pitch) [inch]	friction coeff	Axial Stress [psi]	Nominal shear stress [psi]	Von Mises Stress (ST) [psi]
	31.9	17.33	14.56	2700	0.03937	0.11	2351	52	17944
	52.8	26.78	26.06	2700	0.03937	0.17	2351	86	17962
M38 x 1.0 Raising load	Total Torque Req'd [ft-lbf]	Friction Torque [ft-lbf]	Thread Torque [ft-lbf]	Preload [lbf]	lead (pitch) [inch]	friction coeff	Axial Stress [psi]	Nominal shear stress [psi]	Von Mises Stress (ST) [psi]
	45.0	17.33	27.71	2700	0.03937	0.11	2351	73	17955
	66.0	26.78	39.27	2700	0.03937	0.17	2351	108	17973
M64 x 1.5 Lowering load	Total Torque Req'd [ft-lbf]	Friction Torque [ft-lbf]	Thread Torque [ft-lbf]	Preload [lbf]	lead (pitch) [inch]	friction coeff	Axial Stress [psi]	Nominal shear stress [psi]	Von Mises Stress (ST) [psi]
	36.4	17.33	19.04	2700	0.05906	0.11	1393	12	7081
	65.2	26.78	38.43	2700	0.05906	0.17	1393	22	7086

Table A4-1: Spreadsheet calculations for the torque required to rotate 10223-DT-459 during the adjustment process. The top two sets are additive pairs as well as the bottom two. Results shown are indicative of friction values present in greased threads. Other stress values are from stresses induced in the threads during adjustment.

Later in the design process just before a full redesign of the spline coupling, a vendor recommended Lubri-Bond A, a dry film lubricant, for this application. Its specified friction coefficient ranges from 0.02 – 0.04 [**43**], a nearly 3 fold decrease from greased threads [**37**]. Results for this range are shown in Table A4-2.

M64 x 1.5 Raising load	Total Torque Req'd [ft-lbf]	Friction Torque [ft-lbf]	Thread Torque [ft-lbf]	Preload [lbf]	lead (pitch) [inch]	friction coeff	Axial Stress [psi]	Nominal shear stress [psi]	Von Mises Stress (5T) [psi]
	26.2	3.15	23.05	2700	0.05906	0.02	1393	9	7079
	35.8	6.30	29.53	2700	0.05906	0.04	1393	12	7081

M38 x 1.0 Lowering load	Total Torque Req'd [ft-lbf]	Friction Torque [ft-lbf]	Thread Torque [ft-lbf]	Preload [lbf]	lead (pitch) [inch]	friction coeff	Axial Stress [psi]	Nominal shear stress [psi]	Von Mises Stress (5T) [psi]
	0.4	3.15	-2.71	2700	0.03937	0.02	2351	1	17918
	7.4	6.30	1.13	2700	0.03937	0.04	2351	12	17924

M38 x 1.0 Raising load	Total Torque Req'd [ft-lbf]	Friction Torque [ft-lbf]	Thread Torque [ft-lbf]	Preload [lbf]	lead (pitch) [inch]	friction coeff	Axial Stress [psi]	Nominal shear stress [psi]	Von Mises Stress (5T) [psi]
	13.5	3.15	10.39	2700	0.03937	0.02	2351	22	17929
	20.5	6.30	14.24	2700	0.03937	0.04	2351	33	17935

M64 x 1.5 Lowering load	Total Torque Req'd [ft-lbf]	Friction Torque [ft-lbf]	Thread Torque [ft-lbf]	Preload [lbf]	lead (pitch) [inch]	friction coeff	Axial Stress [psi]	Nominal shear stress [psi]	Von Mises Stress (5T) [psi]
	-6.9	3.15	-10.09	2700	0.05906	0.02	1393	-2	7073
	2.7	6.30	-3.61	2700	0.05906	0.04	1393	1	7075

Tables A4-2: Spreadsheet calculations for the torque required to rotate 10223-DT-459 during the adjustment process using the published maximum friction coefficient of Lubri-Bond A. The top two sets are additive pairs as well as the bottom two. Note: the final set shows a negative torque for a "self-locking" condition, however the additive nature of this configuration shows that adjustment still requires a positive input torque to rotate.

The purpose of finding the required input torque is not to specify a torque but to predict the maximum load seen by components in the adjustment mechanism in order to properly size and select material for them. With this in mind, knowing that the actual torque required is likely to be much lower—and therefore the components used are likely

to be robust—the maximum expected design torque was selected to be 110 ft-lbs, the result of adding the minimum torque results from Table A4-1 from the first additive set. This choice builds in a natural safety margin that ensures the components will not fail during the adjustment process.

Figure A4-2 shows a graphical representation of the reaction that occurs when an input torque is applied to the adjustment mechanism. The selected values from in Table A4-1 can be substituted for the generic terms "Input Torque", "M64 Reaction Torque", and "M38 Reaction Torque".

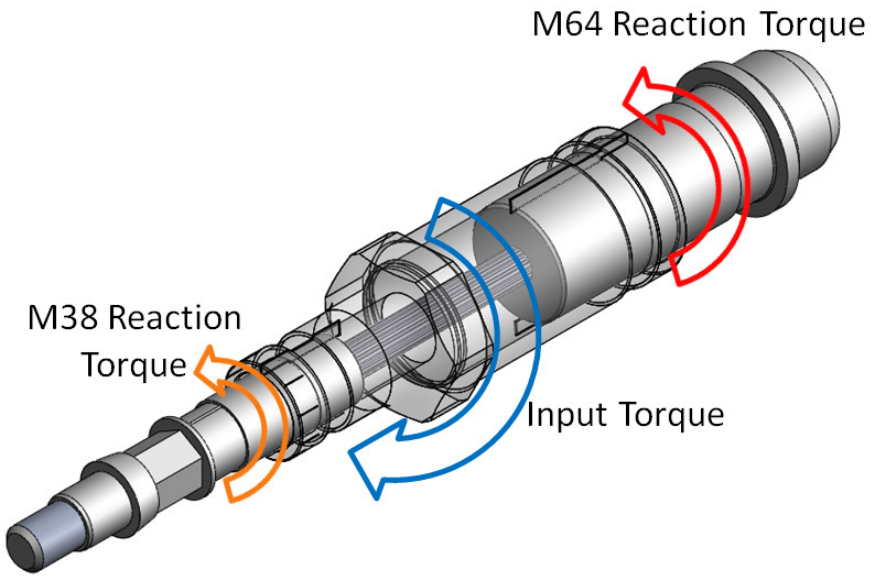

Figure A4-2: Graphical representation of the input and reaction torques that arise during the adjustment process.

Section 2: Effects of torque on 10223-DT-461 geometry

Part 1: Assumptions

To ensure worst-case stresses are used in the design and sizing of components, no torque required to overcome angular deflections due to non-infinite torsional stiffnesses were considered. Additionally, even though the spline shaft is likely seeing only the difference between the two reaction torques (since the torques act in the same direction) it will be treated as if the full 110 ft-lbs (150 N-m) is applied to the M64 end and the M38

end is fixed. The splined shaft will be modeled as a solid rod of diameter equal to the root diameter of the spline profile. These assumptions ensure the splined shaft coupling will withstand a worst case scenario.

Part 2: Determining minimum spline root diameter

Given 150 N-m of torque applied to the splined shaft and the Von Mises yield-criterion estimate of the modulus of rupture it is possible to find the minimum root radius that can be used in this application [**37**]. Equation A4-3 shows this relationship.

$$r_{min} = \left(\frac{2 * T_{applied}}{0.577 \pi \sigma_{yield}} \right)^{1/3} \qquad \textit{Eq A4-3}$$

Where r_{min} is the minimum root radius of the splined shaft that can be used in this configuration at this applied torque, $T_{applied}$ is the applied torque, and σ_{yield} is the yield strength of the chosen material.

Since a stainless steel would eliminate the need for a nitrocarburizing process and is an available material from which to obtain the spline, it would be an ideal choice. The minimum root radius for 316L stainless steel is 5.1 mm for a minimum root diameter just under 0.4".

So now any size 316L spline shaft above 0.4" in root diameter can be used. However, there are a few more requirements. The first is the press fit.

Part 3: Spline press fit analysis

Rearranging Eq A1-15 for pressure required in the press fit give the following relation:

$$P_{press\ fit} = \frac{2T_{applied}}{\pi f l d^2} \qquad \textit{Eq A4-4}$$

where $P_{press\ fit}$ is the pressure required of the press fit, f is the coefficient of friction present in the press fit, l is the depth of the hole into which the shaft is pressed, and d is the nominal diameter of the shaft.

An additional complication arises in that the hole for the press fit needs to be of low enough diameter that it does not risk damaging the M38 threaded component, 10223-DT-458. This puts an upper cap on the splined shaft diameter.

The length, diameter, and interference were then solved for while using Eq A1-8 from Appendix 1, Section 2, Part 2 using the methods described therein.

This resulted in a nominal press fit diameter of 15.87 mm, 38 mm deep, with an interference of 5 microns minimum.

Part 4: Spline fillet geometry

The final critical area is the transition radius that takes 10223-DT-467 from the press fit diameter to the full spline at the end of the press fit. This radius must be large enough that the stress concentration factor it induces does not cause the splined shaft to fail when loaded at the maximum design load.

Professor Alexander Slocum created a design spreadsheet for his 2.007 class that incorporated common shaft geometries that includes the one seen in this situation. This spreadsheet was then slightly modified and used to find the maximum stress expected at the fillet using the design load.

Large diameter, D [mm]	**16.103**
Small diameter, d [mm]	**15.875**
Shaft torque (N-m)	**150.000**
Major shaft diameter [mm]	**16.103**
transition radius (mm)	**0.25**
Fillet stress concentration factor, Kt	**1.24**
Shaft length (mm)	**150**
Shaft modulus, E (GPa)	**2.05E+11**
Shaft Poisson ratio	**0.29**
Shear modulus, G (GPa)	**7.95E+10**
Fillet design torsion stress (MPa)	**236.4**

Table A4-9: Spreadsheet calculations for the stress induced at the fillet at the end of the press fit that arises from the input torque. By changing the transition radius for a given pair of diameters, torsional load and material properties, the spreadsheet will calculate the approximate stress concentration factor and stress in the fillet [**50**].

Bibliography

[1] "Scanning the Universe with the Hobby-Eberly Telescope," *Sky & Telescope*, vol. 98, no. 4, pp. 24-25, October 1999.

[2] Thomas A. Sebring, "Hobby-Eberly Telescope Cuts Costs to Track Stars," *Laser Focus World*, vol. 33, no. 7, pp. 75-81, July 1997.

[3] McDonald Observatory. HETDEX Website. [Online]. http://hetdex.org/hetdex/het.php

[4] McDonald Observatory. HETDEX Website. [Online]. http://hetdex.org/dark_energy/discovery.php

[5] Adam G. Reiss et al., "Observational Evidence From Supernovae For An Accelerating Universe And A Cosmological Constant," *The Astronomical Journal*, vol. 116, pp. 1009-1038, September 1998.

[6] S. Perlmutter et al., "Measurements of Omega and Lamda From 42 High-Redshift Supernovae," *The Astrophysical Journal*, vol. 517, pp. 565-586, June 1999.

[7] McDonald Observatory. HETDEX Website. [Online]. http://hetdex.org/dark_energy/index.php

[8] McDonald Observatory. HETDEX Website. [Online]. http://hetdex.org/dark_energy/what_is_it/

[9] Gary J. Hill, Karl Gebhardt, Eiichiro Komatsu, and Phillip J. MacQueen, "The Hobby-Eberly Telescope Dark Energy Experiment," in *AIP Conference Proceedings*, vol. 743, 2004, pp. 224-233.

[10] Karen Olsson, "The Final Frontier," *Texas Monthly*, vol. 36, no. 4, pp. 162-169, April 2008.

[11] Center for Electro-Mechanics HETDEX Team, HETDEX Upgrade Rendering, 2010, Contains models created by members of the CEM HETDEX team, model rendering by Rex Jackson, and graphic work by Patrice Palmer.

[12] Richard Hayes, HETDEX Tracker and Fiber Management System Specification DRAFT, August 17, 2009, RF272 CEM Internal Document.

[13] J.C Faugere and D. Lazard, "Combinatorial Classes of Parallel Manipulators," *Mechanical Machine Theory*, vol. 30, no. 6, pp. 765-776, 1995.

[14] Xiao-Shan Gao, Deli Lei, Qizheng Liao, and Zhang Gui-Fang, "Generalized Stewart-Gough Platforms and Their Direct Kinematics," *IEEE Transactions on Robotics*, vol. 21, no. 4, pp. 141-151, April 2005.

[15] Carlo Innocenti and Vincenzo Parenti-Castelli, "A Novel Numerical Approach to the Closure of the 6-6 Stewart Platform Mechanism," in *Fifth International Conference on Advanced Robotics, "Robots in Unstructured Environments"*, 1991, pp. 851-855.

[16] Satheesh G. Kumar, M. Bikshapathi, T. Nagarajan, and Y.G. Srinivasa, "Stiffness Analysis and Kinematic Modeling of Stewart Platform for Machining

Applications," in *American Society of Precision Engineering Annual Proceedings*, Orlando, 2004, pp. 1516-1519.

[17] John McInroy, Farhad Jafari, and John O'Brien, "Tri-Symmetric Orthogonal Gough-Stewart Platforms," in *IEEE International Conference on Robotics and Automation*, Barcelona, Spain, 2005, pp. 936-941.

[18] Ping Ji and Wu Hongtao, "A Closed-Form Forward Kinematics Solution for the 6-6p Stewart Platform," *IEEE Transaction on Robotics and Automation*, vol. 17, no. 4, pp. 522-526, August 2001.

[19] Xiguang Huang, Qizheng Liao, and Shimin Wei, "Closed-Form Forward Kinematics for a Symmetrical 6-6 Stewart Platform Using Algebraic Elimination," *Mechanism and Machine Theory*, vol. 45, pp. 327-337, 2010.

[20] Tae-Young Lee and Shim Jae-Kyung, "Algebraic Elimination-Based Real-Time Forward Kinematics of the 6-6 Stewart Platform with Planar Base and Platform," in *IEEE International Conference on Robotics & Automation*, Seoul, Korea, 2001, pp. 1301-1306.

[21] Alexander Slocum. (2005) FUNdaMENTALS of Design on 2.007 Course Homepage. [Online]. http://stellar.mit.edu/S/course/2/sp09/2.007/materials.html

[22] Karl T. Ulrich and Steven D. Eppinger, *Product Design and Development*, 3rd ed. New York, United States of America: McGraw-Hill, 2003.

[23] McDonald Observatory, HET Operations Staff Requirements, January 14, 2008, Presentation to CEM by MDO.

[24] Center for Electro-Mechanics HETDEX Team, HETDEX Solid Model, 2010, Contains models made by members of the HETDEX team retrieved from the project database.

[25] Joseph Zierer, Hexapod, PFIP Support Structure, and Rho Stage, December 16, 2008, Presentation given at Critical Design Review I meeting with MDO.

[26] Joseph Zierer, PFIP Hexapod, Support Structure, and Rho Stage, May 29, 2008, Presentation given at Preliminary Design Review meeting.

[27] Richard Savage, SYSTEM LAYOUT DRAWING NO HX0037, 2009, McDonald Observatory Technical Drawing Sheet 1 of 4.

[28] McDonald Observatory and Center for Electro-Mechanics, Tracker Travel Range and Shim Requirements, July 16, 2009, HX0055-01-01 Internal Document.

[29] Joseph Zierer, Pupil Assembly Beam Force Summary, August 10, 2009, Internal CEM document.

[30] Center for Electro-Mechanics HETDEX Team, 10223-DT-015 Solid Model, 2010, Contains concept design work by Nick Mollison and Homar Molina and detail design work by Homar Molina and Rex Jackson.

[31] Center for Electro-Mechanics HETDEX Team, Upper Rho Assembly Solid Model, 2010, Contains models created by Joey Zierer, Rex Jackson, Sarah Hinze, and Homar Molina.

[32] Center for Electro-Mechanics HETDEX Team, 10223-DT-083 Solid Model, 2010, Contains concept work by Nick Mollison, Rex Jackson, and Homar Molina and detail work by Rex Jackson and Homar Molina.

[33] Aurora Bearing Company. 2003-04 Internet Catalog. [Online]. http://www.aurorabearing.com/Files/articles/2003-04_Internet_Catalog.pdf

[34] Center for Electro-Mechanics and McDonald Observatory, Preliminary Design Review, May 29, 2008, A meeting hosted by CEM in which concept-level design was discussed with members of MDO.

[35] Serope Kalpakjian and Steven R. Schmid, *Manufacturing Engineering and Technology*, 4th ed., Laura Curless et al., Eds. Upper Saddle River, New Jersey, United States of America: Prentice Hall, 2001.

[36] Nitreg Corporation. Nitreg and Nitriding - Heat Treating Solutions. [Online]. http://www.nitrex.com/english/metal_technologies.htm

[37] Richard Budynas and Keith Nisbett, *Shigley's Mechanical Engineering Design*, 8th ed. New York, United States of America: McGraw-Hill Primis, 2006.

[38] Automation Creations, Inc. (2010, May) MATWEB: Online Materials Information Resource. [Online]. http://www.matweb.com

[39] Center for Electro-Mechanics and McDonald Observatory, Critical Design Review II, May 12, 2009, A meeting hosted by CEM in which detail-level design and assembly were discussed with members of MDO.

[40] Whittet Higgens Corporation. (2010, June) BLM Bearlok. [Online]. http://www.whittet-higgins.com/part.php?series_id=2

[41] Center for Electro-Mechanics HETDEX Team, 10223-DT-459 Solid Model, 2010, Contains concept work by Nick Mollison, Rex Jackson, and Homar Molina and detail work by Rex Jackson and Homar Molina.

[42] ASME International, ASME B1.13M-2005 Metric Screw Threads: M Profile, 2005, Metric Thread Standard.

[43] Everlube Products. (2003, October) Lubri-Bond A Technical Data Sheet. [Online]. http://www.everlubeproducts.com/products/docs/pdfdisplay.php?dir=tds&pdf=LubriBondATDS.pdf

[44] Rex Jackson, Interview with Rex Jackson, June 1, 2010, Interview regarding the "thread blocking" feature, how it is accomplished, and its potential uses.

[45] Center for Electro-Mechanics HETDEX Team, 10223-DT-458 Solid Model, 2010, Contains concept work by Nick Mollison, Rex Jackson, and Homar Molina and detail work by Rex Jackson and Homar Molina.

[46] Scott P Pish, Surface Coating Specification, DRAFT, June 17, 2010, 10223-DT-199 REV 2 CEM Internal Document.

[47] Bruce R Somers, "Introduction to the Selection of Carbon and Low-Alloy Steels," in *ASM Handbook Vol. 6: Welding, Brazing, and Soldering*.: ASM International, 1993, pp. 405-407.

[48] McMaster-Carr. (2010, June) McMaster-Carr - Online Catalog - Shaft Clamps. [Online]. http://www.mcmaster.com/#shaft-clamps/=8a2lun

[49] Whittet-Higgins Company. Bearlok Precision Retaining Devices: Installation Instructions for 4-screw Bearloks. [Online]. http://www.whittet-higgins.com/BearlokAssemblyInstructions4Screw.pdf

[50] Alexander Slocum. (2002, February) shaft_torsion.xls. [Online]. http://stellar.mit.edu/S/course/2/sp09/2.007/materials.html

Vita

Homar Molina Jr. was born in Harlingen, TX—the first of four in his family. He grew up in Monte Alto (Rollo), TX and graduated from Edcouch-Elsa High School in 2004. In 2008 he earned a Bachelor of Science degree in mechanical engineering from the Massachusetts Institute of Technology in Cambridge, MA under Professor Seth Lloyd. He began at the University of Texas in Austin in 2008 where he pursued a Master of Science degree in mechanical engineering specializing in design and manufacturing under Professor Steven Nichols.

Permanent e-mail: omj@alum.mit.edu

This thesis was typed by the author.